An energy-based representation of a counter flow single phase heat exchanger

SB Smuts

21796432

Dissertation submitted in fulfilment of the requirements for the degree *Magister Ingeneriae* in Computer and Electronic Engineering at the Potchefstroom Campus of the North-West University

Supervisor: Prof G van Schoor

Co-supervisor: Prof KR Uren

November 2015

PREFACE

Foremost I want to thank my Lord Jesus Christ for the wonderful opportunity to be able to do this study. I also want to thank Him for His grace, blessing and strength I received during this study without whom I would not have been able to complete this study.

I would like to thank my study leaders, Prof George and Prof Kenny. It was truly a blessing to have them as my supervisors. I learned much from them not only about the academic world but also about life. Their support and guidance made this study not only possible but also a great learning experience for me.

I want to thank my dear friends in office 212. It has been a great two years learning and growing together. The time spent making jokes, working hard and taking an abnormal amount of coffee breaks each day, was a blessing to share with you. You will all be sorely missed.

I want to thank my family, mom Hanlie, dad Andre and sister Corlia for their love, support and prayers. This study was not always easy and their encouragement and support helped me when I needed it most. I also want to express my gratitude to my roommate Iddo. He has truly been a blessing to me. He spent late nights listening to my problems and always had a word of encouragement. He kept me going even when my study wasn't going very well.

Lastly I want to thank M-Tech Industrial (Pty) Ltd and THRIP for funding this research. Without their financial support this research would not have been possible. I would also like to thank M-Tech Industrial (Pty) Ltd for access to the Flownex® simulation software.

But thanks *be* to God, who gives us the victory through our Lord Jesus Christ. Therefore, my beloved brethren, be steadfast, immovable, always abounding in the work of the Lord, knowing that your labor is not in vain in the Lord.

1 Corinthians 15:57-58 NKJV

ABSTRACT

Energy is a fundamental part of human civilisation and the expected rise in global energy demand is approximately 1.7% per annum until 2030. With limited fossil fuels available for energy generation, other ways of energy production and conservation must be investigated. One way to achieve this objective is to evaluate the energy used in an industrial process and to determine if this energy evaluation can be used to increase efficiency of the said industrial process.

In order to address the problem of evaluating the energy representation of a heat exchanger, an analytical model must be derived, verified and validated. The sensitivity of the energy representation for several fault conditions is evaluated and possible applications of the energy representation are identified.

The analytical model is derived by applying the staggered grid approach and the laws of conservation of mass, momentum and energy to the heat exchanger. Verification was done by comparing the analytical model results to the results of a Flownex® simulation. Flownex® is validated thermodynamic and hydraulic simulation software that excels at simulations where a fluid is a driving factor. Validation was done using a supercritical CO_2 test bench that consists of a compressor, gas cooler, expansion valve, and an evaporator. The gas cooler can be approximated as a heat exchanger, as it is where hot CO_2 is cooled with water. The gas cooler was therefore used for validation.

Bejan [1] created entropy interaction–energy interaction graphs, using the first two laws of thermodynamics and visualises the changes in energy and entropy of a system. Faults induced include fluid leakage, heat leakage, and fouling. The purpose of faults in the heat exchanger system is to measure the sensitivity of the energy representation to changes in the heat exchanger operation.

An emerging property of the graphing technique is that entropy generated is also shown. The entropy generation number is an indication of the efficiency of the system. Because the energy representation is sensitive to changes in the operating conditions of the heat exchanger and the efficiency of the heat exchanger can be seen, possible applications include fault detection and isolation (FDI) and optimisation. Future research includes a more accurate model encompassing more detail regarding the real world system and improved manners to detect faults as not all faults could be identified.

Keywords: Heat exchanger model, energy-based representation, Flownex®, entropy interaction–energy interaction graphs

TABLE OF CONTENTS

LIST OF TABLES

LIST OF FIGURES

NOMENCLATURE

ROMAN LETTERING (LOWERCASE)

Symbol	Unit	Description
c_p	J/kg.K	Specific heat at constant pressure
d	m	Diameter
e	-	Error code
f	-	Darcy-Welsbach friction factor
f	-	Fault residual vector
h	W/m^2.K	Convection heat transfer coefficient
h	J/kg	Enthalpy
k	W/m.K	Thermal conductivity
l	m	Length
$\dot{m}$	kg/s	Mass flow rate
n	-	Normal residual vector
r	m	Radius
r	-	Residual vector
s	J/kg.K	Specific entropy
t	s	Time
q	W/m^2	Net energy transfer due to thermal radiation
x	-	Direction of transfer

ROMAN LETTERING (UPPERCASE)

Symbol	Unit	Description
A	m^2	Cross sectional area
B	Pa	Bulk Modulus
E_b	W/m^2	Thermal radiation energy emitted per unit area
E_h		Entransy of a system
$\dot{E}_{system}$	W	Energy change of a system
E_x	J	Exergy of a system
$\boldsymbol{F}$	-	Fault vector
$\boldsymbol{G}$	W/m^2	Rate of thermal energy absorption
K_s	-	Secondary Losses

Symbol	Unit	Description
L	-	Length
M	kg	Mass
P	Pa	Pressure
$\dot{Q}$	W	Heat transferred
Q_{vh}	J	Thermal energy stored
S	J/K	Entropy of a system
$\dot{S}_{gen}$	W/J	Generated Entropy
S^{tot}	J/K	Entropy of a system at a deviation from equilibrium
S^{tot}_{eq}	J/K	Entropy of a system at thermodynamic equilibrium
T	K	Thermal potential
T	K	Temperature
U	K	Thermal potential
V	m^3	Volume
$\dot{W}$	W	Work done by a system

GREEK LETTERS

Symbol	Unit	Description
σ	$W/m^2.K^4$	Stefan-Boltzmann constant
ε	-	Emissivity of an object
α	-	Thermal absorptivity
ρ	kg/m^3	Density

SUBSCRIPTS

Symbol	Description
amb	Ambient conditions
c	Cold side
C	Cold side
conv	Convection heat transfer
h	Hot side
H	Hot side
in	Inlet
L	Leak

Symbol	Description
out	Outlet
s	Surface
w	Wall
∞	Fluid
0	Initial value

ABBREVIATIONS

FDI	Fault detection and isolation
S–E	Entropy interaction–energy interaction diagram
T–E	Temperature energy interaction diagram
PLC	Programmable logic controller

CHAPTER 1 INTRODUCTION

1.1 Background

The development of new technologies and the increased population growth have led to an increase in energy usage [2]. The expected rise in global energy demand is approximately 1.7% annually until 2030. The main source of energy generation, approximately 80%, originates from fossil fuels, while renewable energy sources only generate about 11% of the world's energy [3]. With the increase in energy consumption and the negative impact of fossil fuels on the environment, energy conservation has received more attention [4].

Energy is present and used in all industrial processes. Power plants, for instance, produce electrical energy by burning coal, while petroleum plants use energy to convert natural gas to usable petrol. Large industrial processes consist of smaller processes or subsystems. A power plant for instance has a boiler, a turbine and a cooling tower. Each of these systems work together to execute the purpose of the process. A heat exchanger is such a subsystem that utilizes energy to achieve the intended purpose of the process.

Heat exchangers are devices that assist in the flow of thermal energy between two fluids separated by a solid [5]. Heat exchangers used in energy conversion applications range from power, transportation and air-conditioning to heat recovery, alternate fuels and manufacturing industries [6].

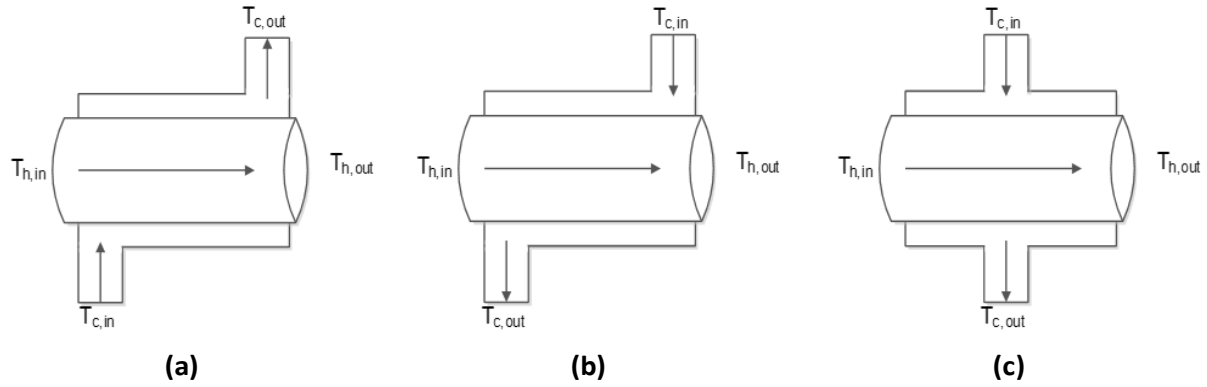

Figure 1-1: Heat exchanger flow arrangements. (a) Parallel-flow, (b) Counter flow, (c) Cross flow

Heat exchangers come in a variety of configurations and flow arrangements depending on the application of the heat exchanger. The most common configurations used, include: shell-and-tube

heat exchangers, plate heat exchangers and double-pipe heat exchangers. Typical flow arrangements include parallel-flow, counter flow and crossflow heat exchangers. In parallel-flow heat exchangers (Figure 1-1 (a)), the fluids flow in the same direction with respect to each other as opposed to a counter flow heat exchanger (Figure 1-1 (b)) where the fluids flow in opposite directions. In a crossflow heat exchanger (Figure 1-1 (c)), the cold fluid flow in a zigzag pattern over the hot fluid [7].

Two-phase heat exchangers change the phase of the fluid as it passes through the heat exchanger. Examples of two-phase heat exchangers include heat pumps, heat pipes, evaporators and gas coolers [8]. Single-phase heat exchangers purely extract or add energy to the fluid without the fluid changing phase inside the heat exchanger. Two-phase heat exchangers have several applications including distillation of vapour in chemical plants, the boiling of water in a nuclear reactor and the use of gas coolers to cool steam in fossil fuel power plants [9].

Once one understands the fundamental mechanics of a heat exchanger, a model can be derived. The purpose of a heat exchanger model is to produce a representation of a real-world system where theories can be tested without the effort or cost involved in implementing the system. The model can accurately calculate the parameters needed to create the energy-based representation of the heat exchanger.

Energy related heat exchanger properties, like heat transfer or fluid flow, comes to mind when the energy of a heat exchanger is considered. The purpose of the energy-based representation is to be a visualisation of the energy of the heat exchanger. An example of what an energy-based representation might look like is given in Figure 1-2.

The effects of heat transfer and fluid flow, on the energy of the heat exchanger, can be seen in Figure 1-2. Energy can flow in and out of the heat exchanger in various manners. Some manners increase the energy of the heat exchanger and some decrease it. It is important that these effects, as well as the influence they have on the heat exchanger, are visible in the energy-based representation. The energy-based representation can also be created under other working points or fault conditions. The change in the representation relative to a defined normal representation can be visually observed. Characteristics such as these make the energy-based representation a valuable heat exchanger evaluation tool.

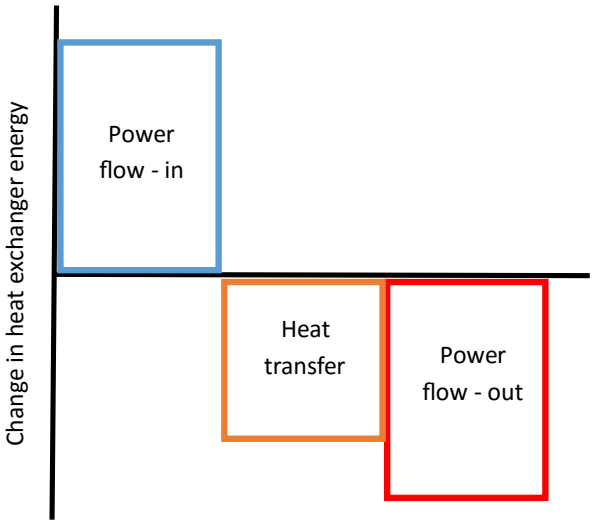

Figure 1-2: An illustration of what an energy representation might look like

It is now clear that describing a heat exchanger in terms of energy is advantageous due to three important reasons. Firstly, energy is a unifying concept and is more easily understood than fundamental equations. Energy can be used to describe the multi-domain behaviour of heat exchangers resulting in a unified depiction of the processes in the heat exchanger. Secondly, the energy crisis is forcing industries to be more energy conscious, especially consumers of vast quantities of energy such as industrial plants. Heat exchangers are a vital component in many industrial plants, thus, evaluation and optimisation of heat exchangers in terms of energy can lead to a more efficient industrial process. Thirdly, it is possible that when the energy of the system as a whole is viewed, additional information may be present in the energy representation that one may not be able to see in the solutions of the fundamental equations. The focus, therefore, of this research is: (i) to evaluate the energy of a heat exchanger by means of an energy-based representation and (ii) to identify possible applications of the energy-based representation.

1.2. Problem statement

The aim of this research is to develop an energy-based representation of a counter flow single phase heat exchanger. The energy-based representation must depict the energy as well the effects that change the energy of the heat exchanger. The energy-based representation must also be sensitive to changes in the operation of the heat exchanger. The counter flow single phase heat exchanger that will be modelled is a double pipe super critical heat exchanger that cools warm CO_2 with water.

1.2.1 Research scope

The type of heat exchanger used in this study is a double-pipe single-phase counter flow heat exchanger. Software that will be used during this study include MATLAB® and Flownex®. Experimental data will be gathered on the gas cooler that forms a part of the CO_2 test bench to be used during model validation. The energy analysis is restricted to the cold fluid. The hot fluid has more energy than the cold fluid (because of increased temperature and different molecular composition) and therefore yields energy diagrams that are difficult to interpret. The analysis is also restricted to modelling both fluids as incompressible.

1.3. Issues to be addressed

This section will discuss the issues that need to be addressed by this research.

1.3.1 Development of an analytical model

The real-world system, that must be modelled, is a gas cooler that is part of a CO_2 test bench. The gas cooler can be approximated as a double pipe heat exchanger as it is where hot CO_2 is cooled with water.

1.3.2 Verification of the analytical model

Verification is the process of confirming that the model is correctly implemented in the sense that it matches certain specifications and assumptions that one would expect from the process or system that is modelled [10].

1.3.3 Validation of the analytical model

Validation can be defined as the process followed to ensure that the analytical model, within its domain of applicability, has a satisfactory range of accuracy when compared to the real-world system that was modelled [11].

1.3.4 Energy representation

The energy representation is a visual illustration of the energy of the heat exchanger. The representation can include the energy stored in the system, the change of the energy of the system, and the flow of energy in and out of the system.

1.3.5 Sensitivity of the energy representation

The sensitivity of the energy representation is a measure of how the energy representation changes when the heat exchanger operating conditions change. For the energy representation to be useful, it must change even in the presence of minute changes in heat exchanger operation.

1.4 Methodology

The methodology followed for this research is given in this section. Figure 1-3 illustrates the high-level methodology followed.

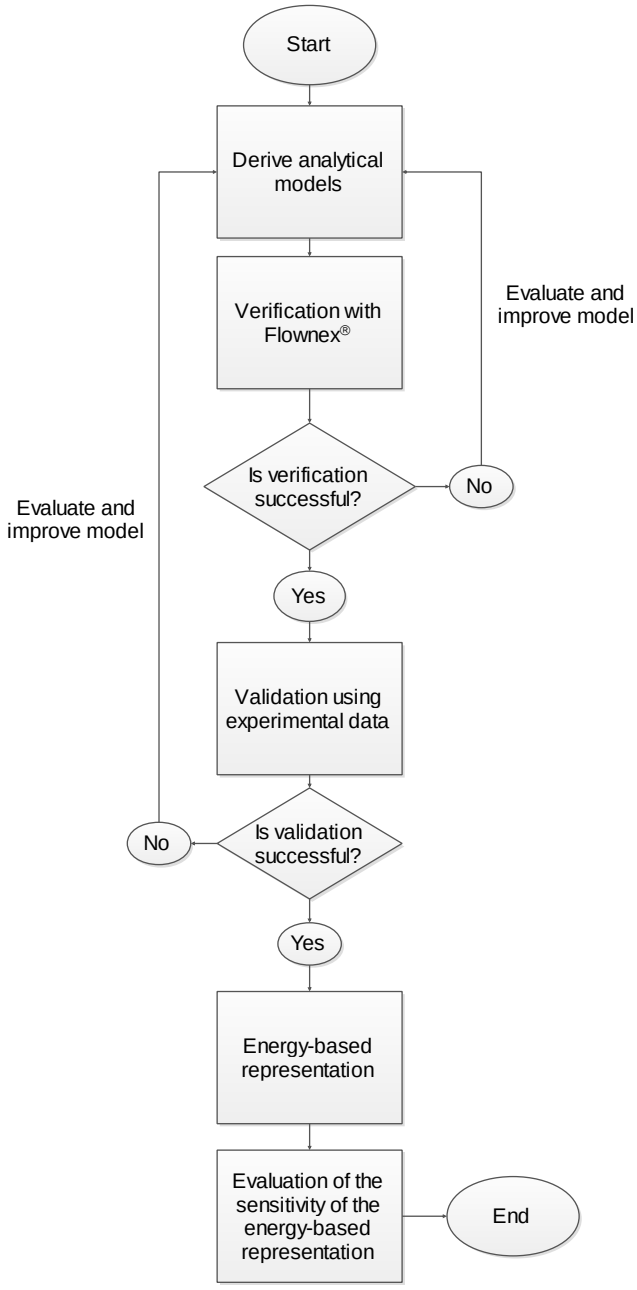

Figure 1-3: The high level methodology followed for this research

1.4.1 Development of an analytical model

The analytical model will be derived based on the properties of the fluids and the real-world system. The laws of conservation of mass, momentum, and energy will be used to derive equations that describe the heat exchanger. The model will be implemented and solved in MATLAB®. Two additional models will be derived to be used as fault models when the sensitivity of the heat exchanger is evaluated. The fault models will simulate a fluid leak and a heat leak.

1.4.2 Verification of the analytical model

The heat exchanger will be modelled in Flownex® on a component level to solve for the variables of interest. Verification will be done by comparing the results of the Flownex® model to the analytical model.

1.4.3 Validation of the analytical model

The mechanical engineering department at the North-West University has a CO_2 test bench where experiments can be conducted. The test bench consists of a compressor, gas cooler, expansion valve, and an evaporator. The experiments will be done on the gas cooler as the gas cooler is a type of heat exchanger. The gas cooler is where hot CO_2 is cooled with water. The experimental data and the results of the analytic model can be compared to validate the analytical model.

1.4.4 Energy representation

The energy of the heat exchanger will be visualised using entropy interaction–energy interaction (S–E) graphs [1]. These energy representations depict the energy and entropy present in the heat exchanger system based on the second law of thermodynamics. It is beneficial to describe the heat exchanger in entropy and energy, because both of these quantities are sensitive to changes and entropy can be used for optimisation.

1.4.5 Sensitivity of energy representation

In order to measure the sensitivity of the energy representation, changes must be induced in the heat exchanger operation. Changes will be induced in the operation of the heat exchanger by changing the operating point or by inducing faults into the heat exchanger operation.

1.5 Outline of Dissertation

This dissertation consists of six chapters and two appendices.

Chapter 2 provides an overview of heat exchanger configurations and manners of heat transfer. Common heat exchanger modelling techniques and energy concepts such as entropy, exergy, and heat exchanger optimisation techniques are described as well. Chapter 2 concludes with a critical review of the presented literature.

Chapter 3 describes the derivation process of the analytical model using the laws of conservation of mass, momentum and energy. Two fault models are also derived to be used during the

evaluation of the sensitivity of the energy representation. Chapter 3 concludes with the simulation results of the analytical model and the fault models.

Chapter 4 presents verification of the analytical and fault models with Flownex® models. The validation procedure, experimental setup, and validation of the analytical model are also given in Chapter 4. Appendix B includes the tables listing the raw experimental data.

Chapter 5 provides an overview of the technique used to create the energy representation along with an illustrative example. The energy representation created under normal and fault conditions is also shown. Chapter 5 concludes with the evaluation of the sensitivity of the energy representation.

Chapter 6 concludes the research with conclusions, recommendations and closure.

CHAPTER 2 LITERATURE STUDY

2.1 Introduction

The literature, regarding the modelling and visualisation of the energy of the heat exchanger, can be broken down into sections, namely: (i) heat exchanger theory, (ii) heat exchanger modelling techniques, (iii) energy concepts, (iv) visualisation, and (v) optimisation. Each of these sections is discussed briefly in the literature survey regarding current research. The literature study then continues with heat exchanger theory regarding heat exchanger configurations and heat transfer mechanics. An overview of four common heat exchanger modelling techniques is given and concepts such as energy, entropy and exergy are reviewed. Four heat exchanger optimisation techniques are discussed briefly, after which this chapter concludes with a critical review of all the literature presented.

2.2 Literature survey

The concept of heat transfer has been around since the dawn of civilisation. Scientific studies regarding heat transfer can be dated back to 1700 when Newton conducted studies on the capabilities of heating a solid with steam from a hot fluid. It was not until the late 19th and early 20th centuries that the value of heat transfer for technical purposes was realised. With the invention of the steam machine and the need for more effective heat transfer, heat exchangers truly became a fundamental part of industrial processes.

Heat exchanger technology has rapidly advanced in the last century due to the increasing demand for more efficient and cost effective heat exchangers [12]. Heat exchangers come in a variety of configurations depending of the application the heat exchanger was designed for. Shell-and-tube heat exchangers, for example, have a large heat transfer area but cannot operate at very high pressure [13]. Double-pipe heat exchangers, on the other hand, can operate at high pressure and are particularly advantageous when small heat transfer areas are a requirement [5].

In order to understand and analyse the phenomena present in a heat exchanger, a model can be used. A model is a mathematical, logical or mechanical representation of a system designed in such a way that a study of the model results in a summary of the complex processes of the real-world system or the illustration of a theory [14]. A few common methods used to model heat exchangers include: analytical modelling, CFD software [15], artificial networks modelling [16], and object-orientated modelling [17]. Once the model is completed, analysis and optimisation of

the system can begin. Energy is a concept that is sometimes used when analysing and optimising a heat exchanger [18].

Energy is closely linked to industrial processes and it is estimated that almost 80% of energy consumption in the industry is related to heat transfer [19]. Current research is focused on using energy and two energy related concepts namely exergy and entropy, for analysis and optimisation purposes. Exergy is a measure of the usable energy of a system with respect to the environment. Exergy is destroyed whenever an irreversible process occurs in a system. Exergy destruction can, thus, be used as a basis for optimisation [20]. Entropy is a measure of the discord of a system [20]. Entropy generation, on the other hand, is a measure of the efficiency of a system and can be used as a means of optimisation [1].

Bejan [1] proposed that a visual representation of a system can be a valuable analysis tool. Heat exchanger representations, however, are an area that little work has been done on. Bejan [1] developed two thermal system representation techniques, namely the entropy interaction–energy interaction (S–E) diagram and the temperature–energy interaction (T–E) diagram. S–E diagrams visually show the entropy and energy flows and changes of a system. It is beneficial when modelling open systems with one or more mass flow rates across the system boundary. T–E diagrams are useful when visualising the imperfect performance of closed thermodynamic systems that operate steadily or in cycles [1].

Muralikrishna et al. [21] used a pressure drop diagram to determine the feasible region for the design of a shell-and-tube heat exchanger. The feasible region was defined in such a way to eliminate the trial-and-error process often encountered during the design phase. Picón-Núñez et al. [22] proposed a graphing approach that aids in the preliminary design of heat exchangers. Several geometric parameters, including shell diameter and tube length, are used as axis values. Curves, such as heat load and pressure drop, are plotted on the graph surface and the optimal design space is where these curves intersect. This graphing approach allow the designer to change certain parameters in order to achieve an optimal design.

In pursuit of improved heat transfer, substantial efforts have been made to define various optimisation methodologies. Optimisation research can be divided into two main categories: (i) the evolutionary algorithm optimisation method and (ii) the mathematical programming optimisation method [23]. Different perspectives on these methods can include, but is not limited to, second law analysis, distinctive evolutionary optimisation, single-geometric optimisation, and multi-objective optimisation. Second law analysis includes techniques such as entropy generation minimisation [24] and entransy dissipation theory [25]. Distinctive evolutionary algorithm

techniques include using a particle swarm [26] and a chaotic quantum-behaved particle swarm [27] for heat exchanger optimisation. Single-geometric optimisation is done by optimising a single geometric parameter of the heat exchanger such as the space between the baffles of a shell-and-tube heat exchanger to reduce the capital investment [28]. Multi-objective optimisation is the process where the most optimal solution is found when considering several parameters. Sanaye et al. [29] used multi-objective optimisation to maximise the efficiency and minimise the cost of a shell-and-tube heat exchanger.

Another focus of heat exchanger optimisation is to increase the thermodynamic properties of the fluid and to increase the heat transfer area. The heat transfer area of a heat exchanger can be increased by adding fins inside the tubes. Recent studies conducted to improve heat transfer potential are centred on nanofluids. Nanofluids are liquid suspensions containing particles that are smaller than 100nm [30]. Nanofluids have been proven to be effective in heat transfer due to enhanced properties such as conductivity when compared to the carrier fluid alone [31]. Nanofluids with suspensions such as Al_2O_3, TiO_2 and SiO_2 have been proven to have increased conductivity [32]. Nanofluids have been shown to be advantageous in several heat exchanger configurations, including shell-and-tube heat exchangers [33], double pipe heat exchangers [34], and plate heat exchangers [35].

2.3 Heat exchangers

Heat exchangers have many uses in industrial processes and are classified according to certain criteria. The classification criteria include aspects such as heat transfer mechanisms, geometry and flow arrangement [5]. This section provides a broad overview on the different configurations of heat exchangers, as well as more detail concerning the three most common heat exchangers used in industry. An overview on the different heat transfer mechanisms is also provided.

2.3.1 Heat exchanger configurations

This section provides a brief overview of the three most common heat exchanger configurations used in industry, including a summary of the uses, advantages and disadvantages of each type of heat exchanger.

2.3.1.1 Shell-and-tube heat exchanger

Shell-and-tube heat exchangers are constructed from two main components: the shell and the tubes. The shell side is where the cold fluid flows and inside the tubes are where the hot fluid flows. The shell can contain several baffles forcing the cold fluid to flow in a criss-cross pattern

over the tubes. The baffles cause leakage streams. These leakage streams reduce the velocity of the fluid and as a consequence the heat transfer coefficient is reduced in exchange for a longer contact time between the two fluids [36]. Roughly 35-40% of all heat exchangers used in global industry are shell-and-tube heat exchangers. [12].

2.3.1.2 Plate heat exchanger

Plate heat exchangers consist of flow channels made of plates that are corrugated. The plates are stacked together with gaskets between them. Once assembled the corrugations on successive plates form narrow flow channels [37]. A plate heat exchanger exposes the fluids to a much larger surface area. The increase in surface area increases the heat transferred. Plate heat exchangers can be manufactured in three ways depending on the method used to seal the flow channels: gasket, welded, or module welded [38].

2.3.1.3 Double-pipe heat exchanger

A double-pipe heat exchanger consists of two concentric pipes with the hot fluid in the centre pipe and the cold fluid in the outer pipe. In order to improve the heat transfer, axially placed fins can be inserted into the bigger pipe to increase the heat transfer surface area. The fluids usually flow in opposite directions resulting in a counter-flow heat exchanger. Manufacturing of double-pipe heat exchangers occurs in modules such that these modules can be connected to produce any desired heat transfer capacity [7]. Table 2-1 provides a few advantages, disadvantages, and main uses of the three heat exchanger types discussed.

Table 2-1: Uses, advantages, and disadvantages of different heat exchangers

Configuration	Main Uses	Advantages	Disadvantages
Double-pipe	• Sensible heating or cooling of process fluids where small heat transfer areas are required [5]	• Particular advantages when the fluids are at high pressure that would cause increased costs to strengthen the shell of a conventional shell-and-tube heat exchanger [7]	• Bulky and expensive per unit transfer area [5]
Shell-and-tube	• Transformer oil cooling • Exhaust gas heat recovery	• Large heat transfer area per unit volume • Wide range of operating conditions	• High pressure drop • Low shell side mass flow rate • Short operation time [40]

Configuration	Main Uses	Advantages	Disadvantages
	• Solvent distillate processes [39]	• Versatile materials used in construction [13]	
Plate	• A wide range of chemical and industrial applications • Preferred in the food industry for easy cleaning, suitability in hygienic applications, and temperature control needed for sterilisation and pasteurisation [38]	• More compact designs • Large surface area in small volume • Easily modifiable by increasing or decreasing the number of plates [38]	• Not suitable for heat exchange between gasses because of large pressure drop [37] • Limited operational range [38]

2.3.2 Heat transfer mechanisms

Heat is transferred from one medium to the other due to a temperature difference. Transfer of heat occurs in three ways. Conduction heat transfer involves the transfer of heat through a surface. Convection heat transfer describes the transfer of heat between flowing fluids and a surface such as a fluid flowing in a pipe. Radiation heat transfer describes the transfer of heat via electromagnetic waves. The next section discusses each of these methods of heat transfer shortly.

2.3.2.1 Conduction

Conduction heat transfer occurs inside a solid that has a temperature difference across it. The difference in temperature causes energy to move from the higher temperature area to the lower temperature area [41]. The equation for conductive heat transfer is known as Fourier's law and is given by

$$\dot{Q}_x = -k\frac{dT}{dx}. \tag{2.1}$$

The heat flux, $\dot{Q}_x$, [W/m^2] is the heat transfer rate per unit area while k symbolises the thermal conductivity [W/m.K] of the solid. The temperature gradient of the solid is given by dT/dx [K/m] for the x-direction. If one considers the temperature distribution to be linear, Fourier's law is written as

$$\dot{Q}_x = k\frac{T_1 - T_2}{L}. \tag{2.2}$$

Equation (2.2) is only valid when conduction takes place through a flat plate or surface. In the case of a pipe (cylinder), the general form of the heat equation (Fourier's law) is given as [41],

$$\frac{1}{r}\frac{\partial}{\partial r}\left(kr\frac{\partial T}{\partial r}\right)+\frac{1}{r^2}\frac{\partial}{\partial \phi}\left(k\frac{\partial T}{\partial \phi}\right)+\frac{\partial}{\partial z}\left(k\frac{\partial T}{\partial x}\right)+\dot{q}=\rho c_p\frac{\partial T}{\partial t}. \tag{2.3}$$

2.3.2.2 Convection

Convection heat transfer is the transfer of energy from a surface to a fluid or vice versa. Two types of convection are typically investigated: forced convection and natural convection. Forced convection occurs when the fluid is flows over the surface much like a fan forces air over a heat sink. Natural convection occurs when the fluid moves due to density changes within the fluid caused by the addition or extraction of thermal energy [41]. The convection heat transfer equation is known as Newton's law of cooling and is given by

$$\dot{Q} = h(T_s - T_\infty). \tag{2.4}$$

The convective heat flux, $\dot{Q}$ [W/m^2] is proportional to the difference between the fluid temperature, T_∞ [K] and the surface temperature, T_S [K]. The convective heat transfer coefficient, h [W/m^2.K] is the proportionality constant and is dependent on variables such as fluid and solid properties as well as the motion of the fluid [41].

2.3.2.3 Thermal radiation

Every form of matter that is at a finite temperature emits thermal radiation in the form of electromagnetic waves. Unlike convection or conduction heat transfer, radiation heat transfer does not require a medium and is most efficient in a vacuum [41]. The Stefan-Boltzmann law gives the maximum energy that can be emitted from an ideal object as

$$E_b = \sigma T_s^4, \tag{2.5}$$

with E_b the energy emitted [W/m^2], σ the Stefan-Boltzmann constant (5.67x10^{-8}W/m^2.K^4) and T_s the absolute temperature [K] of the matter. However, all matter is not ideal, therefore, there is a non-ideal form of (2.5) as given by

$$E_b = \varepsilon\sigma T_s^4, \tag{2.6}$$

with $0 \leq \varepsilon \leq 1$ termed the emissivity of the object. Objects can not only emit thermal radiation but also absorb thermal radiation at a rate of G [W/m^2]. As with the emission of thermal radiation, non-ideal objects also absorb radiation at a non-ideal rate as given by

$$G_{abs} = \alpha G \,. \tag{2.7}$$

The thermal absorptivity, $0 \leq \alpha \leq 1$, is a measure of how well the object absorbs or reflects thermal radiation. The net change in the thermal radiation emitted and absorbed by an object is given by

$$q''_{rad} = \frac{q}{A} = \varepsilon E_b(T_s) - \alpha G = \varepsilon\sigma(T_s^4 - T_{sur}^4) \,. \tag{2.8}$$

2.4 Heat exchanger modelling techniques

This section will provide an overview of different heat exchanger modelling techniques that are common in the literature. These techniques include analytical modelling, CFD modelling, artificial neural network modelling, and object orientated modelling.

2.4.1 Analytical models

Analytical modelling of heat exchangers usually start with the three governing equations. The conservation of mass, momentum and energy equations describe the processes of the heat exchanger in both the hydrodynamic and thermodynamic domains. The conservation of mass, momentum and energy equations, respectively, are given by

$$\frac{\partial}{\partial t}\int_{CV} \rho dV + \int_{CS} \rho \mathbf{v} \bullet \hat{\mathbf{n}} dA = 0 \,, \tag{2.9}$$

$$\frac{\partial}{\partial t}\int_{CV} \mathbf{v}\rho dV = -\int_{CS} \mathbf{v}\rho \mathbf{v}.\hat{\mathbf{n}} dA + \int_{CS} \bar{\tau} dA + \int_{CV} \bar{\beta}\rho dV \quad \text{and} \tag{2.10}$$

$$\frac{\partial}{\partial t}\int_{CV} e\rho dV = -\int_{CS} e\rho \mathbf{v}.\hat{\mathbf{n}} dA + \dot{Q} + \dot{W} \,. \tag{2.11}$$

In order to simplify the governing equations, methods like control volumes and discretising of the equations can be implemented. The concept of control volumes involves dividing the system to be modelled into non-overlapping volumes [42]. The control surface separates the control volume from its surroundings. The control surface may be open or closed to mass and energy inflow and outflow [43]. The main advantage of the control volume approach is that control volumes are a small representation of the system. If the governing equations are valid for a single control volume, they are valid for all similar control volumes and the system as a whole [44].

Discretising the governing equations is the process used to simplify them by deriving them for only certain points in space and time. The points where the differential equations will be derived for are known as main grid points. When one solves all three the governing equations on the same main grid point, several difficulties may arise in the solution [42]. Patankar [42] solved this problem by defining what is known as a staggered grid. By inserting control volumes around each main grid point one can define secondary grid points on the control surface of each control volume.

On the staggered grid the conservation of mass and conservation of energy equations are solved on main grid points and the conservation of momentum equation is solved on secondary grid points. This eliminates the problems of using a single grid point for each of the three governing equations [42]. The main advantage of analytical models are that one gains a deeper insight into the physical properties of the real-world system being modelled. The main disadvantage of analytical models are the complexity of the equations and the assumptions that have to be made to decrease the complexity of the model [16].

2.4.2 CFD software

With the increase in the processing power of modern-day computers, research into fluid flow is taking advantage of this in the form of computational fluid dynamic (CFD) software. CFD software takes advantage of a computer's power to numerically solve the fundamental non-linear differential equations that describe fluid flow (such as the Navier-Stokes equation). The main advantage of CFD software is that engineers can simulate complete systems and easily make changes without the effort and cost of implementing the real-world system [45]. The main disadvantages of CFD software are the cost of the software and the additional training time needed to use the software.

2.4.3 Artificial neural networks

Analytical models involve complex mathematics and assumptions and experimental methods require expensive equipment. Artificial neural network (ANN) based models were developed to overcome these difficulties. The ANN can identify the nonlinear relationship between the input and output data based on the provided sets of training data. When developing the ANN to model the heat exchanger it is important to accurately select the ANN parameters like the number of neurons in the input layer or the network architecture. Incorrectly selecting the ANN parameters can affect the accuracy of the model. The number of neurons in the input layer is equal to the number of heat exchanger parameters needed to optimise the heat exchanger. The number of

neurons in the output layer is equal to the number of heat exchanger parameters that need to be optimised. Once the ANN has been designed, training can begin [16].

The ANN is trained with sets of matching input and output data and a learning method. The value of the weight coefficients between the neurons are adjusted as the training data are learned. The performance of the trained ANN must then be evaluated using statistical methods such as the root mean square error and the absolute fraction of variance. The ANN parameters can be adjusted by a trial-and-error process to obtain the optimal values for these parameters. The main advantage of an ANN is the increased accuracy and that no equations or system descriptions are required. The main disadvantage is that an ANN is regarded as a black box. This implies that only the inputs and outputs of the ANN is known and the calculations made to get the output values from the given input values are unknown [16].

2.4.4 Object-orientated modelling

Object-orientated modelling (OOM) is an approach used to model the components of heat exchangers as a set of interconnected objects. For instance a heat exchanger has two fluid streams and a separation wall. The cold fluid can be modelled as an object connected with a terminal to the separation wall object. Objects need to be properly defined in terms of properties and terminals in terms of transfer mechanics. The main advantages of defining the components of a heat exchanger as objects are the possibility of multiple inheritance and the declaration feature. These advantages result in a clear model structure and increased model flexibility [46]. A result of the object-orientated approach is the Modelica® project. Modelica® is described as a non-proprietary, object-oriented, equation-based modelling tool [47].

2.5 Energy, exergy and entropy

When one attempts to describe a process in terms of energy it is important to know the meaning of energy, and the different forms of energy used to describe systems. The unit of energy is the Joule [J] and is a measure of the amount of work a system can do [20]. However, not every last joule a system possesses can be used for work. Some of the energy is physically captured in the molecules of the matter as internal energy [48]. A new quantity is needed that takes into consideration not only the energy of the system but also the quality or work potential of the energy. To this end, two quantities were defined: entropy and exergy [48].

2.5.1 Energy

Energy is the capability of a system to produce an effect. Energy can be transferred through various ways (heat transfer, chemical change, combustion) and can be stored in various systems [43]. The first law of thermodynamics states that energy cannot be created or destroyed but only transferred from one form to another [48]. The first law of thermodynamics can be expressed in equation form as given by

$$\Delta \dot{E}_{system} = \dot{E}_{in} - \dot{E}_{uit} . \tag{2.12}$$

The term on the left of (2.12) symbolises the change in energy of the system. The first term on the right is the inflow of energy and the second term on the right represents the outflow of energy. Any heat transfer interaction, $\dot{Q}$ [W], or work, $\dot{W}$ [W], done on the system is positive when entering the system and negative when leaving the system. Although energy is a valuable tool in heat transfer analysis, entropy and exergy analysis has many advantages over a purely energy-based approach [48].

2.5.2 Exergy

Some thermodynamic systems are in equilibrium within itself but not in mutually stable equilibrium with the surroundings. Exergy is defined as the maximum amount of useful work that a reversible system can produce with respect to a specific environment or ambient condition [49]. The properties of the environment, for instance, temperature, pressure and chemical composition, need to be specified. Exergy is not only a thermodynamic property but also a co-property of the system and the environment [48]. The exergy of a system may be expressed as follows:

$$E_x = T_0(S_{eq}^{tot} - S^{tot}) . \tag{2.13}$$

The temperature of the environment is given by T_0 [K] while S_{eq}^{tot} and S^{tot} represent the entropies [J/K] at thermodynamic equilibrium and a certain deviation from equilibrium respectively. Exergy and exergy destruction have become valuable tools in heat exchanger analysis and optimisation [50]–[53].

2.5.3 Entropy

The first law of thermodynamics describes the quantity of the energy of the system but does not give any indication of the quality of the energy. On the other hand, the second law of thermodynamics describes the quality of the energy and shows that not all the energy of a system

can be used effectively or used at all [54]. The entropy of a system has the following three characteristics. Firstly, the entropy of a system is a measure of its disorder. Secondly, a system can only generate entropy and not destroy it. Thirdly, entropy can be increased or decreased by energy being transported over the system boundary [48]. The second law of thermodynamics is stated by the following two equations:

$$\sum_{in} \dot{m}s - \sum_{out} \dot{m}s + \frac{\dot{Q}}{T} \leq \frac{dS}{dt}, \tag{2.14}$$

$$\dot{S}_{gen} = \frac{dS}{dt} - \sum_{in} \dot{m}s + \sum_{out} \dot{m}s - \frac{\dot{Q}}{T} \geq 0. \tag{2.15}$$

The term on the right of the equal sign in (2.15) is the entropy generation rate and can never be smaller than zero. The first term on the left of the equal sign is the change in entropy. The second and third terms on the right of the equal sign represent the inflow and outflow of entropy with $\dot{m}$ the mass flow rate [kg/s] and s the specific entropy [J/kg.K]. Any entropy entering or leaving the system due to heat transfer is given by $\dot{Q}/T$ [W/K]. Entropy generation ($\dot{S}_{gen}$) is used to evaluate the irreversibility of a process. A process that generates zero entropy is completely reversible [55]. The application of entropy to the optimisation and analysis of a heat exchanger was investigated thoroughly with special attention to the entropy generation minimisation technique [1][56].

2.6 Heat exchanger optimisation techniques

The optimisation of heat exchangers and heat transfer, in general, has received increased attention due to the energy crisis [57]. A number of optimisation techniques were developed including second law analysis, distinctive evolutionary analysis, single-geometric analysis, and multi-objective analysis, all of which are briefly discussed in this section.

2.6.1 Entransy theory

Guo et al. [58] defined entransy as a physical property for the optimisation of heat transfer and has been derived using the similarities between the electrical and thermal domain. Entransy corresponds to the electrical energy stored in a capacitor and is given by

$$E_h = \frac{1}{2} Q_{vh} U_h = \frac{1}{2} Q_{vh} T. \tag{2.16}$$

Q_{vh} gives the thermal energy [J] stored in an object at constant temperature and U_h or T the thermal potential [K]. Guo et al. found that, during experimentation, entransy describes an object's ability to transfer heat. The authors also found that entransy is dissipated due to thermal resistance when heat conduction through a medium takes place. This observation leads to a definition of entransy transfer efficiency that is the basis for the extremum principle of entransy dissipation and the minimum thermal resistance principle. Both of these principles can be used as a means of optimisation.

2.6.2 Entropy generation minimisation

Every irreversible operation in a system generates entropy, therefore the purpose of entropy generation minimisation is to identify and optimise the components responsible for the entropy generation [1]. In a real-world heat exchanger, the most common form of entropy generation is heat transfer and fluid flow with friction.

Bejan [1] proved that by choosing an optimal flow path and heat transfer area, entropy generation can be minimised. The implications of this are that the optimal flow path is inversely related to the mass velocity. This relation means that the faster the fluid flows, the shorter the optimal path length will be. This allows one to make a sensible choice regarding the length needed for the heat exchanger for minimum entropy generation during the design phase. Secondly, the entropy can be minimised by using a larger heat transfer area. Bejan found that when the heat transfer area is sufficiently large, less entropy will be generated [1]. A direct consequence of a larger heat transfer area is lower fluid velocities and, as a result, less entropy generation.

Minimising the entropy during the design phase might not always be the best approach as one will overlook things like cost or space. In most heat exchanger applications there will always be a cost or space constraint. Simply increasing the heat transfer area, therefore, might not be an easy task or cost effective.

2.6.3 Distinctive evolutionary optimisation

A common evolutionary computation technique is particle swarm optimisation (PSO). PSO has key features of evolutionary computational techniques such as the initialisation of a population with random solutions and searching for the optimal solution by updating the particles. Each potential solution of the problem modelled with PSO is represented by a particle. Each particle has current unique coordinates and the coordinates of the optimal solution it has found thus far. The coordinates of the most optimum solution found by any particle in the swarm is also recorded.

The solution of the particle swarm is done by updating the velocity of each particle towards the coordinates of its personal best and the global best solutions [26].

The equations governing the velocity change consist of random values and weighted velocity constants. The purpose of these constants is to change the behaviour of the swarm. Lower values for these constants allows the particles to roam further away from the current optimal solutions, while higher values result in sudden movements towards or past the current optimal solution. The choice of constants greatly affect the performance of the particle swarm and by carefully choosing optimal values for the constants the performance of the swarm can be greatly increased [26].

2.6.4 Multi-objective optimisation

Multi-objective optimisation is the process by which a heat exchanger is optimised based on more than one parameter. Most cases of multi-objective optimisation in literature is the maximising of a heat exchanger parameter, like efficiency, and the minimising of a cost or emission parameter. Once the parameters of interest have been decided upon, optimisation usually occurs by employing an algorithm that iterates through the different solution sets until an optimal solution has been reached [59], [60].

Kang [59] et al. used multi-objective optimisation to minimise the annual cost and total CO_2 emissions of a heat exchanger network retrofitted with a heat pump. The optimal solution of these two objectives is derived by solving the heat exchanger model and plotting the Pareto front. Wang [60] et al. proposed the optimal design of plate fin heat exchangers using an improved multi-objective cuckoo search algorithm. The authors optimize the heat exchanger by simultaneously minimizing the entropy generated due to heat transfer and fluid friction. It can be seen from the studies discussed above that multi-objective optimisation always occurs in two steps: the definition of the parameters to optimize and the optimising of the selected parameters using.

2.7. Critical review of literature

Chapter 2 provided a broad overview on the configurations of heat exchangers including a discussion on the three most common type of heat exchangers found in the industry: shell and tube heat exchangers, plate heat exchangers, and double-pipe heat exchangers. A short review of the three manners of heat transfer, conduction, convection, and radiation was also provided.

Once the phenomena of a heat exchanger are understood a model for the heat exchanger can be created. Several modelling approaches were reviewed including analytical modelling, CFD software, artificial neural network modelling and object-orientated modelling. The advantages and

disadvantages of these techniques were discussed and after careful evaluation the method to be used in this study was chosen as analytical modelling. The use of an analytical model allows one to calculate and evaluate the parameters needed to create the energy representation. Complexity is not a requirement for this study, thus, a representative heat exchanger model will be sufficient.

When evaluating the energy of a heat exchanger, an entropy or exergy analysis usually accompanies the energy analysis. A review on energy, entropy and exergy was provided in this chapter and it was decided to base the heat exchanger of this study on energy and entropy. The reason for choosing entropy and energy is twofold. Firstly, the heat exchanger is regarded as an open system. Entropy and energy are useful for analysis of open systems; because the entropy and energy flows in and out of the system are useful parameters for fault detection and optimisation. Secondly, the method that will be used to create the energy representation of the heat exchanger is energy and entropy based.

Little literature is available on the application of graphing techniques as a means of creating an energy-based representation of a heat exchanger. Several graphing techniques were identified, but only the entropy interaction–energy interaction (S–E) diagram developed by Bejan [1] is suitable to this study. The S–E diagram depicts the flows of the entropy and energy of the heat exchanger system and is advantageous when used for an open system. This visual indication of the energy and entropy of the system can be used as a means to identify the current state of the system and possibly the detection of faults.

The optimisation of heat exchangers is a research area that has gained increased attention over the last few years. Several optimisation techniques were discussed in this chapter including entransy theory, entropy generation minimisation, particle swarm optimisation, and multi-objective optimisation. After a review of these techniques it was concluded that entropy generation minimisation is the technique best suited for this study. Entropy generation minimisation has been verified in literature as being an excellent optimisation technique and the energy-based representation is compatible with the entropy generation minimisation technique. For these reasons entropy generation minimisation is deemed as the best choice for optimising the heat exchanger of this study. Although optimisation of a heat exchanger is not part of this study, it is important to evaluate the possibility to use the energy representation of the heat exchanger as a means for optimisation for the purposes of further study.

CHAPTER 3 SYSTEM MODEL

3.1 Introduction

An analytical model is a mathematical representation of a real-world system. In order to derive an analytical model, the physical system that needs to be modelled must be defined in terms of certain parameters. An overview of the CO_2 test bench is provided, with specific attention to the gas cooler on which the analytical model is based. The methodology followed to derive the analytical model is also provided. The analytical model is derived by applying the staggered grid approach [42] to the heat exchanger in order to discretise the heat exchanger in one-dimensional space. The differential equations, describing the phenomena present in the heat exchanger, are derived by using the laws of conservation of mass, momentum and energy. The analytical model is simulated to evaluate the correctness of the equation responses. The derivation of the mathematical models for two fault conditions, is also given in this chapter. The fault models will be used when evaluating the sensitivity of the energy-based representation. This chapter concludes with the simulation of the fault models.

3.2 Physical system

The test bench, on which the experiments are to be conducted, is a closed CO_2 cycle test bench. The test bench consists of a compressor (Figure 3-1 (2)), a gas cooler (Figure 3-1 (1)), an expansion valve (Figure 3-1 (3)), and an evaporator (Figure 3-1 (5)). The compressor is a reciprocating compressor and increases the pressure of the CO_2 past the critical point of CO_2 and therefore turning into a liquid.

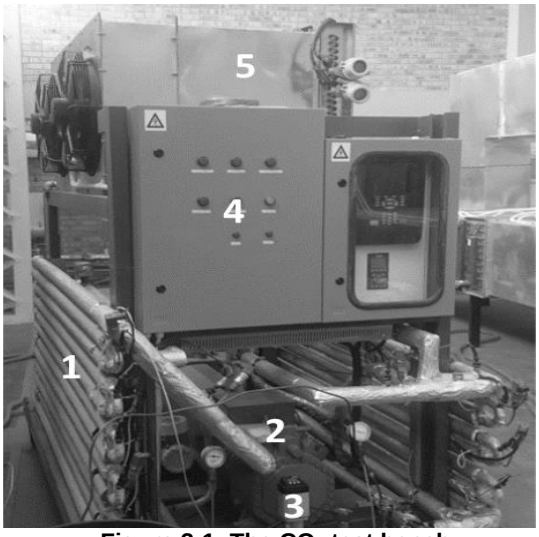

Figure 3-1: The CO_2 test bench

This increase in pressure results in an increase in CO_2 temperature and mass flow rate. The CO_2 is cooled with water in the gas cooler. The expansion valve reduces the pressure of the cooled CO_2 in order to force the CO_2 into a liquid state. Lastly, the evaporator heats the CO_2 until it is in its gaseous state and it is returned to the compressor. This is known as a trans-critical cycle. The P-H diagram of this process is given in

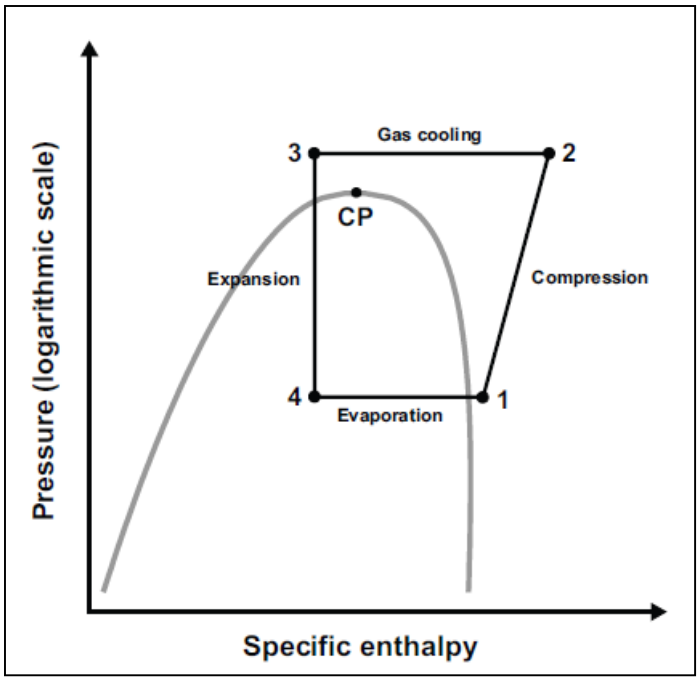

Figure 3-2: The P-H diagram of a trans-critical $C0_2$ cycle

Several sensors are visible in Figure 3-1; including pressure, temperature, and mass flow rate sensors. All the sensors connect to the programmable logic controller (PLC) (Figure 3-1 (4)) where the data of the experiment is logged and made available via a web-based interface.

The gas cooler is a double-pipe counter flow heat exchanger. The hot fluid pipe is made out of AISI 304 stainless steel schedule 40 pipe with a diameter of 15.7 mm and resides inside the cold fluid pipe. The cold fluid pipe is made out of copper with a diameter of 26.6 mm. The total length of the gas cooler is approximately 24 m. A schematic of the gas cooler, with the sensor numbers shown, is given below by Figure 3-3.

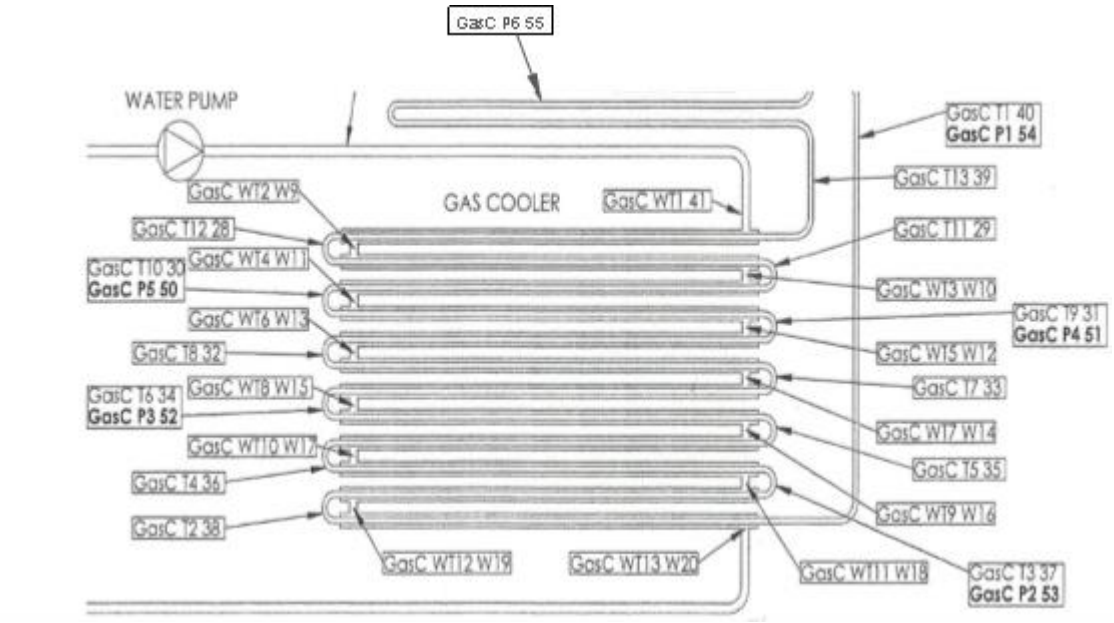

Figure 3-3: The schematic of the condenser of the CO_2 test bench

Data are gathered from the test bench via pressure and temperature sensors. In Figure 3-3 the sensor numbers in bold depict pressure sensors and sensor numbers that contain the letter W depict water temperature sensors. From Figure 3-3 one can see that there are sensors available at the inlet and outlet of the gas cooler for both fluids. The inlet and outlet data are critical for validation. Mass flow rate is measured by mass flow sensors installed on the hot and cold fluid pipes. The mass flow sensors are not connected to the PLC but the mass flow rates can be seen on a screen on the mass flow meter.

3.3 Methodology

The purpose of deriving an analytical model is to get a representative mathematical model of a real-world system. The methodology followed to derive the analytical and fault models are shown below in Figure 3-4.

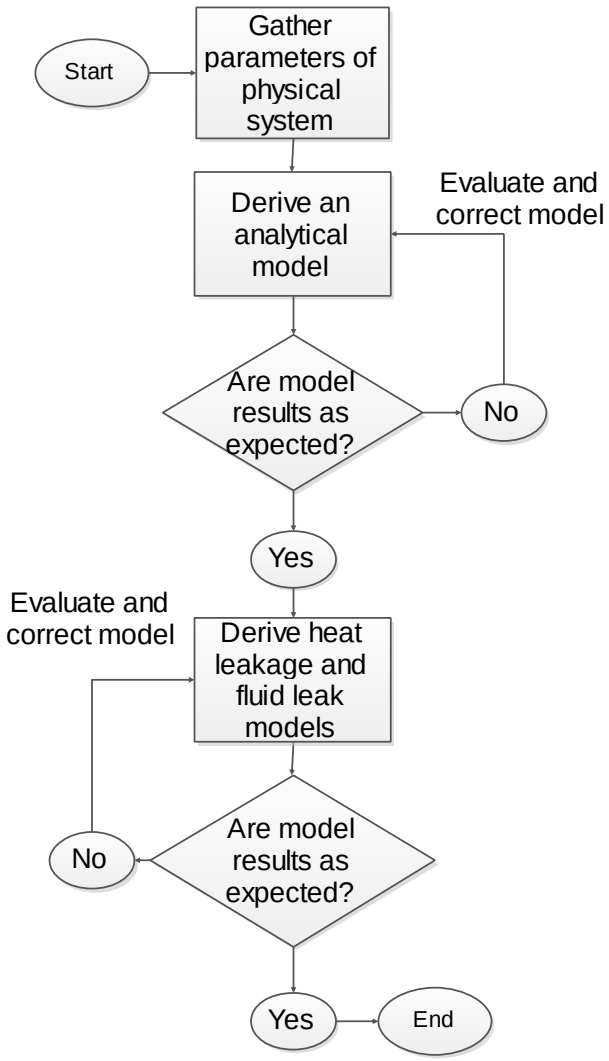

Figure 3-4: The methodology for deriving the analytical model

The first step to creating an analytical model is to gather the parameters of the real-world system. Parameters needed include geometric parameters, such as pipe diameter and heat exchanger length, and pipe and fluid properties, such as density and specific heat. The analytical model will be derived using the laws of conservation of mass, momentum, and energy. The use of these laws of conservation will result in a set of differential equations that describes the heat exchanger. In order to solve the set of differential equations the heat exchanger parameters will be substituted into the equations. The equations will be implemented in MATLAB® and Simulink®.

Once the equations have been derived, a simulation at a specific operating point will be conducted. The results of this simulation will be evaluated and it will be determined whether the results are reasonable. For instance, if the hot side inlet temperature is 320 K an unrealistic

solution would be a cold side outlet temperature of 400 K. Once the model results are satisfactory, the derivation of two fault models will be done. The faults that will be induced in the heat exchanger are heat leakage and fluid leakage.

The heat leakage model simulates an area on the heat exchanger where no insulation is present, resulting in energy leaking out of the heat exchanger system via convection heat transfer with the atmosphere. The fluid leakage model simulates a rupture of the heat exchanger pipe where fluid flows out. Both the fault models will be simulated and the simulation results will be evaluated to determine if the results are reasonable. The purpose of these fault models is to induce changes in the heat exchanger operation that will be used when evaluating the sensitivity of the energy representation.

3.4 Model assumptions

When modelling a real-world system, it is important to know under which assumptions and constraints the system model is derived. In the context of this work, assumptions are regarded as decisions made to reduce the complexity of the mathematical model and constraints are limits or constant values placed on certain parameters to simplify the solution process. Three categories exist for the constraints, namely: (i) fluid, (ii) the separation wall, and (iii) heat transfer.

The first set of constraints apply to the cold fluid. The thermodynamic properties of the cold fluid do not vary significantly enough under the operating conditions of this study to justify variable thermodynamic properties. The density and specific heat of the cold fluid, therefore, remain the same irrespective of where the fluid is in the pipe.

The constraints for the hot fluid must be better defined because the properties of CO_2 change substantially with pressure and temperature. The hot fluid constraints specify that the density of CO_2 is different for every main and secondary grid point and constant for the duration of the simulation. This rule also applies to the specific heat of the nodes and the enthalpy of the elements. The advantages these constraints provide are twofold. Firstly, to increase the accuracy of the model the definition of the properties of CO_2 must occur on more points. Secondly, these constraints reduce the difficulty of the solution process. It is difficult to accurately calculate the thermodynamic properties of the hot fluid during a simulation. As a solution to this problem, the thermodynamic properties of the hot fluid are taken directly from Flownex®. Flownex® uses experimental data to accurately calculate the thermodynamic properties of the fluid at the given pressure and temperature.

The second pair of constraints is related to the separation wall. As with water, the thermodynamic properties of stainless steel do not vary significantly under the operating conditions of this study, for this reason, the density and specific heat of the separation wall are constant.

The last pair of constraints is relevant to the heat transfer coefficients of both fluids. Each main grid point of the fluids has a constant heat transfer coefficient that is calculated by Flownex®. Again this is done to simplify the model due to the difficulty involved in calculating the heat transfer coefficients during a simulation.

Certain assumptions can be made to decrease the mathematical complexity of the model. Listed below are the assumptions made for this study:

- Perfect insulation of the cold pipe against the environment;
- All flow is turbulent;
- The Darcy-Welsbach friction factor is constant;
- The pipes are always regarded as filled with fluid;
- Heat transfer is considered as perfectly uniform across the heat transfer area.

3.5 Analytical model

The derivation process begins with Figure 3-5 showing a simplified two-dimensional layout of a double-pipe heat exchanger.

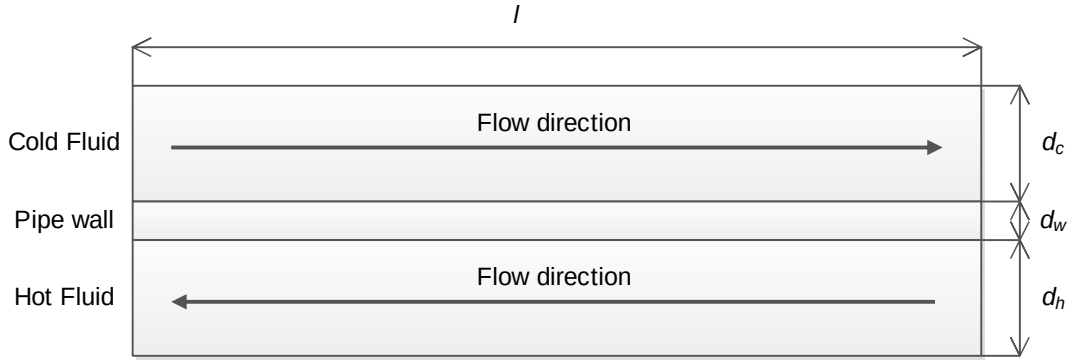

Figure 3-5: A two-dimensional layout of the double pipe heat exchanger

The diameter of the hot fluid pipe is denoted by d_h, d_c indicates the diameter [m] of the cold fluid pipe, and l denotes the length [m] of the heat exchanger. The separation wall signifies the thickness of the pipe and has a diameter of d_w.

The staggered grid approach can be applied to Figure 3-5 by defining two main grid points each for the hot fluid, the separation wall, and the cold fluid respectively. A control volume can then be defined around the main grid points and secondary grid points can be inserted on the faces of the

control volumes resulting in three secondary grid points each for the hot fluid and the cold fluid. This process will result in a lumped-parameter model and is shown in Figure 3-6.

In Figure 3-6 main grid points are represented by rectangles (denoted with the letter M) and will be referred to as nodes. Secondary grid points are represented by circles (denoted with the letter S) and will be referred to as elements. The laws of conservation of mass and energy will be solved at nodes for pressure and temperature respectively. The law of conservation of momentum will be solved at elements for mass flow rate. The nodes of the separation wall (M_{W1} and M_{W2}) will only be used to solve for temperature using the law of conservation of energy.

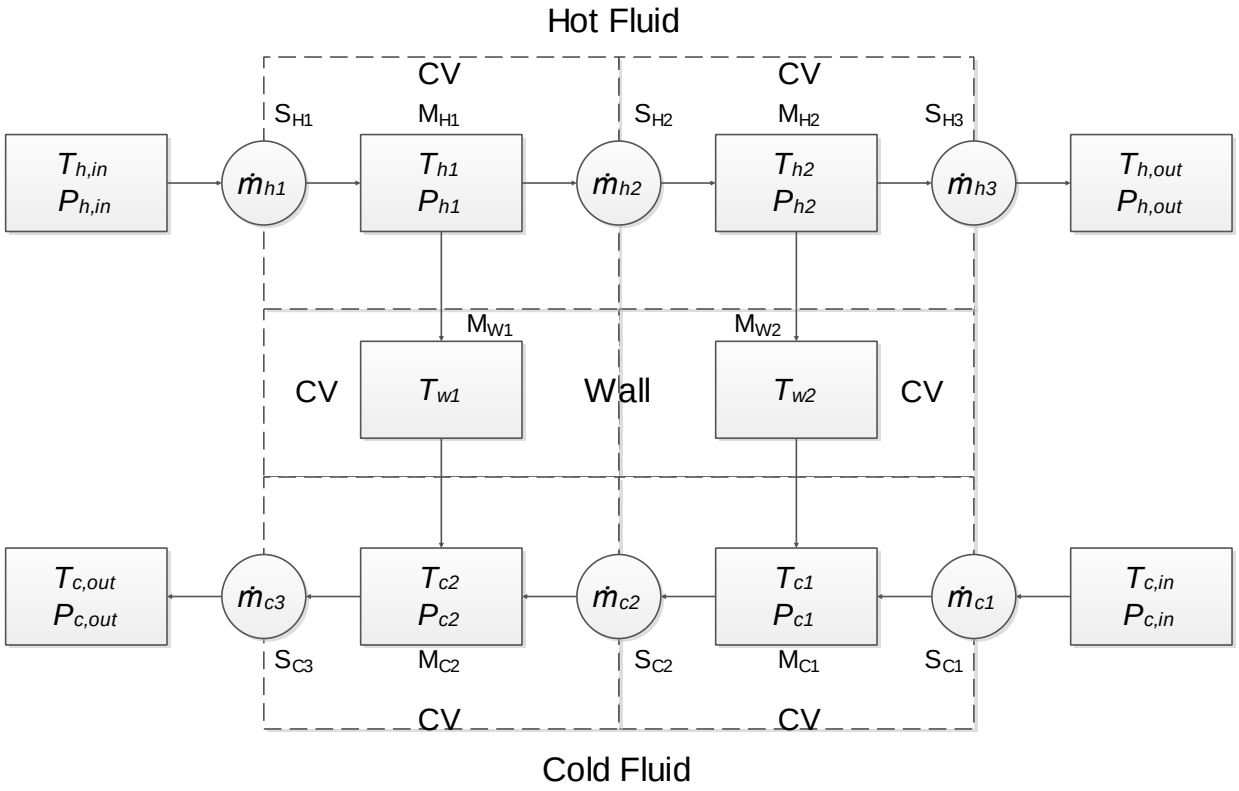

Figure 3-6: The staggered grid approach for the heat exchanger

The model inputs are the inlet temperatures, $T_{h,in}$ and $T_{c,in}$, inlet pressures $P_{h,in}$ and $P_{c,in,}$ and outlet pressures $P_{h,out}$ and $P_{c,out}$. In the fluid-dynamic domain the six elements signify points where the six mass flow rates $\dot{m}_{h1}$, $\dot{m}_{h2}$, $\dot{m}_{h3}$, $\dot{m}_{c1}$, $\dot{m}_{c2}$ and $\dot{m}_{c3}$ will be calculated. The four fluid nodes signify points where the four pressures P_{h1}, P_{h2}, P_{c1} and P_{c2} will be calculated. In the thermodynamic domain, the six nodes signify points where the six temperatures T_{h1}, T_{h2}, T_{w1}, T_{w2}, T_{c1} and T_{c2} will be calculated. Thermal energy is transferred to the separation wall from the hot fluid via convection and from the separation wall to the cold fluid again via convection.

3.5.1 Governing equations

When one models a multi-domain system like a heat exchanger, it is best to start with the three conservation laws governing the behaviour of the heat exchanger. The equation used for calculating the pressure at the main grid points is the conservation of mass equation shown below

$$\frac{\partial}{\partial t}\int_{CV}\rho dV + \int_{CS}\rho \mathbf{v}\bullet\hat{\mathbf{n}}dA = 0\,. \tag{3.1}$$

The first term on the left gives the change of mass of the contents of the control volume with ρ the density [kg/m^3] and V the volume [m^3]. The second term indicates the net rate of change in mass of the control volume. The product, $\rho\mathbf{v}\bullet\hat{\mathbf{n}}$ is the one-dimensional mass flow rate through the control surface. By replacing the integrals with summations the conservation of mass equation becomes

$$\frac{dM_i}{dt} = \sum(Av\rho)_{j-1} - \sum(Av\rho)_j = \dot{m}_{j-1} - \dot{m}_j\,, \tag{3.2}$$

where M_i is the mass [kg] in the i^{th} control volume and $\dot{m}_{j-1}$ and $\dot{m}_j$ are the mass flow rates [kg/s] of the j^{th} and j^{th}*-1* elements. It would be beneficial to describe the law of conservation of mass in terms of pressure. This can be achieved by introducing a change of variable into (3.2) to pressure given by

$$\frac{dM_i}{dP_i}\frac{dP_i}{dt} = \dot{m}_{j-1} - \dot{m}_j\,, \tag{3.3}$$

with P_i the pressure [Pa] in the i^{th} control volume. The term *dM/dP* describes the compressibility of the fluid and can be written in terms of the bulk modulus, B [Pa] as given by

$$\frac{dM_i}{dP_i} = V\left(\frac{d\rho}{dP}\right) = V\rho\,/\,B\,. \tag{3.4}$$

The law of conservation of mass for the i^{th} control volume can, thus, be written as

$$\frac{dP_i}{dt} = \frac{1}{C_h}\left(\dot{m}_{j-1} - \dot{m}_j\right), \tag{3.5}$$

with C_h termed the hydraulic capacitance of the fluid. The hydraulic capacitance is given by

$$C_h = \frac{V\rho}{B}. \tag{3.6}$$

The next governing equation to be considered is the conservation of momentum equation which is given by

$$\frac{\partial}{\partial t}\int_{CV} v\rho dV = -\int_{CS} v\rho v \bullet \hat{n} dA + \int_{CS} \bar{\tau} dA + \int_{CV} \bar{\beta}\rho dV. \tag{3.7}$$

The term on the left hand of the equation is the time rate of change of linear momentum of the control volume. The first term on the right is the rate of linear momentum flow through the control surface. The second term gives the total surface force distribution acting on the control surface. Surface forces arise from direct contact between the fluid and a surface, the most common surface force is losses due to friction caused by the flow of a fluid over a non-smooth surface. The third term represents the total body force distribution acting on the fluid. Body forces are forces that act on the fluid without the need for direct contact such a gravity. After integrating and rewriting the law of conservation of momentum for a secondary grid point, *j*, becomes

$$\frac{d\dot{m}_j}{dt} = \frac{1}{L}(P_i - P_{i+1}) - \frac{R_h}{L}\left|\dot{m}_j\right|\dot{m}_j - \frac{R_{turb}}{L}\left|\dot{m}_j\right|\dot{m}_j, \tag{3.8}$$

with P_i the pressure [Pa] of the node preceding the element *j* and P_{i+1} the pressure [Pa] of the node after the element *j*. The hydraulic inductance is denoted by *L* and given by

$$L = \frac{l}{A}, \tag{3.9}$$

with *l* the pipe length [m] and *A* the cross-sectional area [m^2]. The hydraulic inductance models fluid momentum. The hydraulic resistor, R_h, models turbulent loss and is given by

$$R_h = \left(\frac{fl}{d} + K_s\right)\frac{1}{2\rho A^2} \tag{3.10}$$

with *f* the friction factor, *d* the pipe diameter [m] and *K* the secondary losses. Juslin [61] found in his work that when modelling turbulent flow it is necessary to add an additional loss term. This additional loss term is denoted by R_{turb} in equation (3.8) and given by

$$R_{turb} = -\frac{R_h}{2}, \tag{3.11}$$

with R_h the hydraulic resistor. The conservation of energy equation is used to model the temperature effects of the heat exchanger and is given by

$$\frac{\partial}{\partial t}\int_{CV} e\rho dV = -\int_{CS} e\rho v \bullet \hat{n} dA + \dot{Q} + \dot{W} . \tag{3.12}$$

The energy stored per unit mass is given by e while $\dot{Q}$ represents all the ways in which energy is exchanged between the contents of the control volumes and the surroundings due to a temperature difference. The work done on the control volume is denoted by $\dot{W}$ and is negligible for this study. Replacing the integrals with summations gives

$$V_i \rho_i c_{v,i} \frac{dT_i}{dt} = (\dot{m}_{j-1} h_{j-1} - \dot{m}_j h_j) - \dot{Q}_{conv} , \tag{3.13}$$

with V_i the volume [m^3], ρ_i the density [kg/m^3] and $c_{v,i}$ the specific heat at constant volume [J/kg.K] for the i^{th} control volume. The mass flow rate [kg/s] in and out of the control volume is given by m_{j-1} and m_j respectively and h_{j-1} and h_j is the enthalpy [J/kg] of the fluid at elements j and $j-1$. The convection heat transfer rate $\dot{Q}_{conv}$ [W] is given by

$$\dot{Q}_{conv} = hA(T_i - T) , \tag{3.14}$$

with h the convection heat transfer coefficient [W/m^2.K], A the heat transfer area [m^2] and T_i and T the temperatures [K] of the objects exchanging heat. In the case of the hot fluid the law of conservation of energy can be written as

$$\frac{dT_i}{dt} = \frac{1}{C_t}(\dot{m}_{j-1} h_{j-1} - \dot{m}_j h_j) - \frac{1}{C_t R_t}(T_i - T) , \tag{3.15}$$

with C_t termed the thermal capacitance and given by

$$C_t = V \rho c_v . \tag{3.16}$$

The convection resistance is denoted by R_t and given by

$$R_t = \frac{1}{hA} . \tag{3.17}$$

In the case of the cold fluid, the enthalpy can be set equal to the specific heat times the temperatures. This is only valid if the specific heat can be taken as constant. Thus, for the cold fluid the conservation of energy equation can be written as

$$\frac{dT_i}{dt} = \frac{c_v}{C_t}(\dot{m}_{j-1}T_i - \dot{m}_j T) - \frac{1}{C_t R_t}(T_i - T)\,. \tag{3.18}$$

The same method outlined above can be used to derive equations for the separation wall. The only difference is that the energy inflow into the separation wall is the heat transferred from the hot side and the energy outflow from the separation wall is the energy transferred to the cold side.

3.5.2 System of differential equations

The process described thus far can now be repeated for each main and secondary grid points in order to derive equations for the pressure, temperature and mass flow rates for the heat exchanger system. The system of differential equations is given below in (3.19) to (3.34). The values for the variables are given in Table A-2 in Appendix A.

$$\frac{dP_{h1}}{dt} = \frac{1}{C_{h,h}}(\dot{m}_{h1} - \dot{m}_{h2}) \tag{3.19}$$

$$\frac{dP_{h2}}{dt} = \frac{1}{C_{h,h}}(\dot{m}_{h2} - \dot{m}_{h3}) \tag{3.20}$$

$$\frac{dP_{c1}}{dt} = \frac{1}{C_{h,c}}(\dot{m}_{c1} - \dot{m}_{c2}) \tag{3.21}$$

$$\frac{dP_{c2}}{dt} = \frac{1}{C_{h,c}}(\dot{m}_{c2} - \dot{m}_{c3}) \tag{3.22}$$

$$\frac{d\dot{m}_{h1}}{dt} = \frac{1}{L_h}(P_{h,in} - P_{h1}) - \frac{R_{h,h}}{L_h}|\dot{m}_{h1}|\dot{m}_{h1} - \frac{R_{turb,h}}{L_h}|\dot{m}_{h1}|\dot{m}_{h1} \tag{3.23}$$

$$\frac{d\dot{m}_{h2}}{dt} = \frac{1}{L_h}(P_{h1} - P_{h2}) - \frac{R_{h,h}}{L_h}|\dot{m}_{h2}|\dot{m}_{h2} - \frac{R_{turb,h}}{L_h}|\dot{m}_{h2}|\dot{m}_{h2} \tag{3.24}$$

$$\frac{d\dot{m}_{h3}}{dt} = \frac{1}{L_h}(P_{h2} - P_{h,\text{out}}) - \frac{R_{h,h}}{L_h}|\dot{m}_{h3}|\dot{m}_{h3} - \frac{R_{turb,h}}{L_h}|\dot{m}_{h3}|\dot{m}_{h3} \tag{3.25}$$

$$\frac{d\dot{m}_{c1}}{dt} = \frac{1}{L_c}(P_{c,in} - P_{c1}) - \frac{R_{h,c}}{L_c}|\dot{m}_{c1}|\dot{m}_{c1} - \frac{R_{turb,c}}{L_c}|\dot{m}_{c1}|\dot{m}_{c1} \tag{3.26}$$

$$\frac{d\dot{m}_{c2}}{dt} = \frac{1}{L_c}(P_{c1} - P_{c2}) - \frac{R_{h,c}}{L_c}|\dot{m}_{c2}|\dot{m}_{c2} - \frac{R_{turb,c}}{L_c}|\dot{m}_{c2}|\dot{m}_{c2} \tag{3.27}$$

$$\frac{d\dot{m}_{c3}}{dt} = \frac{1}{L_c}(P_{c2} - P_{c,out}) - \frac{R_{h,c}}{L_c}|\dot{m}_{c3}|\dot{m}_{c3} - \frac{R_{turb,c}}{L_c}|\dot{m}_{c3}|\dot{m}_{c3} \tag{3.28}$$

$$\frac{dT_{h1}}{dt} = \frac{1}{C_{t,h}}(\dot{m}_{h1}h_{h1} - \dot{m}_{h2}h_{h2}) - \frac{1}{C_{t,h}R_{t,h}}(T_{h1} - T_{w1}) \tag{3.29}$$

$$\frac{dT_{h2}}{dt} = \frac{1}{C_{t,h}}(\dot{m}_{h2}h_{h2} - \dot{m}_{h3}h_{h3}) - \frac{1}{C_{t,h}R_{t,h}}(T_{h2} - T_{w2}) \tag{3.30}$$

$$\frac{dT_{c1}}{dt} = \frac{c_{v,c}}{C_{t,c}}(\dot{m}_{c1}T_{c,in} - \dot{m}_{c2}\,\mathrm{T}_{c1}) + \frac{1}{C_{t,c}R_{t,c}}(T_{w2} - T_{c1}) \tag{3.31}$$

$$\frac{dT_{c2}}{dt} = \frac{c_{v,c}}{C_{t,c}}(\dot{m}_{c2}T_{c1} - \dot{m}_{c3}\,\mathrm{T}_{c2}) + \frac{1}{C_{t,c}R_{t,c}}(T_{w1} - T_{c2}) \tag{3.32}$$

$$\frac{dT_{w1}}{dt} = \frac{1}{C_{t,\mathrm{h}}R_{t,\mathrm{h}}}(T_{h1} - T_{w1}) - \frac{1}{C_{t,\mathrm{c}}R_{t,\mathrm{c}}}(T_{w1} - T_{c2}) \tag{3.33}$$

$$\frac{dT_{w2}}{dt} = \frac{1}{C_{t,\mathrm{h}}R_{t,\mathrm{h}}}(T_{h2} - T_{w2}) - \frac{1}{C_{t,\mathrm{c}}R_{t,\mathrm{c}}}(T_{w2} - T_{c1}) \tag{3.34}$$

3.6 Model results

This section will provide the results of the analytical model for a simulation where a change is induced in the hot and cold side inlet pressure and the transient is observed. The model implementation is shown, thereafter the results of the two simulations are shown.

3.6.1 Model implementation

The hydrodynamic domain was implemented in MATLAB® using a self-coded backward Euler solver. This solver, however, produced unsatisfactory results. Due to the non-linear nature of the hydrodynamic domain and the highly dynamic response to the induction of a change in the heat exchanger operation, a better solver was needed to solve the equations. It was decided to implement the hydrodynamic equations as Simulink® block diagrams. The solver used is ode23tb as it allows for the solving of stiff differential equations and employs a variable time step approach for better results. Each of the equations was implemented as separate subsystems, and the subsystems were connected to form the state space model. The subsystem for the hot side pressure and hot side mass flow rate is shown below in Figure 3-7 and Figure 3-8.

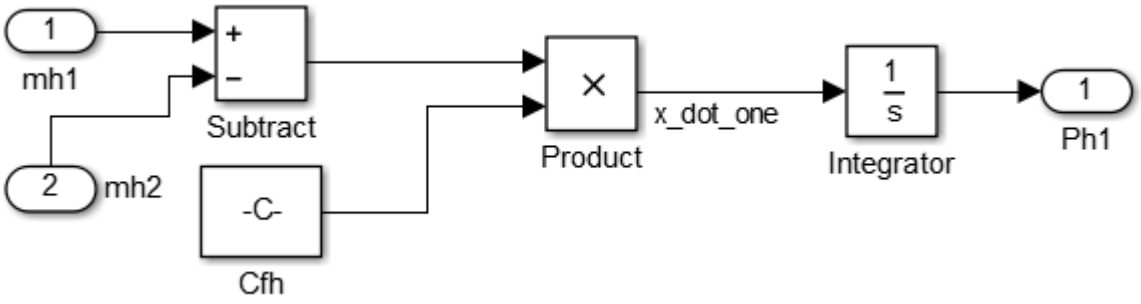

Figure 3-7: The implementation of the conservation of mass equation in Simulink®

The thermodynamic equations were implemented in MATLAB® using a self-coded backwards Euler numerical solving technique. This approach is sufficient for the thermodynamic domain due to the vastly longer settling time and almost no dynamic response to changes in the heat exchanger operation of the thermodynamic domain when compared to the hydrodynamic domain.

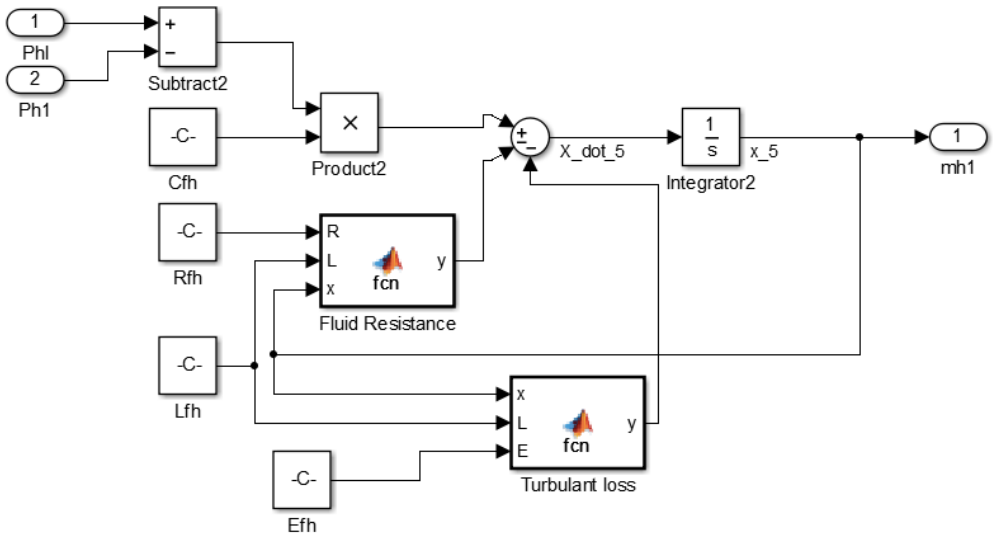

Figure 3-8: The implementation of the conservation of momentum equation in Simulink®

3.6.2 Simulation results

This section will show and discuss the model results for the induction of a transient in the hot and cold fluid. The inlet pressure, $P_{h,in}$, of the hot fluid will be increased by 100 kPa at t=0s and the resulting transient will be plotted. The inlet pressure $P_{c,in}$, for the cold side will be increased by 1 kPa and the resulting transient will be plotted. The reason for the increase in both the hot and cold fluids is that the respective hydrodynamic domains of the fluids are isolated from each other. This means that a change in the hot side pressure will not reflect in the pressure or mass flow rate of the cold side.

The geometric properties of the heat exchanger, such as pipe diameter and length, are given in Table A-1 and the thermodynamic properties of the fluids under the conditions of this simulation are given in Table A-3 and Table A-4 for carbon dioxide and water respectively. The thermodynamic properties of the separation wall is given in Table A-5. The simulation conditions; including the values for the inlet pressure, outlet pressure, and inlet temperature; are given in Table A-6 and the initial conditions; for the pressure, mass flow rates, and temperatures that will be calculated; are given in Table A-7. All these listed tables are in Appendix A. The analytical model results for hot side pressure, mass flow rate and temperature as well as separation wall temperature and cold fluid temperature is shown in Figure 3-9.

Some overshoot and oscillations in the transient of Figure 3-9 (a) and can Figure 3-9 (b) be observed, that can be attributed to the sudden increase in pressure as well as numerical instabilities induced by the solution method. This increase in pressure results in a change in the fluid's flow pattern due to effects such a friction loss and fluid momentum. As the fluid adjusts to the increase in pressure the amplitude of the oscillations decreases until a steady value is reached. The increase in hot side pressure results in an increase in the hot side mass flow rate and, therefore, an increase in the enthalpy entering each hot side control volume. There is more energy available to be transferred to the cold side, therefore, an overall temperature increase as seen in Figure 3-9 (c), Figure 3-9 (d) and Figure 3-9 (e). There is, however, a scenario where an increase in the mass flow rate will not be beneficial. If the mass flow rate is too high, the fluid will not spend enough time in contact with the heat transfer area, for heat transfer to occur properly, and will result in lower temperatures.

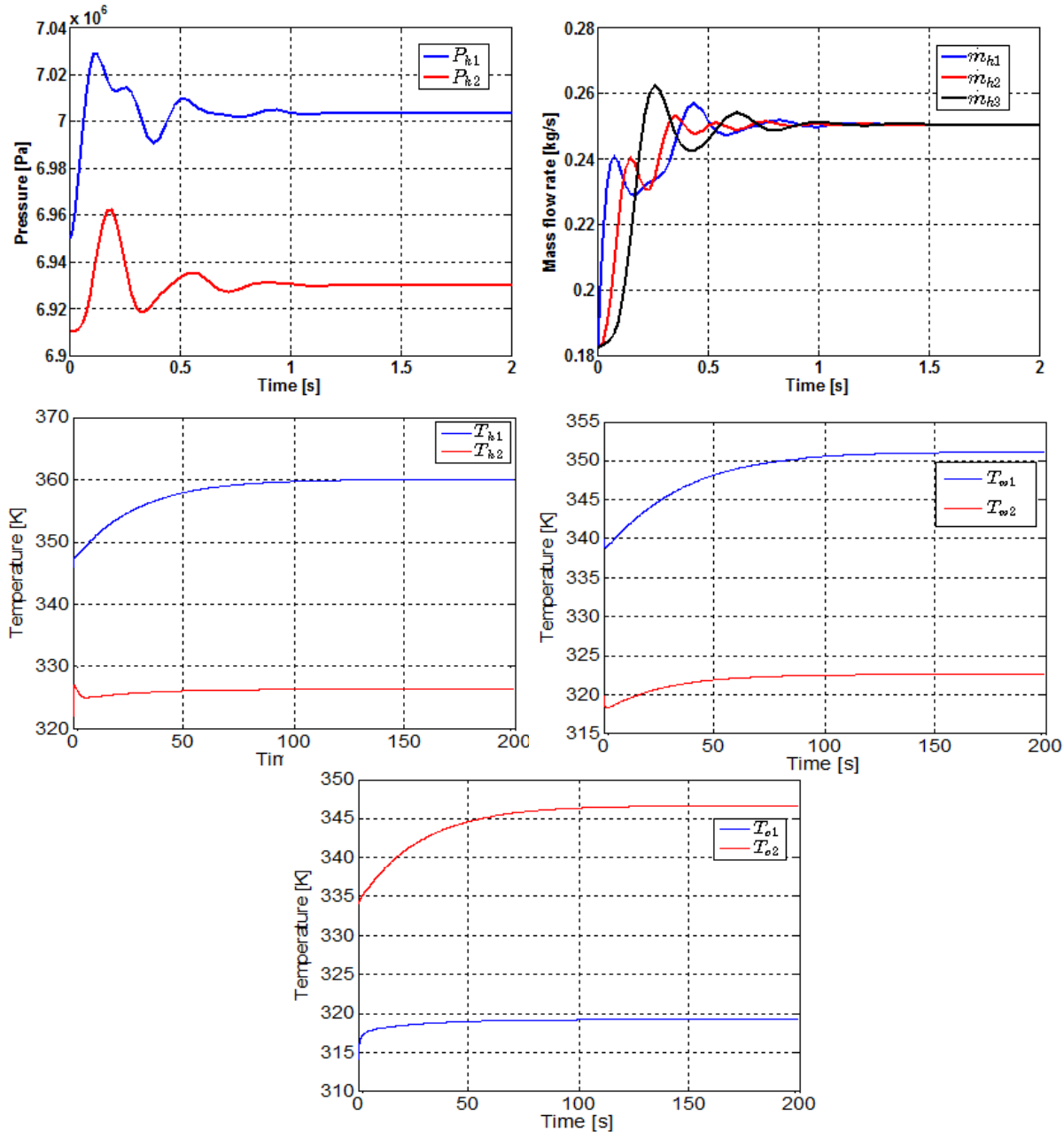

Figure 3-9: Analytical model results: (a) Hot side pressure, (b) Hot side mass flow rate, (c) Hot side temperature (d) Separation wall temperature and (e) Cold Fluid temperature

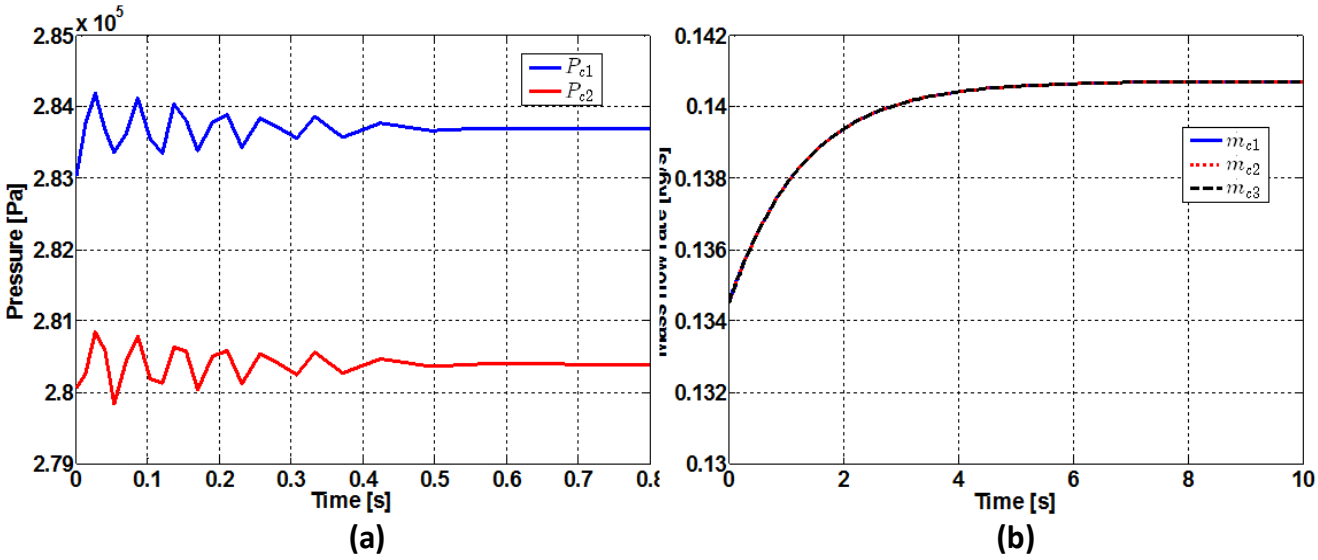

Figure 3-10: Analytical model results: (a) Cold fluid pressure and (b) Cold fluid mass flow rate

From Figure 3-10 (a) a much spikier transient is noticed when compared to Figure 3-9 (a). This is due to the properties of water, like density, being much higher than that of CO_2 and the higher value of the hydraulic inductor of the cold side when compared to the hot side. From Figure 3-10 (b) a much longer settling time of the cold fluid mass flow rate can be seen; this is due to two reasons. Firstly, the larger size of the hydraulic capacitor of the cold fluid when compared to the hot fluid. Secondly, the smaller mass flow rate of the cold fluid when compared to the hot fluid. The hydraulic capacitor takes a longer time to charge up resulting in the longer settling time.

3.7 Fault models

One of the evaluation criteria for the energy representation is that it must be sensitive to small changes in the heat exchanger operation. The sensitivity of the energy representation will be evaluated using three different faults. The three faults are: (i) a fluid leakage, (ii) a heat leakage and (iii) fouling. Only the fluid leak and the heat leak faults require mathematical alteration to the analytical model. The fluid leakage model and the heat leakage model are discussed in this section in terms of the modelling equations and simulation results.

3.7.1 Fluid leak

A rupture or tear of the heat exchanger pipe will result in a leak. This can be visualised as an outflow of energy and fluid; and can be modelled as a very short pipe. The length of the leaking pipe is equal to the thickness of the cold fluid pipe and has a cross-sectional area equal to the size of the hole in the cold fluid pipe. The pressure boundaries of the leaking pipe are the pressure,

P_{c1}, at the cold fluid node M_{C1} and ambient pressure, P_{amb}. The staggered grid approach can be applied to the cold fluid with the leak included and is shown in Figure 3-11.

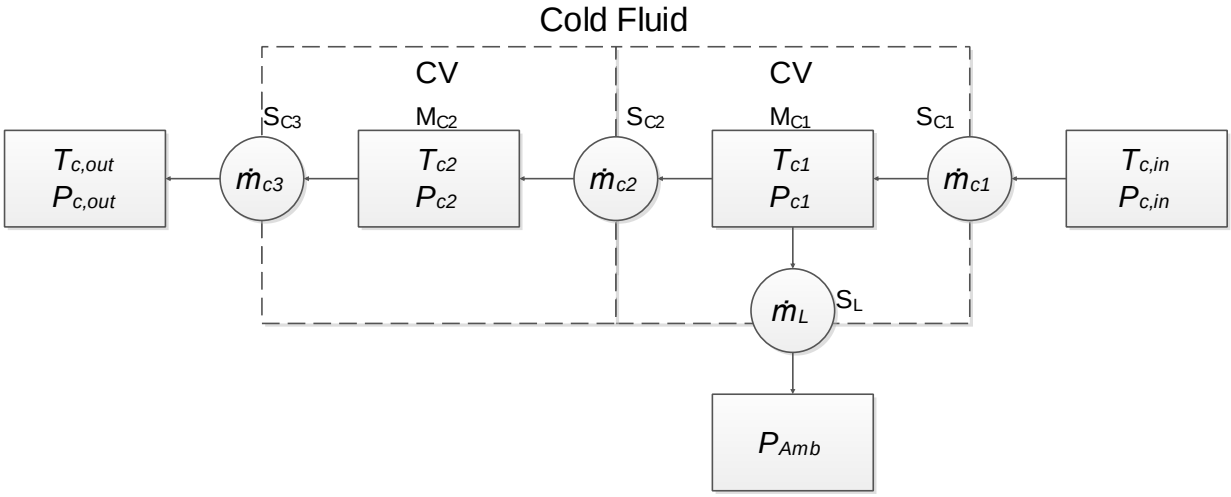

Figure 3-11: The staggered grid approach for the leakage model

Nodes are denoted by the letter M and is where the law of conservation of mass will be solved for pressure. Elements are denoted with the letter S and is where the law of conservation of momentum will be solved for mass flow rate. The element, S_L symbolises the leak mass flow rate. From Figure 3-11 one can observe that the equation for the pressure, P_{c1} needs to be changed to account for the mass flow rate of the leaking fluid. Starting with the equation of conservation of mass, and following the same procedure used during analytical model derivation, the equation for P_{c1} is given by

$$\frac{dP_{c1}}{dt} = \frac{1}{C_{h,c}}(\dot{m}_{c1} - \dot{m}_{c2} - \dot{m}_L), \tag{3.35}$$

with $\dot{m}_L$ the leaking fluid mass flow rate [kg/s]. The conservation of momentum equation must be solved at the element, S_L, of Figure 3-11 for the leakage mass flow rate. Following the same procedure used during derivation of the analytical model the equation for the leakage mass flow rate, $\dot{m}_L$, is given by

$$\frac{d\dot{m}_L}{dt} = \frac{1}{L_L}(P_{c1} - P_{amb}) - \frac{R_L}{L_L}|\dot{m}_L|\dot{m}_L - \frac{R_{turb,L}}{L_L}|\dot{m}_L|\dot{m}_L, \tag{3.36}$$

with L_L the hydraulic inductance, R_L the hydraulic resistance and $R_{turb,L}$ the turbulent loss. The values of these components are given in Table A-2 in Appendix A.

3.7.2 Fluid leak model results

This section will show and discuss the simulation results of the fluid leak. In order to simulate the leak, the heat exchanger is allowed to reach steady state and then the leak is suddenly introduced. The geometry of the pipe used to simulate the leak is given in Table A-8. The initial and simulation conditions of this simulation are given in Table A-6 and Table A-7 respectively. The hot fluid, cold fluid and separation wall properties are given in Table A-3, Table A-4 and Table A-5 respectively. Ambient pressure, P_{amb} is taken as 100 kPa for this simulation. The cold side pressure, P_{c1}, at the node M_{C1} (under normal conditions and during the fluid leak) is given in Figure 3-12 (a). The mass flow rates, $\dot{m}_{c1}$ and $\dot{m}_{c2}$, for the two elements S_{C1} and S_{C2} (under normal conditions and during the fluid leak) are given in Figure 3-12 (b). Figure 3-12 (b) also gives the leakage mass flow rate, $\dot{m}_L$, at the secondary grid point S_L.

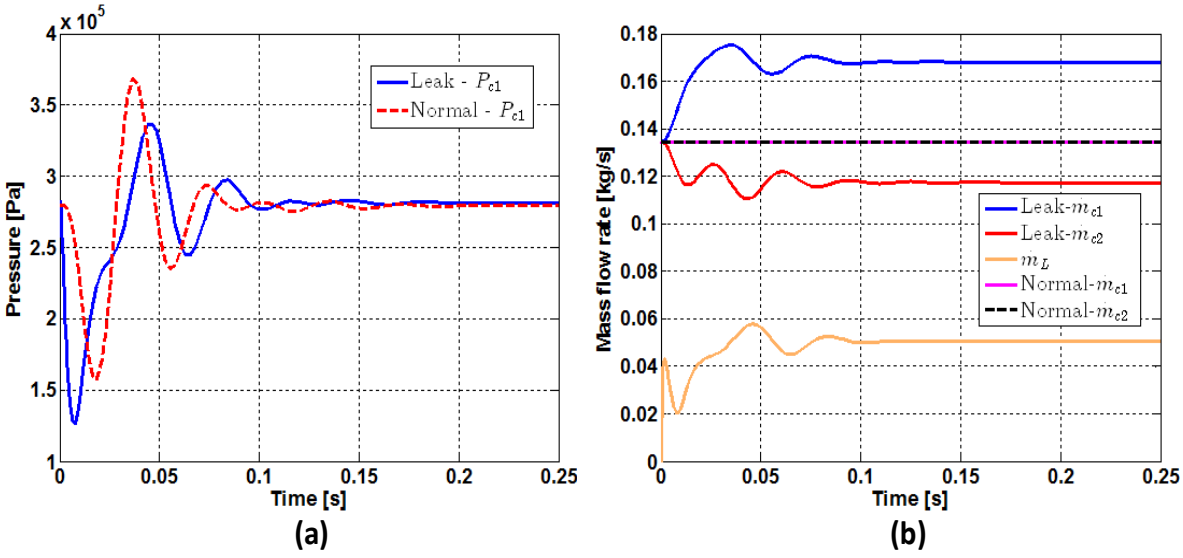

Figure 3-12: Leakage model results: (a) Cold side pressure and (b) Cold side mass flow rate

The mass flow rate though a pipe is limited by the pressure applied and the pipe geometry. The introduction of a leak at node M_{C1} causes an additional mass flow out of M_{C1}. This additional leakage mass flow causes an increase in the inlet mass flow rate, $\dot{m}_{c1}$, to compensate for the increase in mass flow out of M_{C1}. This increase in the inlet mass flow rate causes an increase in the pressure at M_{C1} and can be seen in Figure 3-12 (a). The law of conservation of mass must always be valid, due to this the mass flow rate, $\dot{m}_{c2}$ out of M_{C1} reduces to compensate for the leakage mass flow rate.

3.7.3 Heat leakage

Under normal heat exchanger operation, all the pipes are insulated to reduce heat leakage via radiation and convection to the atmosphere. A heat leak occurs when the insulation is no longer present. The heat leak will be modelled as convection heat transfer from the heat exchanger to the atmosphere. The reason for this simplified model is that the purpose of the heat leakage model is to assist in the evaluation of the sensitivity of the energy representation. Since only a change in heat exchanger operation is needed for this purpose, the simplified heat leakage model is sufficient. The equation of the cold fluid temperature, T_{c1} at node M_{C1} can be altered to include the heat leakage as given by

$$\frac{dT_{c1}}{dt} = \frac{c_{v,c}}{C_{t,c}}(\dot{m}_{c1}T_{c,in} - \dot{m}_{c2}T_{c1}) + \frac{1}{C_{t,c}R_{t,c}}(T_{w2} - T_{c1}) - \frac{1}{C_{t,c}R_{t,c}}(T_{c1} - T_{amb}), \tag{3.37}$$

with T_{amb} the ambient temperature. The last term on the left of the equal sign is the energy leaving node M_{C1} via convection with the atmosphere. The values of the components of (3.37) are given in Table A-2 in Appendix A.

3.7.4 Heat leakage model results

This section will show and discuss the simulation results of the heat leakage model derived in the section above. To simulate the heat leakage, the simulation is allowed to reach steady state and the heat leak is suddenly introduced. The initial and simulation conditions of this simulation are given in Table A-6 and Table A-7 respectively. The hot fluid, cold fluid and separation wall properties are given in Table A-9, Table A-4 and Table A-5 respectively. Ambient temperature, T_{amb} is taken as 280 K for this simulation. The results for the cold side temperature under normal and fault conditions are given in Figure 3-13.

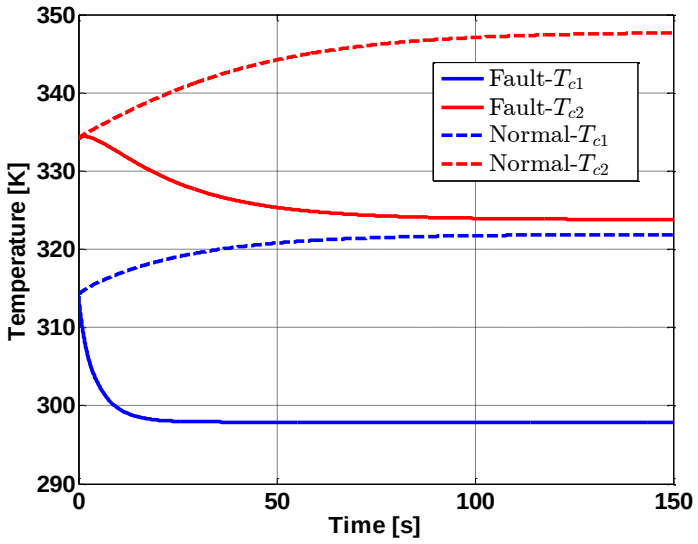

Figure 3-13: Heat leakage model results: Cold side temperature

From Figure 3-13 one can see the difference in temperature between a heat leak and normal operating conditions. The reason for the roughly 20 K difference is that the grid point representing ambient temperature remains constant at 280 K. This implies that the amount of energy leaving grid point M_{C1} is much more than the amount entering the grid point since $(T_{w2}\text{-}T_{c1})<(T_{c1}\text{-}T_{amb})$. As stated during the model derivation, the reason for the ambient node to be at a constant pressure is to reduce the complexity of the heat leakage model.

3.8 Conclusion

Chapter 3 discussed the derivation of the analytical and fault models. The physical system modelled is the gas cooler of a CO_2 test bench. The staggered grid approach was applied to discretise the gas cooler into six main grid points and twelve secondary grid points. The differential equations were derived using the laws of conservation of mass momentum and energy. The simulation results of the analytical model revealed that the response of the model is satisfactory; but there are, however, a few concerns. The first concern is that the number of assumptions made will result in an inaccurate model when compared to the gas cooler. The second concern is related to the CO_2 test bench. The test bench is a closed cycle, therefore, there is a possibility that modelling just one component of the test bench may result in an inaccurate model as the effects of the other components of the test bench are not taken into consideration. Two fault models were derived, namely: a fluid leakage model and a heat leakage model. The purpose of these models are to induce changes in the operation of the heat exchanger. These changes in the heat exchanger operation will be used when evaluating the sensitivity of the energy representation. From the results, shown in this chapter, it is clear that both these fault models affect the heat

exchanger operation enough for use in evaluating the sensitivity of the energy representation. It is evident that, although both fault models have been greatly simplified, the purpose they are intended for can be fulfilled.

CHAPTER 4 VERIFICATION AND VALIDATION

4.1 Introduction

Verification is the process followed to determine if the analytical model was implemented correctly. Validation of the process followed, to ensure that the analytical model is representative of the real-world system. The methodology for verification and validation is discussed briefly and the verification and validation of the analytical model are given. Verification is done by comparing the analytical model to a Flownex® model. The verification procedure and results are shown and the success of verification is evaluated by means of a performance index. Validation is done with data obtained from two experiments conducted on the gas cooler of a CO_2 test bench. The validation results and the performance index, used to evaluate the success of validation, are also given. This chapter concludes with the validation of the two fault models using Flownex®.

4.2 Methodology

The methodology for verification and validation is shown in Figure 4-1. In order to conduct verification, a suitable comparison must be identified. In the case of this study Flownex® was chosen. The Flownex® model is developed in such a way that it mimics the nodes and elements of the staggered grid approach used to develop the analytical model. The reason for developing the Flownex® model in this way is to be able to verify all the variables of interest. The Flownex® model and analytical model results are compared and evaluated with a performance index.

Validation will be done by comparing experimental results obtained from the gas cooler of a heat exchanger test bench with the results of the analytical model. Two experiments will be conducted and both experimental data sets will be used during validation. The success of validation will be measured with a performance index. Once the analytical model is verified and validated, the two fault models will be validated. The fault models will be validated by comparing the results of the fault models with the results of the Flownex® models. As with the analytical model the success of validation of the fault models will be measured with a performance index.

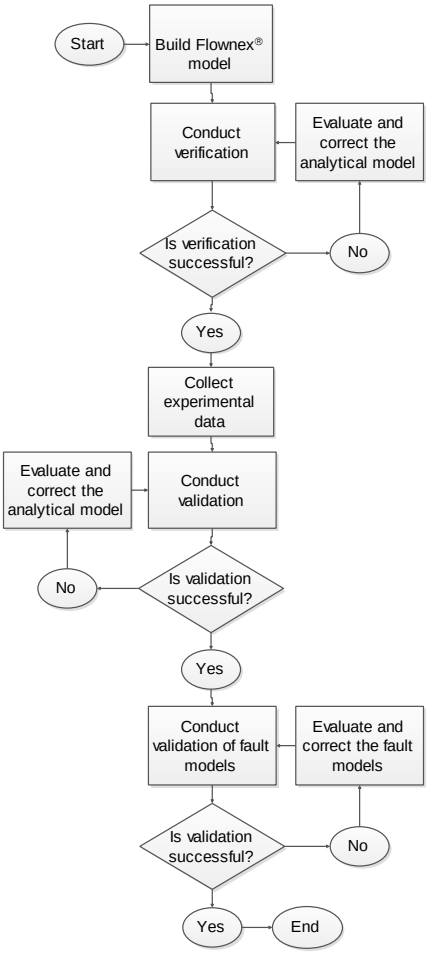

Figure 4-1: The methodology used for verification and validation

4.3 Verification of the analytical model

In order to do a more comprehensive verification and to evaluate all the variables of interest, the results of the analytical model and the Flownex® model will be compared with each other for two different scenarios. Firstly, an increase in hot side pressure after steady state has been reached and, secondly, an increase in cold side pressure after steady state has been reached.

4.3.1 Flownex® model

The Flownex model used for verification is shown in Figure 4-2. The Flownex® model is designed to mimic the staggered grid model of Figure 4-2 in order to compare the results more easily. In Figure 4-2 pipes represent secondary grid points, where mass flow rates will be calculated, while nodes represent main grid points, where temperatures and pressures will be calculated.

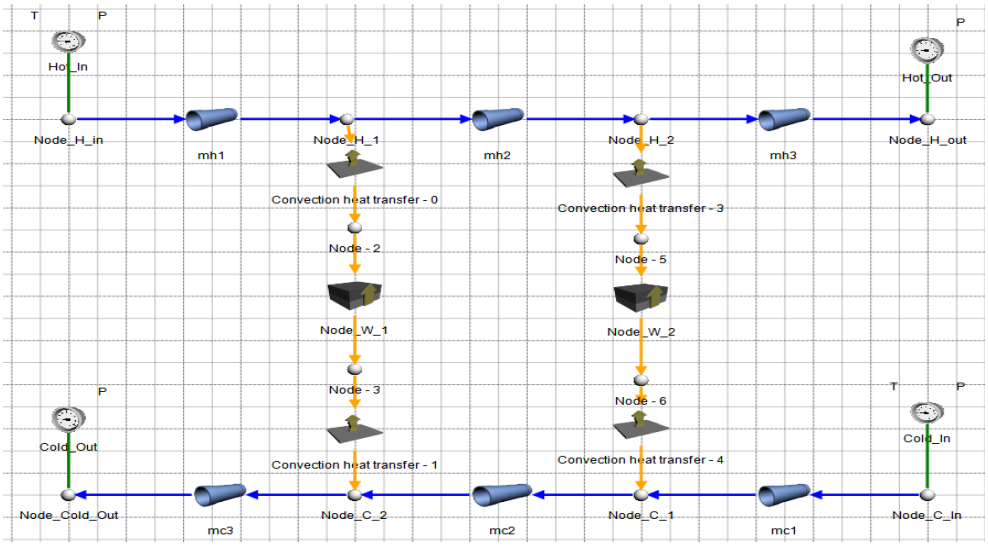

Figure 4-2: The Flownex® model used for verification

4.3.2 Comparison of results

For verification, two different transients will be induced in the heat exchanger system. An increase in hot side inlet pressure of 100 kPa and a cold side inlet pressure increase of 1 kPa will be induced in the heat exchanger system. The reason for this is that the hydrodynamic domains of the hot and cold fluids are isolated. This means that a change in inlet pressure of the hot fluid will not result in a change in cold fluid mass flow rate or pressure. The geometric properties of the heat exchanger, such as pipe diameter and length, are given in Table A-1 and the thermodynamic properties of the fluids under the conditions of this simulation are given in Table A-3 and Table A-4 for carbon dioxide and water respectively. The thermodynamic properties of the separation wall are given in Table A-5. The simulation conditions, including the values for the inlet and outlet pressure and inlet temperature, are given in Table A-6. The initial conditions for the pressure, mass flow rates, and temperatures that will be calculated are given in Table A-7. All these listed tables are in Appendix A. The results of the hot side pressure, mass flow rate and temperature as well as the separation wall temperature and the cold fluid temperature are given in Figure 4-3. The results of the cold fluid pressure and mass flow rate are given by Figure 4-4.

From Figure 4-3 (a) and Figure 4-3 (b) it can be seen that the hot side pressure and mass flow rate compare very well with Flownex®, except for the transients. The difference in transients can be attributed to the solution methods used to solve the model. Flownex® employs an implicit pressure correction solution algorithm discussed in Greyvenstein [62] while MATLAB® employs a numerical method designed to solve any stiff differential equation. It is important for the verification process that the overall trend of the simulation results between Flownex® and the analytical model are similar and that the steady state values are comparable.

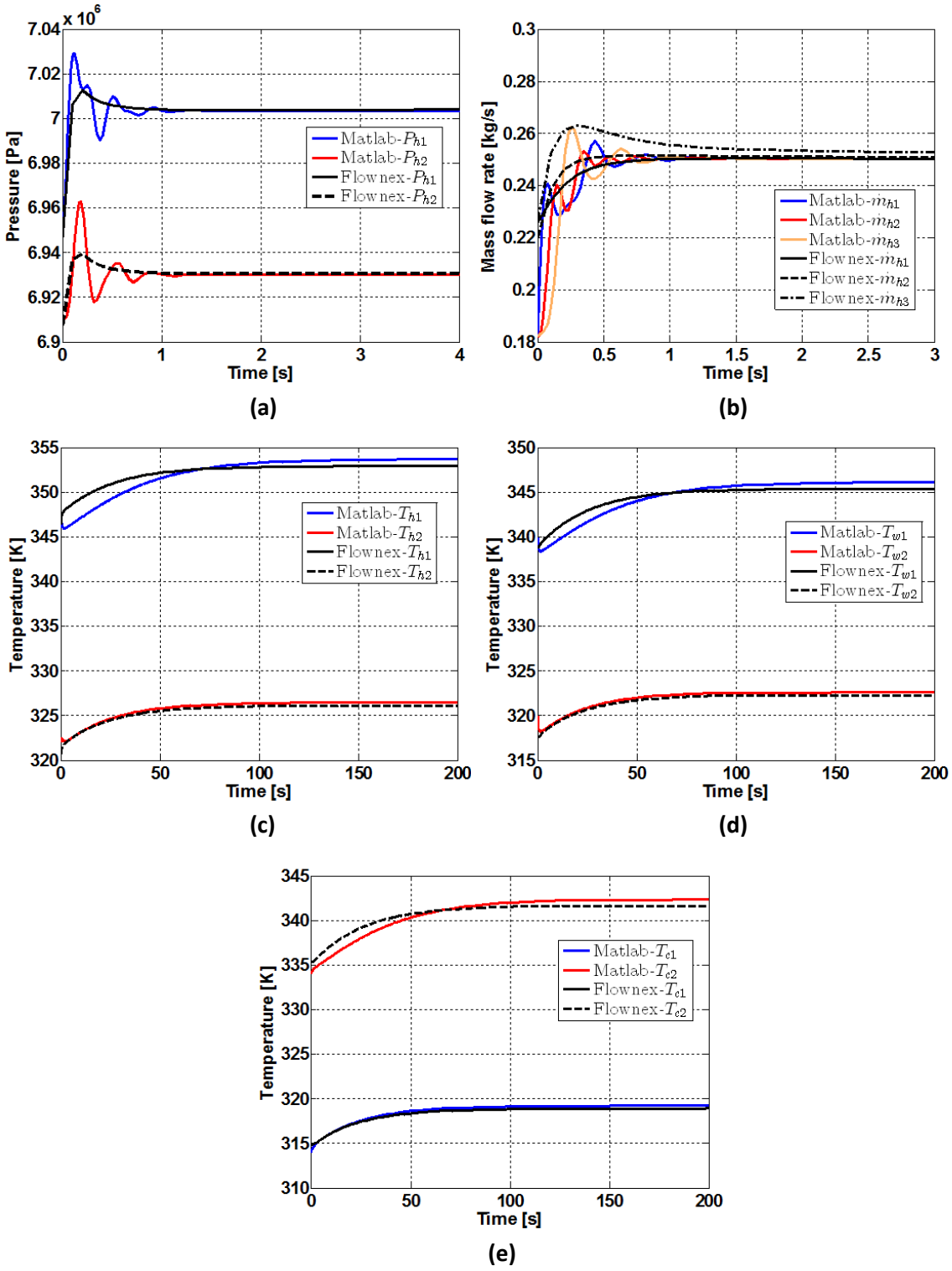

Figure 4-3: Analytical model verification results: (a) Hot side pressure, (b) Hot side mass flow rate, (c) Hot side temperature, (d) Separation wall temperature and (e) Cold side temperature

The hot side, wall, and cold side temperatures are shown in Figure 4-3 (c), Figure 4-3 (d) and Figure 4-3 (e). It can be seen that the overall trend between the MATLAB® and Flownex® results are the same although the steady state values differ slightly. The difference in steady state values

can be attributed to several factors, including fluid characteristics, heat transfer characteristics, and the manner in which heat transfer is modelled.

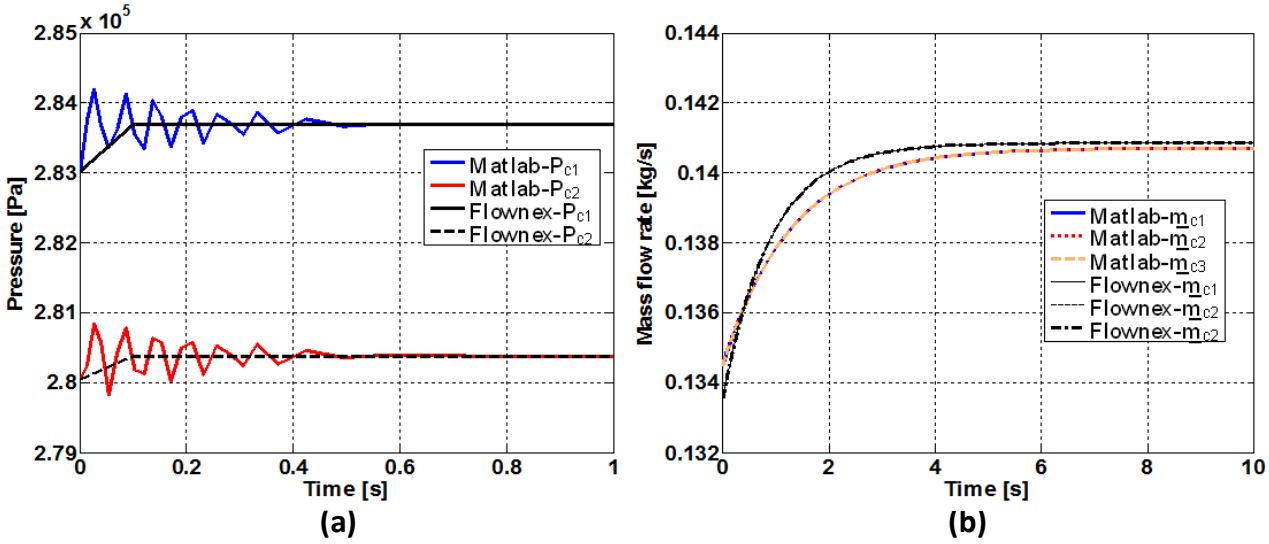

Figure 4-4: Analytical model verification results: (a) Cold Side pressure and (b) Cold side mass flow rate

From Figure 4-4 (a) and Figure 4-4 (b) one can see the transient trend and the steady state values of the results are very similar between Flownex® and MATLAB®. There are small differences between the results in the transient stage of the simulation that can be attributed to small differences in fluid properties such as density and the different solvers. A small difference between steady state values of the mass flow rates is observed and can also be attributed to differences in fluid properties.

4.3.3 Performance index

In order to determine the success of verification, there has to be some form of performance measurement. There are two important performance factors that need to be evaluated: 1) the transient trend and 2) the steady state values. The transient trend will be evaluated by calculating the percentage deviation between the Flownex® and Simulink® transients. To evaluate the steady state, the Simulink® and Flownex® steady state results will be compared, and the difference will be expressed as a percentage relative to the Flownex® steady state value. These performance results are shown below in Table 4-1.

Table 4-1: Performance index for verification

	Transient			Steady state		
Variable	**Flownex Average**	**Simulink Average**	**Deviation**	**Flownex Value**	**Simulink Value**	**Difference**
P_{h1}	7003911 Pa	7003234 Pa	0.009%	7004749 Pa	7003521 Pa	0.017%
P_{h2}	6931041 Pa	6930213 Pa	0.011%	6931436 Pa	6930171 Pa	0.018%
P_{c1}	283687 Pa	283691 Pa	0.001%	283693 Pa	283693 Pa	0%
P_{c2}	280383 Pa	280385 Pa	0.0007%	280386 Pa	280386 Pa	0%
$\dot{m}_{h1}$	0.2487 kg/s	0.2473 kg/s	0.56%	0.2494 kg/s	0.2505 kg/s	0.44%
$\dot{m}_{h2}$	0.2493 kg/s	0.2462 kg/s	1.24%	0.2496 kg/s	0.2505 kg/s	0.36%
$\dot{m}_{h3}$	0.2519 kg/s	0.2456 kg/s	2.5%	0.2509 kg/s	0.2505 kg/s	0.15%
$\dot{m}_{c1}$	0.1403 kg/s	0.1395 kg/s	0.57%	0.1408 kg/s	0.1407 kg/s	0.07%
$\dot{m}_{c2}$	0.1403 kg/s	0.1395 kg/s	0.57%	0.1408 kg/s	0.1407 kg/s	0.07%
$\dot{m}_{c3}$	0.1403 kg/s	0.1395 kg/s	0.57%	0.1408 kg/s	0.1407 kg/s	0.07%
T_{h1}	352.21 K	353.66 K	0.41%	352.90 K	352.18 K	0.2%
T_{h2}	325.57 K	326.46 K	0.27%	326.14 K	325.86 K	0.08%
T_{w1}	318.40 K	319.23 K	0.26%	318.92 K	318.66 K	0.08%
T_{w2}	340.79 K	342.36 K	0.46%	341.63 K	340.91 K	0.21%
T_{c1}	344.55 K	346.10 K	0.44%	345.38 K	346.63 K	0.36%
T_{c2}	321.76 K	322.64 K	0.27%	322.32 K	322.05 K	0.083%

From Table 4-1 it is evident that the MATLAB® and Flownex® results match closely. The biggest difference is present in mass flow rates, but being at around 2% is of no concern. From the figures above one can see that the transient trends closely match and it is reflected in the percentage deviation calculations in Table 4-1. A very small difference in steady state values is observed and from Table 4-1 one can see it is less than 1%.

4.4 Validation of analytical model

Validation is the process of confirming the accuracy of the analytical model with respect to the real-world system that was modelled. This section will discuss the validation of the model including an overview of the test bench, the experimental setup and the results.

4.4.1 Experimental setup

The test bench setup has been discussed in length in chapter 3. Experimental data are logged by the PLC via pressure and temperature sensors installed on the gas cooler. Referring to Figure

3-3 the data that need to be logged can be decided upon. Crucial data for validation are the inlet and outlet temperature for both fluids and the inlet and outlet pressures for CO_2. The mass flow rate for both fluids is equally important, however, the mass flow rate sensors are not connected to the PLC. The mass flow rate of each fluid can be seen on a screen on the mass flow rate sensor. Table 4-2 shows the sensors used to gather experimental data.

Table 4-2: Sensor number, type and the location of sensors used to gather experimental data

Sensor Number	Type	Location
39	Temperature	CO_2 Inlet
40	Temperature	CO_2 Outlet
41	Temperature	H_2O Inlet
W20	Temperature	H_2O Outlet
54	Pressure	CO_2 Inlet
55	Pressure	CO_2 Outlet

Two experiments will be conducted at different conditions in order to obtain two different experimental data sets. In order to induce a transient in the test bench, the frequency of the compressor can be changed. The compressor is a reciprocating compressor. The frequency of the compressor is the rate at which the compressor piston completes one cycle. A cycle is characterised as an up and down movement of the compressor piston. If the frequency of the compressor is 30 Hz then the piston will complete 30 cycles every second. The increase in compressor frequency results in an increase in pressure. Table 4-3 lists the compressor frequency at which these experiments were conducted. The data of the sensors, which were logged during both experiments, can be seen in Appendix B.

Table 4-3: The compressor frequency for the two experiments that were conducted

Experiment	Component	Initial Value	Value after step
1	Compressor	35 Hz	40 Hz
2	Compressor	40 Hz	45 Hz

4.4.2 Validation procedure

The minimum sample time of the PLC was determined to be 5 seconds. This implies that it will be difficult to compare the results of the hydrodynamic domain, as the settling time of the pressure and mass flow rate are around 3 seconds (refer to Figure 3-9 and Figure 3-10). It is acceptable

to assume that if the results of the thermodynamic domain can be validated, the hydrodynamic domain is also validated, since the thermodynamic domain is dependent on the results of the hydrodynamic domain.

It will, therefore, be counterproductive to try and match the pressure and mass flow rate transients of the experimental results and the simulation results. Only the outlet temperatures will be used during validation. Important parameters needed for validation are: simulation and initial conditions, fluid properties, and secondary losses. The following methodology is used to acquire the parameters listed above:

- The simulation conditions (inlet and outlet pressure and inlet temperature) are the steady state values of the experiment at the frequencies after a step has been induced. For experiment 1 the compressor will be at 40 Hz and for experiment 2 the compressor will be at 45 Hz.
- The water inlet and outlet pressure is calculated with p=0.0981hS where p is pressure [Pa], h is the head [m] added by the pump, and S is the specific gravity [] of the fluid.
- The inlet and outlet pressure and the inlet temperature at the frequencies before the step is applied, are used to run a simulation in Flownex®. The initial conditions and fluid properties are then received from Flownex®. For experiment 1 the compressor will be at 35 Hz and for experiment 2 the compressor will be at 40 Hz.
- The losses will be modelled as secondary losses and are represented by $K_{s,h}$ for the hot fluid and $K_{s,c}$ for the cold fluid as seen in Table A-2. Both of the K values can be set by increasing or decreasing its value until the mass flow rate calculated by the analytical model is the same as the experimental mass flow rate.
- The results of the outlet temperatures of the simulation (states T_{h2} and T_{c2}) and the experiments will be compared and evaluated.

4.4.3 Comparison of results

The geometric properties of the heat exchanger, such as pipe diameter and length, are given in Table A-1 and the thermodynamic properties of the fluids under the conditions of this simulation are given in Table A-12 and Table A-13 for carbon dioxide and water respectively. The thermodynamic properties of the separation wall are given in Table A-5. The simulation conditions including the values for the inlet and outlet pressure and inlet temperatures are given in Table A-10. The initial conditions for the pressure, mass flow rates, and temperatures are given in Table A-11. All these listed tables are in Appendix A. Figure 4-5 shows the results of the first experiment for a step of 5 Hz from 35 Hz to 40 Hz for the hot and cold side outlet temperatures. Figure 4-6

shows the results of the hot and cold side outlet temperatures for a step of 5 Hz from 40 Hz to 45 Hz.

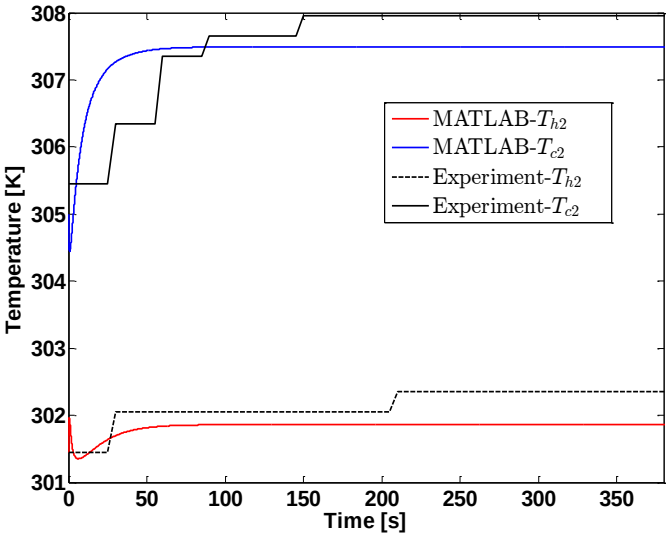

Figure 4-5: Analytical model validation results: Temperature at 40Hz

Observing Figure 4-5 and Figure 4-6 one can see that the settling time and overall transient trend for MATLAB® and the experimental values differ. There are two main reasons for this difference. Firstly, only a single component (gas cooler) of the test bench is modelled. Secondly, because the test bench is a closed cycle the influence of the other components (compressor, expansion valve and evaporator) is not taken into consideration. This also causes the settling time of both the CO_2 and H_2O experimental values to be longer than the MATLAB® values.

Other differences in the transient can be attributed to fluid properties, material properties, such as the copper and steel used for the pipes, and assumptions made in the analytical model. If one looks closely there is some transient behaviour in the water outlet temperature for the MATLAB® results in the first five seconds of the simulation. This is caused by the initial temperature values of the separation wall. The equations are set up with the assumption that heat is always transferred from the hot side to the cold side implying that the hot side temperature will be the hottest with the temperature decreasing towards the cold side.

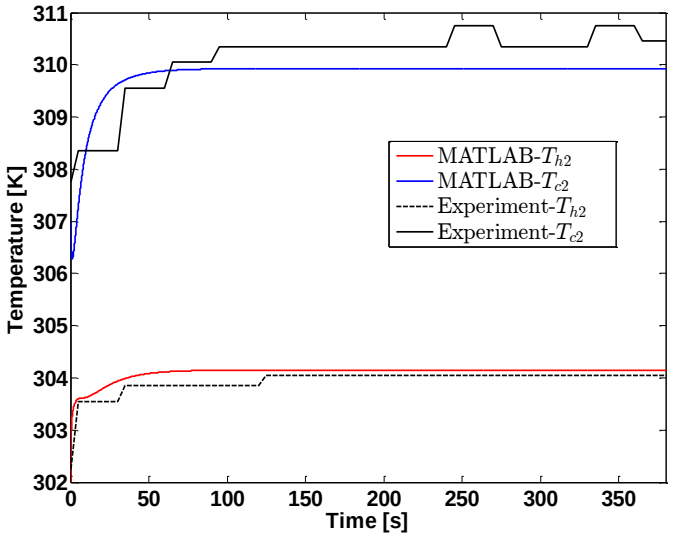

Figure 4-6: Analytical model validation results: Temperature at 45 Hz

In the case of these experiments, the test bench was operated at such a point where the initial value of the cold side was higher than the initial value of the hot side. This causes the dip in the cold side temperature in the first five seconds of the results, since the cold side is hotter that the separation wall. After a short time an equilibrium point is found and the results of the cold side start to follow the correct trend.

4.4.4 Performance index

The purpose of this validation was to determine if the same output temperatures between the analytical model and the experimental data can be reached under the same conditions. It was decided that due to the nature of the test bench it would be impractical to try and get an accurate comparison of the transient values. Therefore a comparison of the steady state values will be made. The difference in steady state values will be expressed as a percentage relative to the experimental value and is shown in Table 4-4 for experiment 1 and in Table 4-5 for experiment 2.

Table 4-4: Validation evaluation for experiment 1

Variable	Experimental Value	Simulink® Value	Difference
T_{h2}	302.35 K	301.86 K	0.162%
T_{c2}	307.95 K	307.49 K	0.149%

Table 4-5: Validation evaluation for experiment 2

Variable	Experimental Value	Simulink® Value	Difference
T_{h2}	304.05 K	304.14 K	0.03%
T_{c2}	310.45 K	309.93 K	0.17%

From Table 4-4 and Table 4-5 one can see that the steady state values match closely. There are small deviations due to the differences between the model and the test bench. The purpose of this model is to be a representation of a real world heat exchanger with sufficient accuracy in order to do an energy based analysis. Considering the purpose that this model must serve and the validation results presented, this model is regarded as validated only for its specific purpose.

4.5 Validation of fault models

Both the fault models need to be validated. For the purposes of validation it was decided to use Flownex®. The fluid leakage and heat leakage models were developed in Flownex® and the results were compared to the analytical model.

4.5.1 Fluid leakage model

The fluid leak was modelled as a small pipe that allows an additional mass flow to flow out of the heat exchanger. The Flownex® model used to validate the fluid leak model is shown below in Figure 4-7.

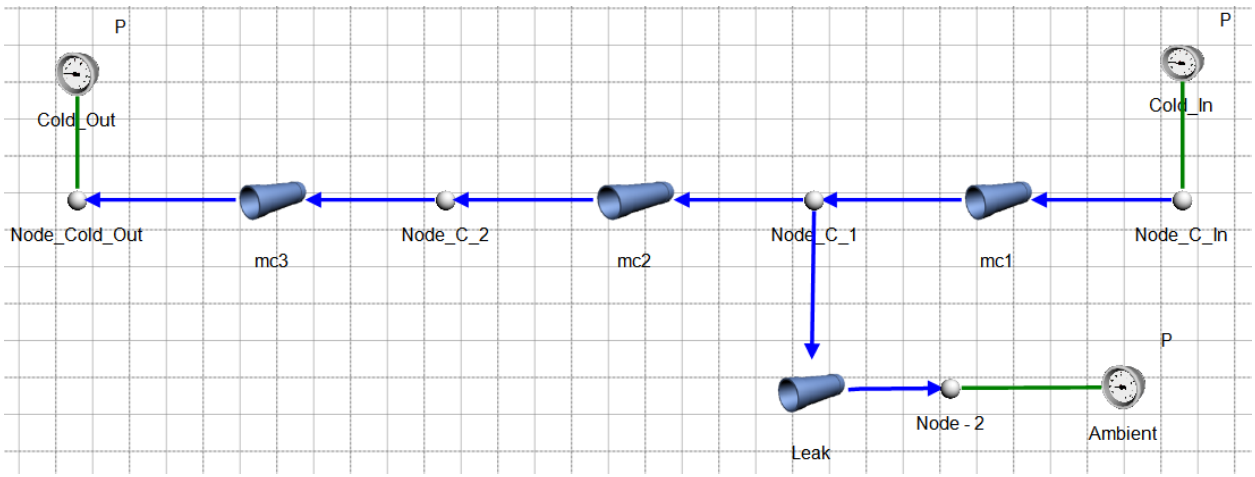

Figure 4-7: Flownex model used for validation of fluid leakage model

4.5.1.1. Validation results

The geometric properties of the heat exchanger, such as pipe diameter and length, are given in Table A-1. The thermodynamic properties of the fluids under the conditions of this simulation are given in Table A-3 and Table A-4 for carbon dioxide and water respectively. The thermodynamic properties of the separation wall are given in Table A-5. The simulation conditions, including the values for the inlet and outlet pressure and inlet temperature, are given in Table A-6 and the initial conditions for the pressure, mass flow rates, and temperatures that will be calculated are given in Table A-7. All these listed tables are in Appendix A. The heat exchanger is allowed to reach steady state before the leak is suddenly introduced. The validation results of the fluid leak are shown below in Figure 4-8 (a) for the cold side pressure and Figure 4-8 (b) for the cold side mass flow rate.

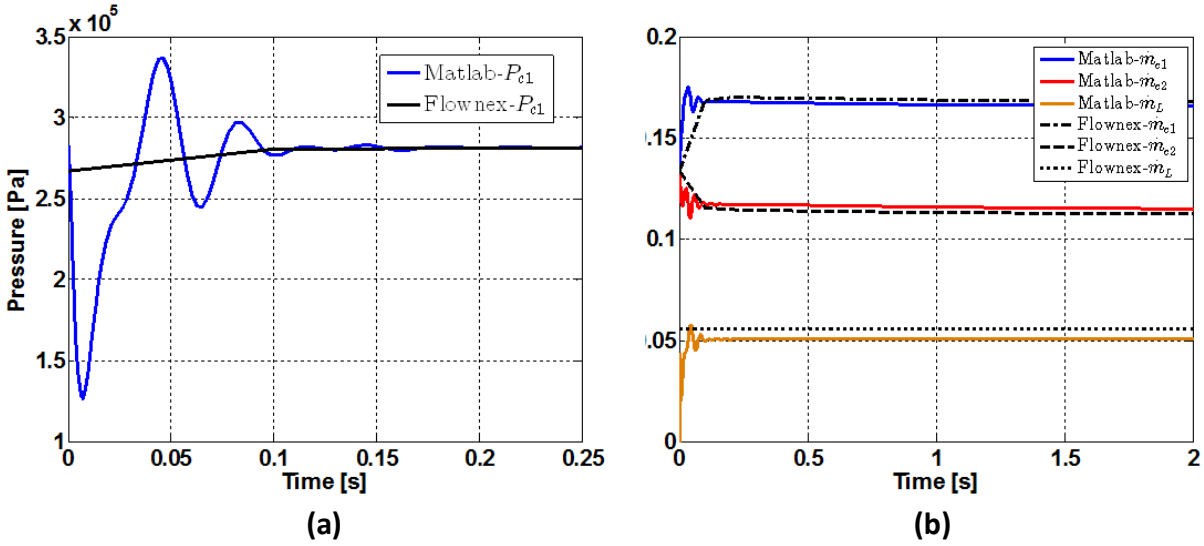

Figure 4-8: Fluid leakage model validation results: (a) Cold side pressure and (b) Cold side mass slow rate

From Figure 4-8 (a) one can see that the steady state values of the pressures of the analytical model and Flownex® correlated well, but there is a difference in the transient. The main reasons for this difference are the solution methods used and differences in fluid properties. Figure 4-8 (b) shows that there are small differences in the steady state values of the mass flow rate. This can be attributed to small differences in the fluid properties between Flownex® and MATLAB®.

4.5.1.2. Performance index

The success of verification and validation are measured by a performance index. The performance index for the leakage model is shown below in Table 4-6. Two important performance factors that need to be evaluated are the transient trend and the steady state values.

Table 4-6: Performance index for the validation of the fluid leak model

	Transient			Steady state		
Variable	**Flownex Average**	**Simulink Average**	**Deviation**	**Flownex Value**	**Simulink Value**	**Difference**
P_{c1}	281150 Pa	271070 Pa	3%	281296 Pa	281452 Pa	0.05%
P_{c2}	279110 Pa	275580 Pa	1,2%	279188 Pa	279266 Pa	0.02%
$\dot{m}_{c1}$	0.1682 kg/s	0.1631 kg/s	3%	0.1680 kg/s	0.1650 kg/s	1.7%
$\dot{m}_{c2}$	0.1127 kg/s	0.1175 kg/s	4%	0.1125 kg/s	0.1144 kg/s	1.6%
$\dot{m}_{L}$	0.0555 kg/s	0.0475 kg/s	14%	0.0555 kg/s	0.0506 kg/s	8%

From Table 4-6 one can see that there is a small difference in pressure during a transient. The difference in transient results are mostly due to the different solution methods used by Flownex® and MATLAB®. There is a bigger difference in mass flow rates, especially for the pipe leak. This can be attributed to two reasons. Firstly, small differences in fluid properties; and secondly, the way in which the pipe leak is modelled in Flownex®. There is no way to prohibit a mass flow through a pipe in Flownex® except by using a valve. Valves are highly non-linear and greatly influences the results of the simulation. The solution to this problem was to introduce a pipe leak after the steady state was solved and before the Flownex® simulation was started. Although accurate results were obtained, small differences are observable. Considering everything, the fluid leak model can be seen as validated as these results are accurate enough for the intended purpose of the fluid leak model.

4.5.2 Heat leakage model

The heat fluid leak was modelled as convection heat transfer between the cold side node, M_{C1}, and the atmosphere. The Flownex® model used to validate the heat leak model is shown below in Figure 4-9.

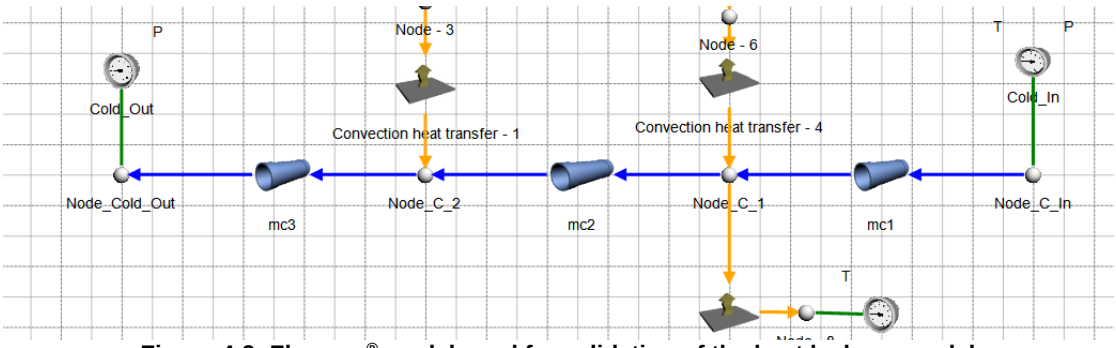

Figure 4-9: Flownex® model used for validation of the heat leakage model

4.5.2.1 Validation results

In order to simulate the heat leakage the simulation is allowed to reach steady state, whereafter the heat leak is suddenly introduced. The initial and simulation conditions of this simulation are given in Table A-6 and Table A-7 respectively. The hot fluid, cold fluid, and separation wall properties are given in Table A-9, Table A-4 and Table A-5 respectively. Ambient temperature, T_{amb}, is taken as 280 K for this simulation. These tables can be viewed in Appendix A. The results of the cold side temperature are shown below in Figure 4-10.

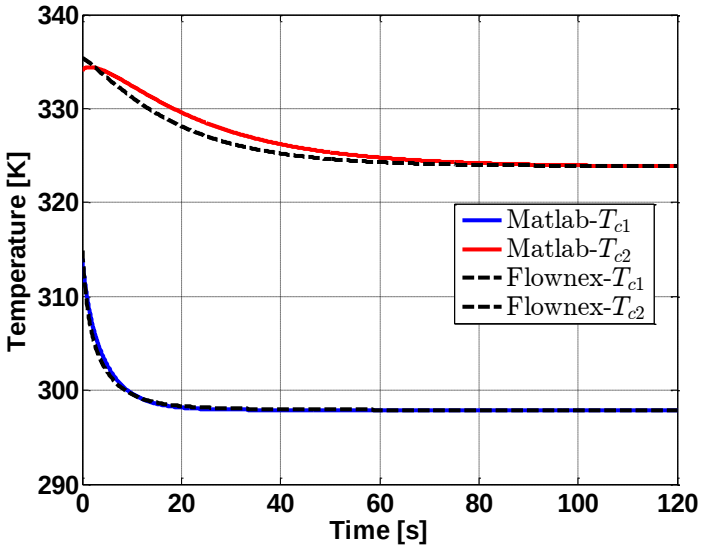

Figure 4-10: Heat leakage validation results: Cold side temperature

From Figure 4-10 one can see a very small difference in the transient and the steady state values. The small differences can be attributed to the difference in properties of carbon dioxide between Flownex® and MATLAB®. Although the heat leakage is on the cold side, the hot side is thermally connected to the cold side and can influence the cold side temperatures. The transient trend is the same, so the small deviations are of no concern for the intended purpose of this fault model.

4.5.2.2 Performance Index

A performance index for the heat leakage model is done exactly as with the fluid leakage model of section 4.4.1.2 but only for the cold side temperatures and is shown below in Table 4-7.

Table 4-7: Performance index for the validation of the fluid leak model

	Transient			Steady state		
Variable	**Flownex® Average**	**Simulink® Average**	**Deviation**	**Flownex® Value**	**Simulink® Value**	**Difference**
T_{c1}	298.23 K	298.18 K	0.01%	297.89 K	297.90 K	0.0003%
T_{c2}	324.99 K	325.00 K	0.003%	323. 87 K	323.78 K	0.02%

From Table 4-7 one can see that both the steady state and transient values barely differ. These results are more that accurate enough for the intended purpose of the heat leak model.

4.6 Conclusion

The same scenario, as in the model results of chapter 3, was used during verification in order to do a comparison between the analytical model and Flownex®. The verification results indicate a good correlation between the analytical model and Flownex®. The last step is to perform validation. Validation was performed with data gathered by conducting experiments on a CO_2 test bench. The model and the experimental data were compared and it was found that although the model matched the data with relative accuracy, there were some significant differences. The reasons behind these differences are mostly due to the differences in the real-world system and that of the model. The differences were determined to be of no large significance when taking into account the level of accuracy needed in order to validate the model for its intended purpose. The model is now considered representative of the real-world system and will be used in the energy calculations. The fault models derived in chapter 3 were also validated using Flownex®. From the results one can see that there is almost no deviation and that the steady state values nearly match. This is a good indication that the fault models can also be considered as validated.

CHAPTER 5 ENERGY REPRESENTATION

5.1 Introduction

The energy representation is based on a technique developed by Bejan [1], namely entropy interaction–energy interaction graphs. The methodology for this chapter, regarding the energy-based representation and the steps followed to evaluate the sensitivity of the energy representation, is given. The energy representation under several fault conditions — including shift of operating point, fluid leakage, heat leakage, and fouling — are given and some key features of the energy representation are identified. The key features identified will aid in the definition of the residuals. The residuals will be used to see how the energy representation changes when changes in the heat exchanger are induced. Changes in the operation of the heat exchanger are induced in the form of faults. The focus of the energy analysis is on the cold fluid. This is due to two reasons; 1) the cold fluid has less energy than the hot fluid therefore yielding better results for the specific technique used and 2) it is mathematically less complex to induce faults (specifically a leak) in the cold fluid pipe. The reason for this is that the boundary conditions outside the cold fluid pipe is atmospheric pressure and temperature. This chapter concludes with the evaluation of the sensitivity of the energy representation by means of three test cases.

5.2 Methodology

The methodology for this chapter is shown below in Figure 5-1.

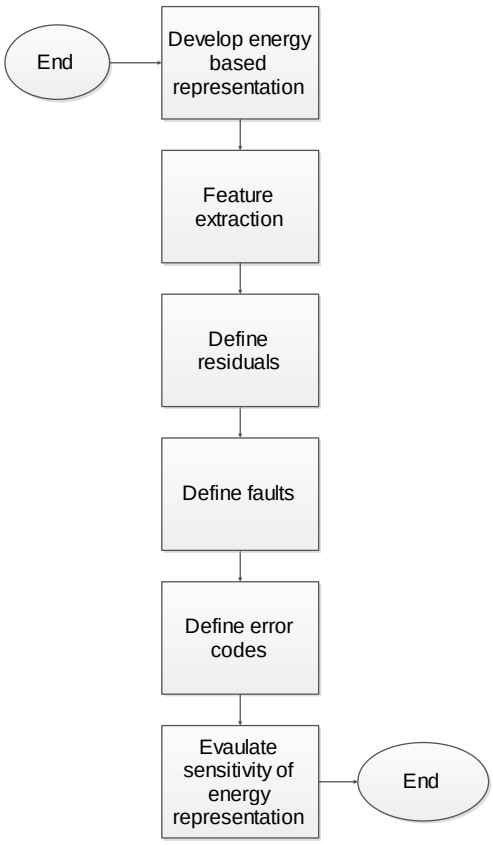

Figure 5-1: The methodology used to derive and evaluate the energy representation

The energy representation is created by using a graphing technique known as entropy interaction–energy interaction graphs [1]. Before the energy representation is developed, the graphing techniques are explained along with an illustrative example. The energy representation under normal and under four fault conditions, including shift of operating point, fluid leakage, heat leakage, and fouling, are developed. The reason for creating the energy representation under normal and fault conditions is to evaluate the sensitivity of the heat exchanger when changes are induced into the heat exchanger operation.

The sensitivity of the energy representation will be evaluated by observing how key features of the energy representation change when faults are induced. The identified key features will be used to define a residual. The change in the residual when a fault is induced, will be evaluated by means of error codes. The purpose of the error codes is to uniquely identify each fault that is induced in the heat exchanger operation. The evaluation of the sensitivity of the energy representation will be done by means of three test cases. In test case one, only single faults will be induced. In test case two, faults will be induced in pairs and in test case three, faults of varying severity will be induced. The reason for inducing faults of varying severity is to see if the energy representation is not only sensitive to large changes but also to small changes induced in heat exchanger operation.

5.3 Energy visualisation technique

Bejan [1] developed two energy based visualisation techniques that are of particular use to this study, namely entropy interaction–energy interaction (S–E) graphs and temperature–energy interaction (T–E) graphs. T–E graphs are used when analysing closed systems, such as a Brayton cycle, and S–E graphs are used to analyse open systems where mass flow and heat transfer occur across the control surface into the control volume. The technique can be explained by considering the illustration of a control volume shown in Figure 5-2.

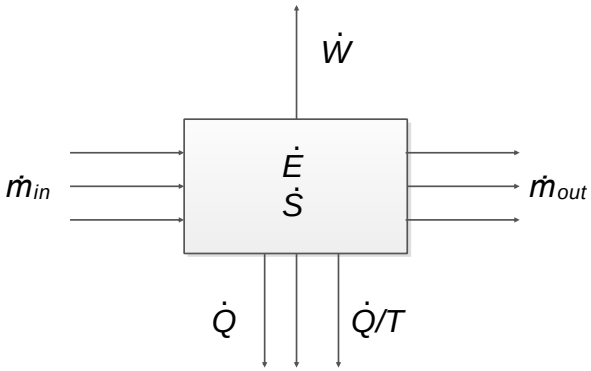

Figure 5-2: A basic illustration of a control volume

From Figure 5-2 it can be seen that there is a mass inflow and outflow across the control surface into the control volume. The mass flow carries with it an enthalpy, h, and specific entropy, s. Heat is transferred to and from the control volume at a rate $\dot{Q}$ and entropy is transferred to and from the control volume at a rate $\dot{Q}/T$ because of the heat transfer. Inside the control volume the energy and entropy is changing at a rate $\dot{E}$ and $\dot{S}$ respectively, due to the mass and heat transfer. Any irreversible process such as heat transfer generates entropy inside the control volume at a rate of $\dot{S}_{gen}$. Any work done on or by the control volume is denoted by $\dot{W}$.

Mass flow and heat transfer can be seen as interactions, since they interact with and change the energy and entropy of the control volume. The energy inlet mass flow interaction ($\dot{m}_{in}h$) and the entropy inlet mass flow interaction ($\dot{m}_{in}s$) can be combined to form the inlet mass flow interaction vector, $\mathbf{m_{in}}$. The same process can be used to define the outlet mass flow interaction vector, $\mathbf{m_{out}}$ with components ($\dot{m}_{out}h$, $\dot{m}_{out}s$) and the heat transfer interaction vector **Q** with components ($\dot{Q}$,$\dot{Q}$/T). These interaction vectors can now be plotted one by one on the entropy-energy (S–E) graphing plane. Figure 5-3 shows a basic illustration of an S–E graph.

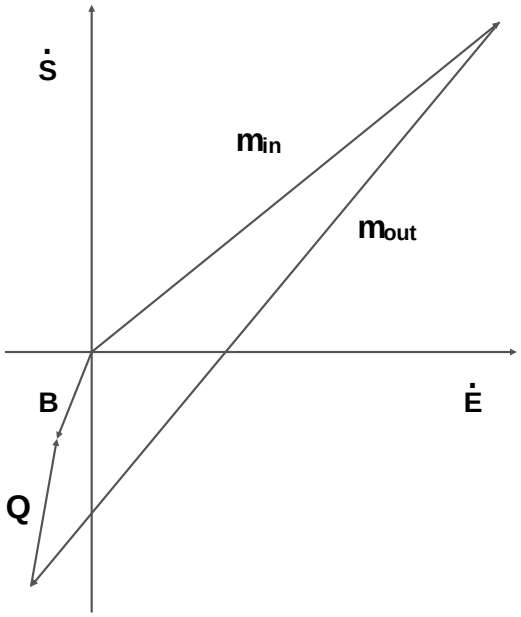

Figure 5-3: An example of an S–E diagram

From Figure 5-3 the interaction vectors can be seen, as well as the influence that the components of the interaction vectors have on the change in energy and entropy of the control volume. The difference between interaction vectors and the origin of the S–E graph is termed the **B** vector. The components of the **B** vector are the negative of the entropy generated ($-\dot{S}_{gen}$) and the work done ($\dot{W}$) on the control volume. In pure heat transfer application, the work done is zero. The entropy generated can never be smaller than zero, thus the **B** vector will always point to the lower half of the S–E plane. To illustrate the process described above an example will be discussed next that applies the S–E graph to a basic heat transfer problem. Although this energy visualisation technique can be used to model he energy during a transient, in the case of this study, only the steady state energy of the cold fluid is evaluated.

5.3.1 An illustrative example

In this section the S–E graph will be applied to a basic heat transfer problem in order to illustrate the graphing technique. In order to apply the S–E graph method to a basic heat transfer problem, the problem must first be defined. Consider the pipe segment of a heat exchanger given by Figure 5-4.

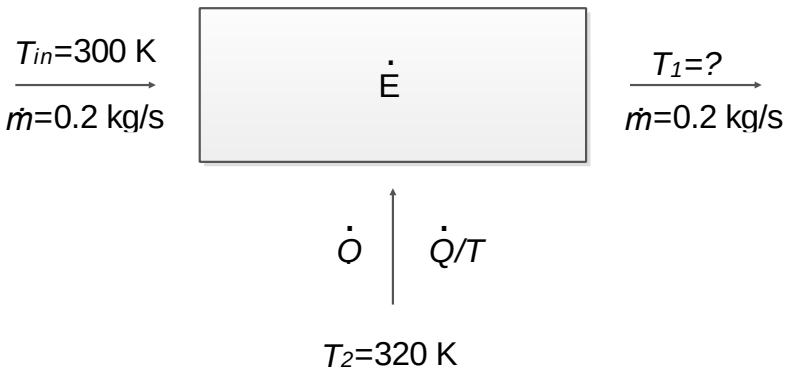

Figure 5-4: The pipe segment used to illustrate the S–E graphing approach

Cold water flows in the pipe segment of Figure 5-4 and receives energy from a hot fluid via convection heat transfer. For this problem friction loss in the pipe can be neglected and the inlet mass flow rate is equal to the outlet mass flow rate. The outlet temperature T_1 is unknown and must be calculated.

The pipe segment can be simplified by applying the staggered grid approach. One main grid point, two secondary grid points, and one control volume can be defined. The staggered grid approach for this problem is shown in Figure 5-5.

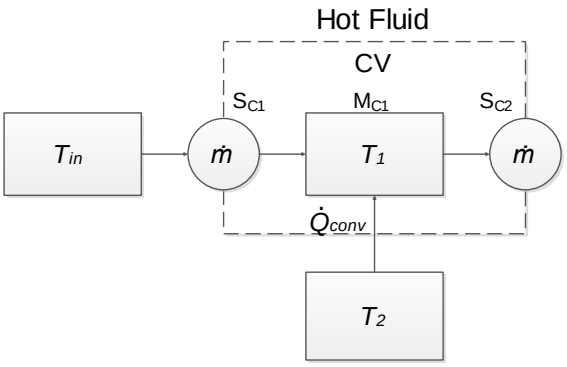

Figure 5-5: The staggered grid approach applied to the example pipe segment

The unknown temperature T_1 at the main grid point can be calculated with the first law of thermodynamics, as given by

$$\frac{dE}{dt} = m\left(h_{in} - h_{out}\right) + \dot{Q}_{conv}\,. \tag{5.1}$$

Since the working fluid is water, the assumption that $h=c_vT$ is valid. Including this relation and rewriting, the first law of thermodynamics becomes

$$\frac{dT_1}{dt} = \frac{\dot{m}c_v}{V\rho c_v}(T_{in} - T_1) + \frac{hA}{V\rho c_v}(T_2 - T_1)\,. \tag{5.2}$$

Substituting the thermodynamic properties of water given in Table A-4 into (5.2), the unknown temperature T_1 can be solved and the S–E graph can be constructed. The inlet mass flow interaction vector $\mathbf{m_{in}}$, has components $\dot{m}_{in}c_vT_{in}$ (since $h=c_vT$ is valid for water) and $\dot{m}_{in}s$. Both of these elements can readily be calculated. The heat transfer interaction vector **Q** has components $\dot{Q}$ and $\dot{Q}/T_{in}$. Both of these components can easily be calculated. The S–E graph for this example is shown in Figure 5-6.

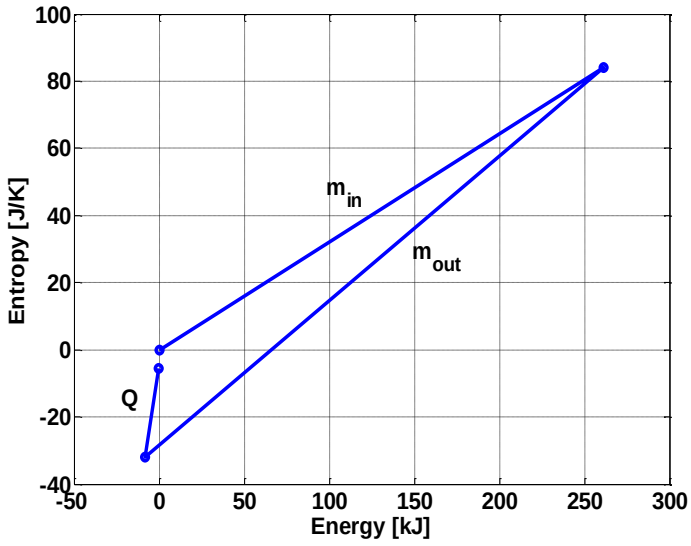

Figure 5-6: The S–E graph of the example problem

A few important observations can be made about the graphing approach. Firstly, the interaction vectors are in rate form (W and W/K). This representation is, therefore, a visualisation of the energy and entropy of the heat exchanger at a specific point in time. Therefore, although the interaction vectors are in rate form, the graph axis are not. Secondly, the influence that each of the different interactions has on the control volume, in terms of energy and entropy, is clearly visible. Thirdly, the **B** vector is visible on the graph and has component values [0,-5.5]. The advantage of being able to see the effect that each different interaction has on the control volume

along with the information added by the **B** vector, indicates that the S–E graphs have the ideal characteristics needed to visualise the energy of the heat exchanger.

5.4 Heat exchanger visualisation

This section will provide the energy visualisation of the heat exchanger under normal and four fault conditions, including a shift in operating point, fluid leakage, heat leakage, and fouling.

5.4.1 Normal conditions

The purpose for creating a graph of the heat exchanger under normal conditions is to serve as a means of comparison and to aid in the definition of the residual. The heat exchanger parameters and simulation conditions are exactly as given in section 3.2.6, with the exception of the entropy values of water which are given in Table A-14 for this simulation. The S–E graph for the cold fluid under normal conditions is given by Figure 5-7 for cold fluid nodes M_{C1} and M_{C2}.

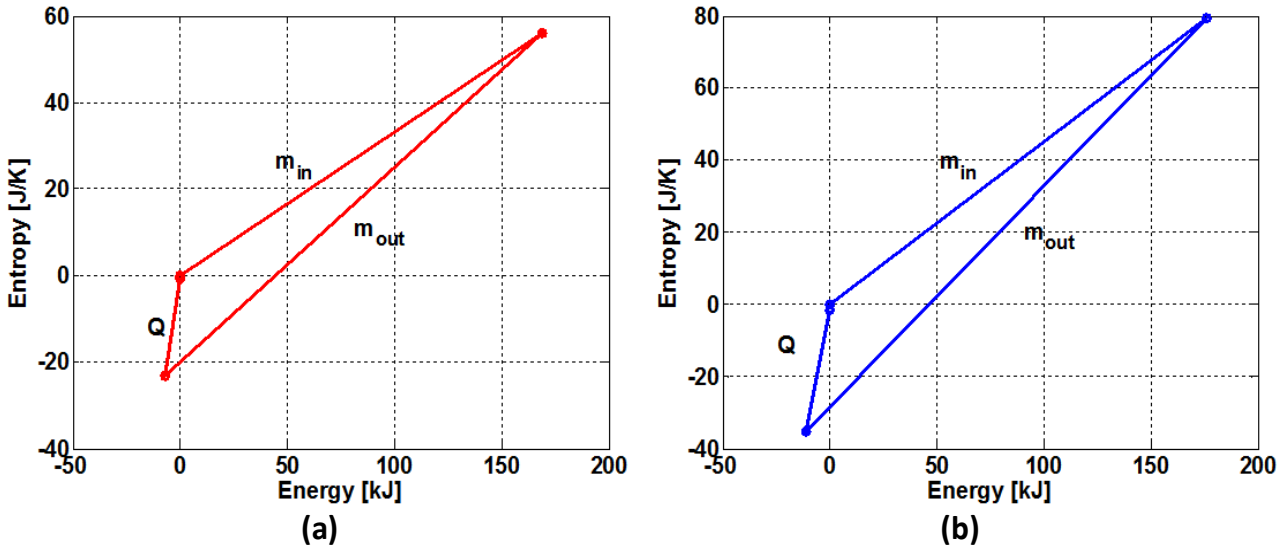

Figure 5-7: S–E diagram for the cold fluid under normal conditions for a) M_{C1} and b) M_{C2}

From Figure 5-7 one can observe that node M_{C2} has more energy and entropy than node M_{C1}, because node M_{C2} is at a higher temperature. One can also observe that the outlet mass flow interaction vector $\mathbf{m_{out}}$ is longer than the inlet mass flow interaction vector $\mathbf{m_{in}}$. This is due to the energy node M_{C1} and M_{C2} receive via heat transfer. Entropy is generated at a rate of 0.3599 [W/K] for node M_{C1} and 1.3363 [W/K] for node M_{C2}.

5.4.2 Shifting of operating point

In some cases during normal heat exchanger operation, a shift in operating point can occur caused by several factors. Causes include an increase in working fluid temperature due to a

defect in a process preceding the heat exchanger or an increase in fluid velocity due to a defective pump. Regardless of the nature of the fault, an change in the heat exchanger operating point can almost always be regarded as a fault, as most industrial processes require working fluids at very specific temperatures. For this simulation the inlet pressure of the cold fluid is increased by 10 kPa. The heat exchange parameters and simulation conditions are exactly as given in section 3.2.6 with the exception of the entropy values of water which are given in Table A-15 for this simulation. The S–E graph for the cold fluid after a shift in operating point is given by Figure 5-8 for cold fluid nodes M_{C1} and M_{C2}.

The shift of operating point, in the form of a pressure increase, results in a mass flow increase. This increase in mass flow results in more energy passing through the control surface (increased length of $\mathbf{m_{in}}$ and $\mathbf{m_{out}}$) and thus more energy available to be transferred as heat (increased length of **Q**). The increase in pressure also causes more disorder within the fluid and thus a higher specific entropy value. From Figure 5-8 it can be seen that a shift of operating point develops an increase in the length of all vectors by a particular factor. It must be noted that a significant rise in pressure can result in less heat transfer. This is due to the fluid flowing too fast for heat transfer to occur. Another problem with a too high fluid flow is that more entropy is generated. Referring to chapter 2 there is a direct correlation between heat transfer surface area, fluid velocity, and entropy generation. The entropy generated during the transient is 0.405 [W/K] for M_{C1} and 7.4 [W/K] for M_{C2}. The entropy generated after the shift in operating point is more than the entropy generated under normal conditions. Therefore, the heat exchanger is less efficient after the shift in operating point occurred.

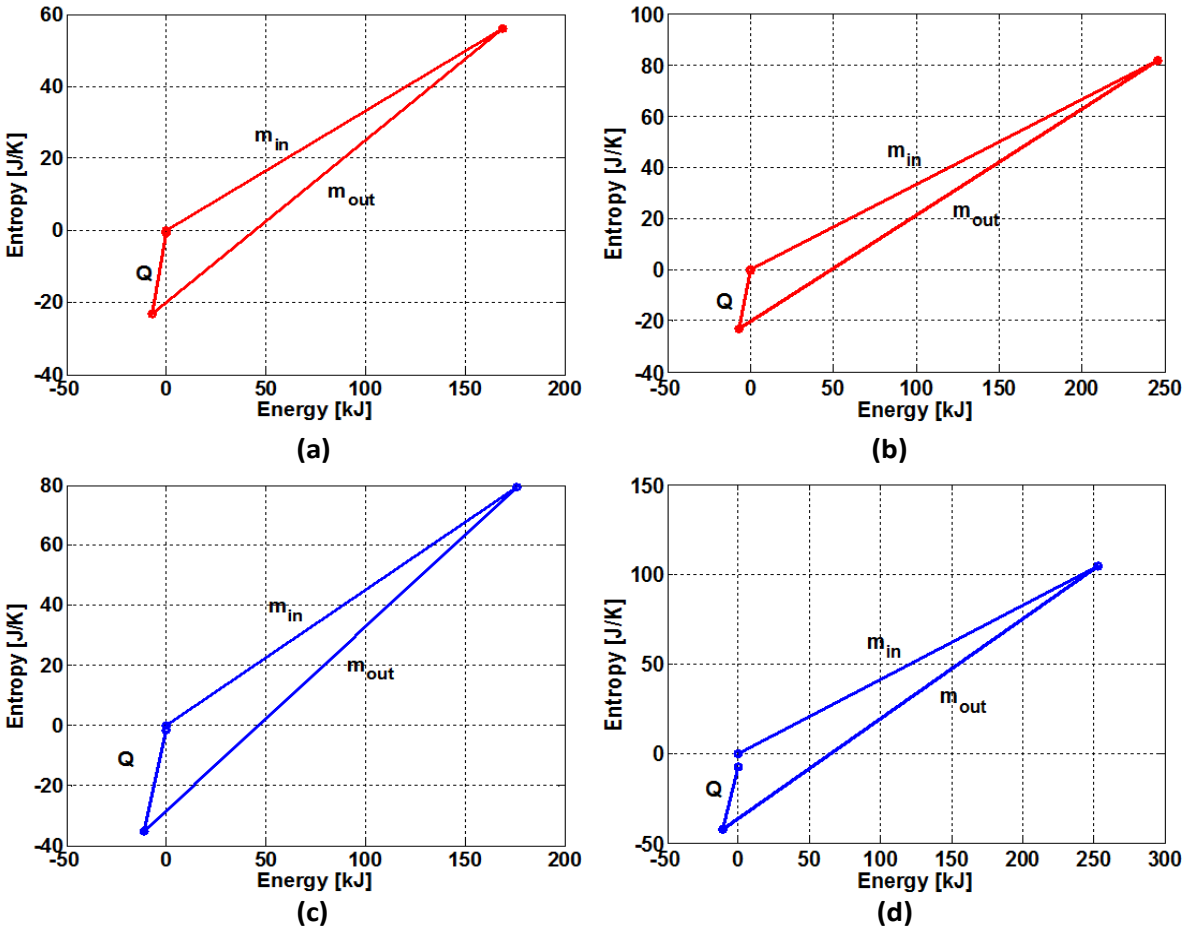

Figure 5-8: S–E for the cold fluid for an increase in cold fluid inlet pressure of 10 kPa for a) M_{C1} normal, b) M_{C1} fault, c) M_{C2} normal and d) M_{C2} fault

5.4.3 Fluid leakage

This section will show and discuss the energy visualisation of the heat exchanger when there is a leak in the cold fluid pipe. A leak in the cold fluid pipe at node M_{c1} of diameter 0.001 m is introduced. The heat exchange parameters and simulation conditions are exactly as given in section 3.2.6, with the exception of the entropy values of water which are given in Table A-16 for this simulation. The resulting energy representation for both cold fluid nodes is shown below in Figure 5-9.

From Figure 5-9 one can observe a much larger inlet mass flow vector when compared to the normal S–E graph. The reason for this is the increased inlet mass flow rate. The mass flow rate of the heat exchanger is mostly dependent on the pressure and the parameters of the pipe. In this simulation, the pressure of the pipe remains constant, but a leak causes the parameters of the pipe to change. The additional mass flow that flows out of the leak causes an increase in inlet mass flow rate for node $M_{C1,}$ and, because the law of conservation of mass must be valid, the

outlet mass flow rate of node M_{C1} decreases. The result of the reduction in outlet mass flow of node M_{C1} is that less energy flows into node M_{C2} as can be seen in the shorter vector length of the inlet mass flow vector ($\mathbf{m_{in}}$) in Figure 5-9 (d).

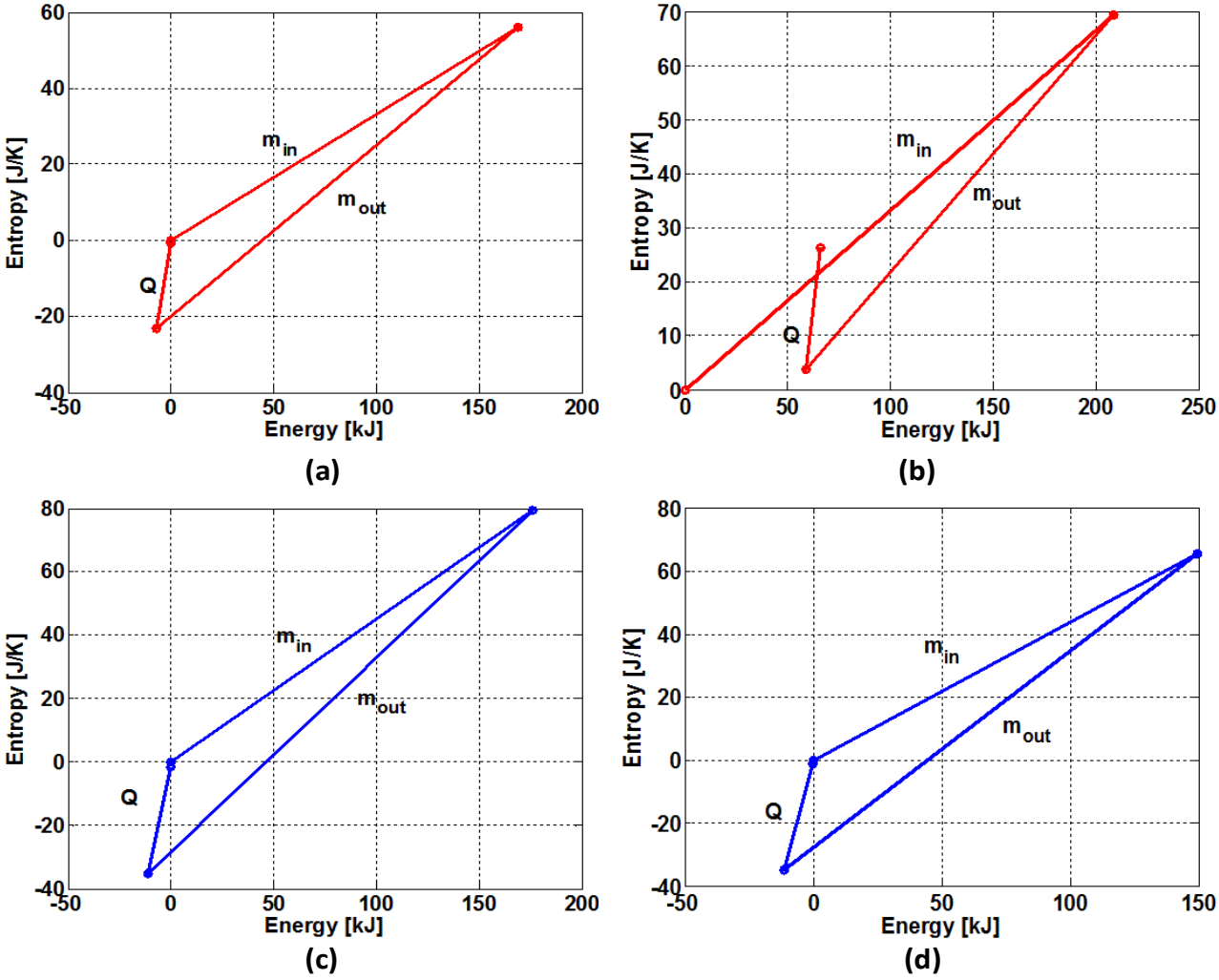

Figure 5-9: S–E for the cold fluid after a fluid leakage for a) M_{C1} normal, b) M_{C1} fault, c) M_{C2} normal and d) M_{C2} fault

5.4.4 Heat Leakage

The heat leakage fault is used to evaluate the change in the energy representation when the fault is induced in the thermodynamic domain. The heat exchange parameters and simulation conditions are exactly as given in section 3.2.6, with the exception of the entropy values of water which are given in Table A-17 for this simulation. A heat leakage is introduced in the cold fluid at node $M_{C1,}$ and the resulting energy visualisation is shown below in Figure 5-10.

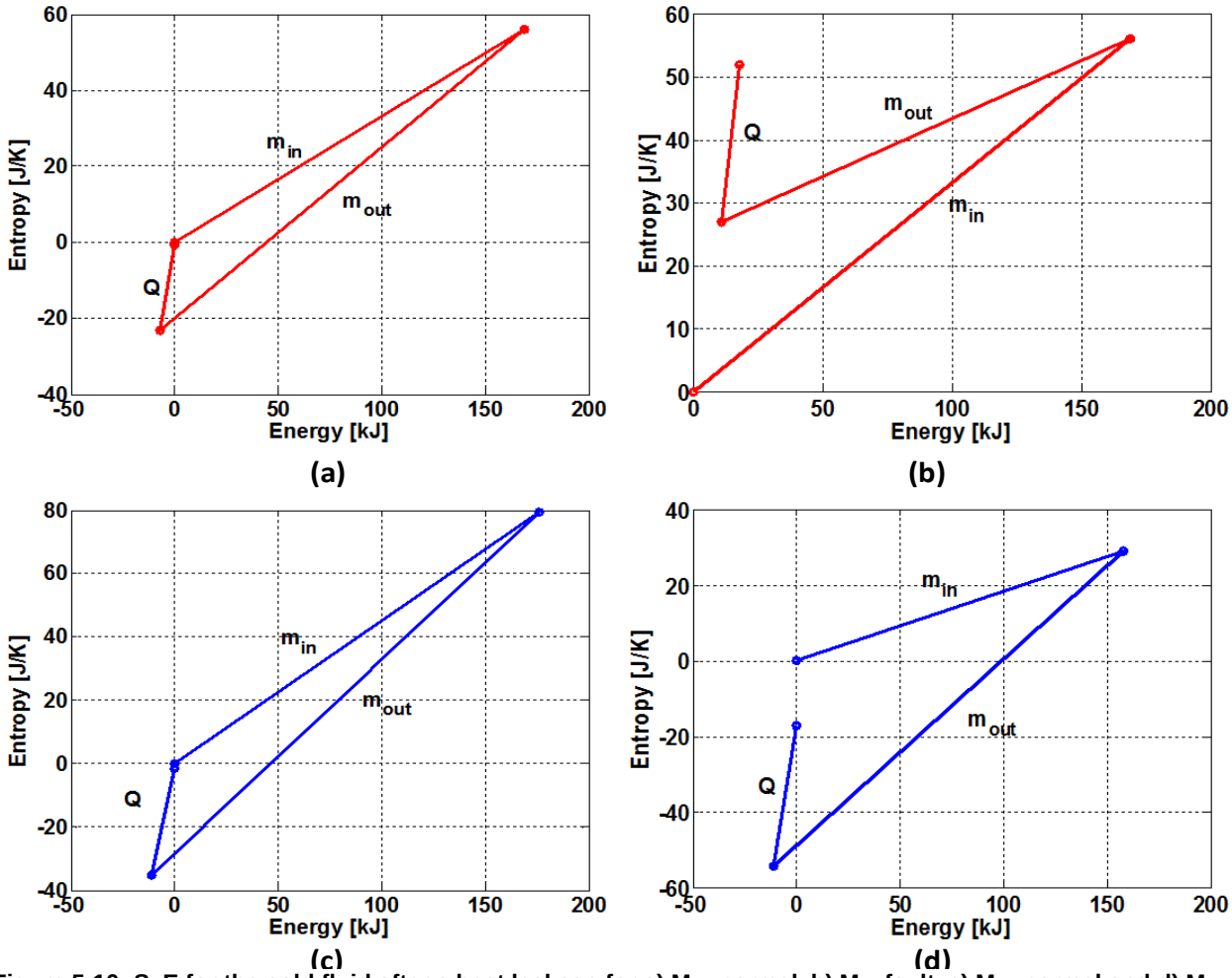

Figure 5-10: S–E for the cold fluid after a heat leakage for a) M_{C1} normal, b) M_{C1} fault, c) M_{C2} normal and d) M_{C2} fault

Heat is lost via convection with the atmosphere around the heat exchanger. The temperature of the atmosphere for this simulation is 280 K. The low atmosphere temperature is chosen in order to induce a sizeable fault. From Figure 5-10 (b) one can see the effect of the heat leak results in a strange shape in the energy representation of node M_{C1}. The reason for this is that the sudden loss of heat energy, via the heat leak, causes the temperature of the node M_{C1} to drop sharply and in turn this reduces the specific entropy of element $S_{C2,}$ which succeeds node M_{C1}. The entropy flow, $\dot{m}s$, leaving node M_{C1} is, therefore, much less than the entropy flow entering node M_{C1}. The heat leak reduces the entropy and energy entering node M_{C2} via the inlet mass flow interaction ($\mathbf{m}_{in}$) and can be seen as the shorter length of $\mathbf{m}_{in}$, $\mathbf{m}_{out}$ and **Q** in Figure 5-10 (d).

5.4.5 Fouling

Fouling occurs in a heat exchanger when impurities in the working fluid such as scale, algae, suspended solids and insoluble salts pack together on the pipe walls [63]. In this simulation the secondary losses is increased to 70 and the convection resistor value is increased by a multiple of 3. The heat exchange parameters and simulation conditions are exactly as given in section 3.2.6, with the exception of the entropy values of water which are given in Table A-17 for this simulation. The S–E graph under normal and fouling conditions for both node is shown in Figure 5-11.

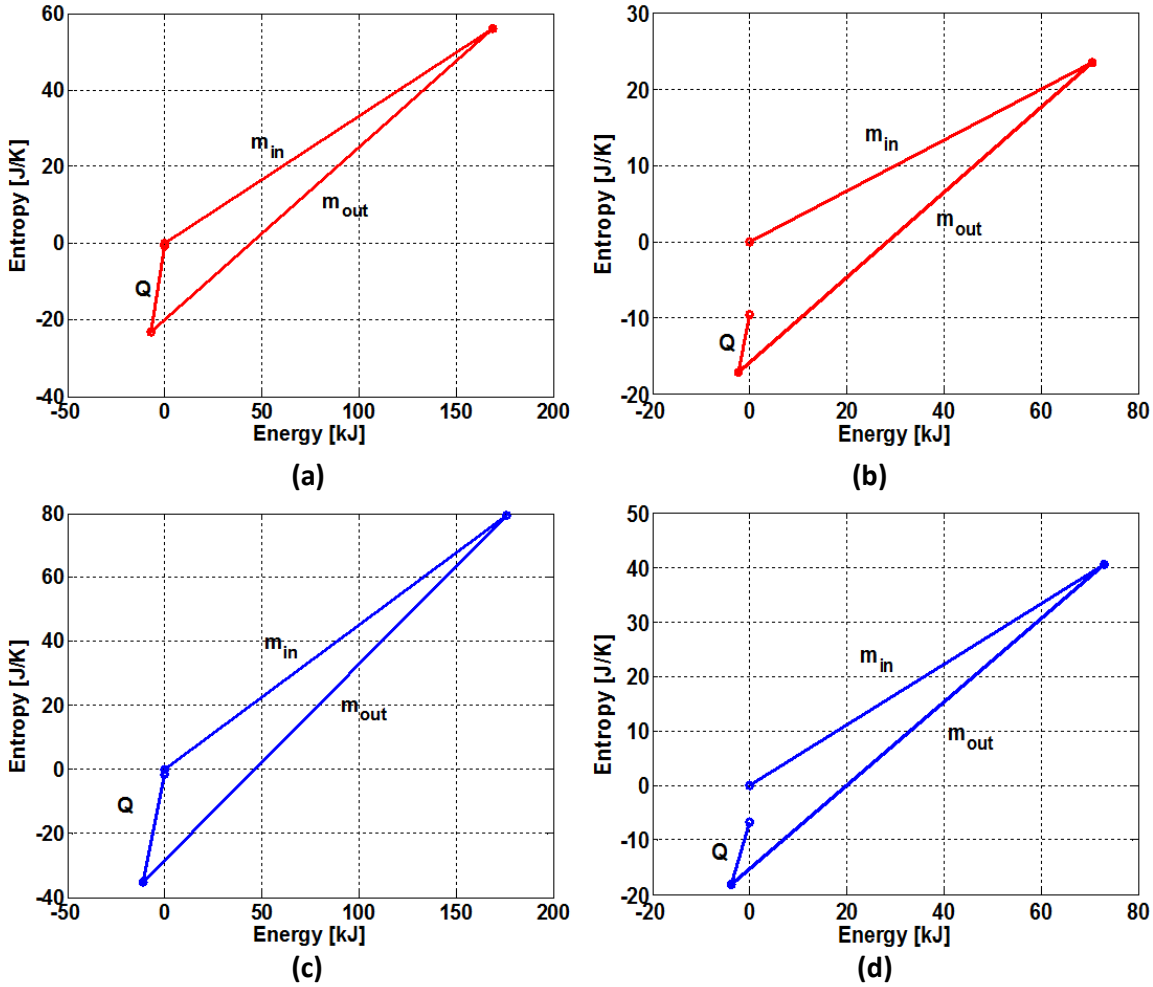

Figure 5-11: S–E for the cold fluid after fouling for a) M_{C1} normal, b) M_{C1} fault, c) M_{C2} normal and d) M_{C2} fault

Fouling has an impact on the heat exchanger in both the thermal and hydrodynamic domains. In the hydrodynamic domain, the fluid has to overcome a larger friction factor and can be modelled as an increase in the value of the hydraulic resistor, R_h. In the thermodynamic domain, the increased fouling reduces the potential for heat transfer and thus reduces the heat transfer coefficient and be seen as a rise in value of the convection heat transfer resistor, R_t. The effect of fouling is twofold. Firstly, the mass flow rate is reduced since energy is dissipated when the

fluid needs to do more work to overcome the increased friction. This effect can be seen in Figure 5-11 (b) and (d) as the reduced length of $\mathbf{m_{in}}$ and $\mathbf{m_{out}}$ when compared to the normal energy representation. The second effect of fouling is the reduction in heat transfer effectiveness. When fouling occurs to a certain extent, the convection heat transfer coefficient is reduced and, thus, the total amount of heat that can be transferred and can be seen in both Figure 5-10 (b) and (d) as the reduction in length of the heat transfer vector $\dot{\mathbf{Q}}$. The case outline here is an extreme case of fouling where the convection heat transfer coefficient was drastically reduced.

5.5 Feature extraction

Features are properties of the energy representation that stand out and can aid in uniquely identifying the fault that occurred in the heat exchanger operation. Features can include the area under the graph, the length of the graph, or circumference of the graph. Considering the figures presented thus far, a feature that is present and changing in each graph is the length of the interaction vectors. In each graph the length of the interaction vectors is different depending on the fault induced.

Looking closely at the figures presented thus far, it can be seen that the change in length of the interaction vectors is in some cases the same. For instance, the inlet mass flow interaction vector is longer when a shift of operating point occurs and when a fluid leak is induced. This is an indication that the lengths of the three vectors present are not enough to uniquely identify a fault. Another important observation that can be made is that the ratio of the inlet mass flow vector and the outlet mass flow vector, $\mathbf{m_{out}/m_{in}}$, changes based on the fault that is induced, especially in the presence of a leak. The features of interest are, therefore, the length of the three mass flow interaction vectors, $\mathbf{m_{in}}$, $\mathbf{m_{out}}$ and $\mathbf{Q}$ and the ratio $\mathbf{m_{out}/m_{in}}$.

5.6 Residuals

In order to evaluate the sensitivity of the energy representation, residuals will be used. A residual is used to describe the relationship between two parameters or variables of a system. Typically it would be used to measure the difference between two corresponding sensors in a plant, but can also be used to describe the difference between a measurement and a calculated value [64]. In this case a residual will be used to describe the difference between the heat exchanger under normal and under fault conditions. The faults that will be used to evaluate the sensitivity of the energy representation, include a shift in operating point, fluid leakage, heat leakage, and fouling. The faults will also be induced in varying degrees of severity in order to test if the energy representation is not only sensitive to faults, but also to small or large faults. The faults, the range of the fault, and the fault parameters are given in Table 5-1.

Table 5-1: The nature of the faults and the fault parameters

Fault	Nature of fault	Fault parameter
Shift of operating point	Increase in cold side pressure	5-15 kPa
Fluid leakage	Size of hole	0.001 - 0.0015 mm
Fouling	Increased secondary losses ($K_{s,c}$ and $K_{s,h}$)	50 - 150
Fouling	Increased convection heat transfer resistor	Increase in value of 1.5 to 3 times
Heat leakage	Change in ambient temperature	260 -280 K

The faults, that will be induced, will be described with a number between 0 and 1. If a fault is symbolised with a 0, it indicates that no fault of that type occurred. If a fault is described with a 1, it means that the most severe form of that fault occurred. Anything between one and zero indicates a less severe version of a specific fault occurred. For example, if a shift in operating point occurred and is described with a 1, it means that the cold side pressure increased by 15 kPa. If the shift of operating point occurred and is described with 0.5, it means that the cold side pressure increased by 7.5 kPa.

The discussion, regarding the key features of the energy representation, revealed that the length of the interaction vectors present in the energy representation are ideally suited to be used in the residual. Two vectors can now be defined: **n** will contain the length of the interaction vectors under normal conditions and **f** will contain the length of the interaction vectors under fault conditions. The **n** and **f** vectors are respectively given by

$$\mathbf{n} = \left[\left|\mathbf{m}_{in,norm}\right|, \left|\mathbf{m}_{out,norm}\right|, \left|\mathbf{Q}_{norm}\right|, \left|\frac{\mathbf{m}_{out,norm}}{\mathbf{m}_{in,norm}}\right| \right] \text{ and} \tag{5.3}$$

$$\mathbf{f} = \left[\left|\mathbf{m}_{in,fault}\right|, \left|\mathbf{m}_{out,fault}\right|, \left|\mathbf{Q}_{fault}\right|, \left|\frac{\mathbf{m}_{out,fault}}{\mathbf{m}_{in,fault}}\right| \right]. \tag{5.4}$$

The residual can now be defined as the difference between the **n** and **f** vectors as given by

$$\mathbf{r} = \mathbf{n} - \mathbf{f}. \tag{5.5}$$

If a fault is induced in the heat exchanger system the energy representation will change and so will the residual. The residual will also take on a unique value based on the type and severity of

the fault induced. Advantage can be taken of this unique value of the residual by defining an error code based on the value of the elements in the residual vector. The definition of the error code is given by

$$e = \begin{bmatrix} 1 & if & \mathbf{r}[i] > 0 \\ 0 & if & \mathbf{r}[i] = 0 \\ -1 & if & \mathbf{r}[i] < 0 \end{bmatrix} i = 1,2,3,4\,. \tag{5.6}$$

The error codes will be used to generate a number for each element in the residual vector. These error codes will allow the unique identification of a fault or combination of faults that occurred in the heat exchanger.

5.7 Evaluation of the sensitivity of the energy representation

The sensitivity of the energy representation to changes in heat exchanger operation, will be evaluated by inducing a set of faults in the operation of the heat exchanger. The evaluation of the sensitivity of the energy representation will be conducted with three test cases. In test case one only single faults will be induced and the residuals will be evaluated by means of the error codes. In test case two faults will be introduced in pairs. In test case three faults will be introduced in pairs and at varying degrees of severity. The purpose of test case three is to determine if the residual is sensitive to very small as well as larger changes in heat exchanger operation. The three test cases and the results of each test case are given in the following sections.

5.7.1 Test Case 1: Single Faults

During test case one the faults will be induced one at a time and the residual will be evaluated. The results of test case 1 are provided in Table 5-2 with the residuals and the error codes shown for both cold fluid nodes.

Table 5-2: The faults simulated, the residuals of the fault and the error code for single faults

	Residual M_{C1}	**Residual M_{C2}**	**Error Code N_{C1}**	**Error Code N_{C2}**
Shift of operating point	[-81 -81 0 0]	[-81 -83 -2 0]	[-1 -1 0 0]	[-1 -1 -1 0]
Fluid Leak	[-42 25 0 -0.4]	[30 29 0 0]	[-1 1 0 -1]	[1 1 0 0]
Heat Leak	[0 31 8 -0.2]	[31 29 -4 0]	[0 1 1 -1]	[1 1 -1 0]
Fouling	[82 87 20 0]	[87 97 30 0]	[1 1 1 0]	[1 1 1 0]

From Table 5-2 it can be seen that even though the faults are only induced in node M_{C1}, the effects of those faults are visible in node M_{C2}. The cause of this effect is due to the nodes being linked to each other in both the thermodynamic domain and the hydrodynamic domain. In this test case, only single faults were induced and from the error codes it can be seen that each fault can be uniquely identified.

5.7.2 Test Case 2: Multiple Faults

During test case two, the faults will be induced in pairs. The purpose of this is to observe whether the energy representation changes in the presence of more complex faults. In order to induce more complex faults, a vector describing the faults induced needs to be defined. The fault vector, **F**, is given by

$$\mathbf{F} = \left[f_{transient}, f_{leak}, f_{heatleak}, f_{fouling} \right]. \tag{5.7}$$

The fault vector **F** contains the faults present in the simulation and can be constructed as given by

$$\mathbf{F}[i] = \begin{bmatrix} 1 \; if \; fault \; is \; present \\ 0 \; if \; fault \; is \; not \; present \end{bmatrix}, i = 1,2,3,4 . \tag{5.8}$$

Table 5-3 shows the combination of faults that were simulated, as well as the residuals and the error codes for both nodes.

Table 5-3: The faults simulated, the residuals of the fault and the error code for multiple faults

Fault Vector	Residual M_{C1}	Residual M_{C2}	Error code M_{C1}	Error code M_{C1}
[1 1 0 0]	[-124 -56 0 -0.3]	[-56 -64 1 0]	[-1 -1 0 -1]	[-1 -1 1 0]
[1 0 1 0]	[-81 -44 -2 -0.2]	[-44 -53 -4 0]	[-1 -1 -1 -1]	[-1 -1 -1 0]
[1 0 0 1]	[38 39 20 0]	[39 44 26 0]	[1 1 1 0]	[1 1 1 0]
[0 1 1 0]	[-42 45 1 -0.6]	[45 45 -2 0]	[-1 1 1 -1]	[1 1 -1 0]
[0 1 0 1]	[43 59 22 0.8]	[134 137 31 1]	[1 1 1 1]	[1 1 1 1]
[0 0 1 1]	[82 93 19 0]	[93 104 25 0]	[1 1 1 0]	[1 1 1 0]

In test case two, each test consists of a combination of two faults. If one looks at the error codes of node M_{C1} and M_{C2}, one can observe that each fault combination cannot be identified uniquely. The two fault conditions with the same error codes are: transient and fouling; and heat leakage

and fouling. The reason for these fault combinations having the same error code, is due to the influence of fouling on the residual. Fouling decreases the length of the mass flow inlet and outlet interaction vectors and the heat transfer interaction vector. Since fouling influences both the thermodynamic and hydrodynamic domains, the effect of fouling on the energy representation is more severe. The shift of the operating point merely increases the length of each vector, but not enough to counteract the influence of fouling. The result of fouling and a shift in transient is, therefore, simply the reduction in length of each of the interaction vectors ($\mathbf{m_{in}}$, $\mathbf{m_{out}}$, **Q**) resulting in an error code of [1 1 1 0]. The effect of a heat leak is the reduction of the outlet mass flow vector, $\mathbf{m_{out}}$, and, therefore, the reduction of the relationship $\mathbf{m_{out}/m_{in}}$. Fouling overpowers the effects of a heat leak in the residual and the end result is simply a reduction in length of the vectors.

5.7.3 Test Case 3: Faults of varying severity

The purpose of test case three is not only to induce multiple faults, but also to vary the degree at which the fault is induced. The fault vector, **F**, needs to be adjusted to include not only whether a fault is present or not, but also the severity of the fault. The fault vector will now contain numbers between 0 and 1 as an indication of the severity of the fault. The fault vector, residuals of both nodes, and the error codes are shown below in Table 5-4.

Table 5-4: The fault vector, residuals and error codes for test case 3

Fault Vector	Residual M_{C1}	Residual M_{C2}	Error code M_{C1}	Error code M_{C2}
[0.3 0.9 0 0]	[-158 0 0 -0.8]	[0 -4 1 0]	[-1 0 0 -1]	[0 -1 1 0]
[0.8 0 0.2 0]	[-101 -61 -2 -0.18]	[-61 -71 4 0]	[-1 -1 -1 -1]	[-1 -1 1 0]
[0.5 0 0 0.8]	[70 73 19 0]	[73 83 25 0]	[1 1 1 0]	[1 1 1 0]
[0 0.2 0.7 0]	[-42 51 -2 -0.6]	[51 50 -2 0]	[-1 1 -1 -1]	[1 1 -1 0]
[0 0.4 0 0.4]	[51 70 22 -0.1]	[70 97 29 -0.2]	[1 1 1 -1]	[1 1 1 -1]
[0 0 0.4 0.2]	[82 95 16 0]	[95 104 18 0]	[1 1 1 0]	[1 1 1 0]

The purpose of test case three is to see if the energy visualisation is also sensitive to smaller changes induced in the heat exchanger. From Table 5-4 one can observe that, although the residuals change to reflect the changes in the faults, not every fault combination could be identified uniquely. There are several reasons for this, but foremost is that some combination of faults has similar effects on the energy representation as other combinations of faults. With the addition of varying the severity of the fault in this test case, not all the fault combinations had a significant enough effect on the energy representation to be identified uniquely. The solution to

this problem would be to define a better residual by including additional terms. Referring to the S–E graphs presented thus far, it can be seen that the size of the angles between the vectors in the plots can also be used as elements in the residual. With this new residual the faults may be identified uniquely.

5.8 Conclusion

This chapter provided the energy based representation of a heat exchanger. The graphing technique used is entropy interaction–energy interaction graphs developed by Bejan [1]. The energy and entropy interactions (mass flow and heat transfer) on a control volume are depicted on the graph. This allows one to see the effect each of the interactions has on the energy and entropy of the control volume. The importance of these graphs is that they must be able to change if a fault is present in the heat exchanger. In order to test this, the sensitivity of the graphs to changes in heat exchanger operation will be measured. The sensitivity of the energy representation can be evaluated by means of residuals. Before the residual can be defined, certain features of the energy representation need to be identified.

These features need to be sensitive to changes in heat exchanger operation and must change in the presence of a fault. These features will aid in creating the residual and are the length of the three mass flow interaction vectors, $\mathbf{m}_{in}$, $\mathbf{m}_{out}$ and $\mathbf{Q}$, and the ratio $\mathbf{m}_{in}/\mathbf{m}_{out}$. The residual must be set up in such a way that it changes when the heat exchanger operating conditions change. The residual is defined as the difference in the four features between normal and fault conditions. The purpose of the residual is to determine if a fault has occurred and what the fault might be. In order to determine what the fault induced might be, error codes can be defined that change based on the value of the residual.

The evaluation of the sensitivity of the energy representation was done in three separate test cases. The reason for this is to gradually increase the complexity of the faults in order to evaluate whether the energy representation is sensitive to a wide range of faults. It was determined that although the residuals change for each fault, or fault combination induced, the error codes were unable to uniquely determine each of the faults. Possible solutions to this problem include a better defined residual by defining more features such as the angle between the interaction vectors.

CHAPTER 6 CONCLUSION

6.1 Introduction

This chapter provides conclusions regarding the analytical model and the energy representation, with respect to its usefulness, shortcomings and problems experienced. Recommendations are made for future work regarding the problems experienced with validation of the analytical model and possible applications of the energy representation. This chapter concludes with a verdict regarding the success of the research.

6.2 Conclusions

Global energy usage is drastically rising and fossil fuels, being the primary source of power generation, are being depleted. The impact of fossil fuel usage in power generation has significant adverse effects on the environment coupled with the rising energy demand. Research is, therefore, shifting towards energy conservation. Heat exchangers are components used in many industrial processes. It is estimated that almost 80% of energy consumption in the industry is related to heat transfer. Heat exchangers, therefore, are industry components that warrant analysis and optimisation regarding energy usage. The purpose of this study is to develop an energy based representation for a counter flow single-phase heat exchanger.

In order to visualise the energy of a heat exchanger a representative model is needed. During this study, a model was derived based on the parameters and attributes of a real-world heat exchanger. The model was obtained using the staggered grid approach presented by Patankar [42]. The staggered grid approach aids significantly in deriving fundamental equations for the thermodynamic and hydrodynamic domains. The laws of conservation of mass, momentum, and energy were used to derive the necessary differential equations. Some challenges were encountered during the simulation of the analytical model particularly the definition of the thermodynamic properties of the working fluids. This problem was solved by using the thermodynamic properties supplied by Flownex®.

The next step in the methodology of this study was to complete verification and validation. Verification is the process by which the output of the model was compared to the output of a Flownex® model. Flownex® is advanced simulation software that specialises in simulations where fluids are the working force. Although the steady state values were mostly the same during the comparison, there was a difference in the transients. The differences can mostly, but not solely, be attributed to the different approaches used to solve the analytical and Flownex® models. The

solver Flownex® uses is an implicit pressure correction solution algorithm, while the analytical model is solved using a standard stiff differential equation solver. As with any numerical method, both these solvers impact the results differently. Other factors influencing the difference in solutions include small differences between the thermodynamic properties of the fluids between the Flownex® and MATLAB® models. The results, however, match close enough to deem verification successful.

Validation of the model was done using experimental data obtained from a heat exchanger test bench. The test bench is a CO_2 cycle consisting of a gas cooler, expansion valve, evaporator, and compressor. The gas cooler was used as validation for this model, as the gas cooler is where water cools hot CO_2. A few problems were encountered during validation, foremost among them is that the test bench is a closed cycle. Because the CO_2 flows continuously in a closed cycle the inlet temperature of the CO_2 continuously changes until steady state has been reached. This temperature change is contrary to the assumptions used during simulation of the analytical model where inlet temperatures are constant. Another problem that became apparent is the placement of the sensors on the test bench. The nodes, where temperatures and pressures are calculated for the analytical model, do not correspond to the places on the heat exchanger where sensors are. This problem made it impossible to validate every state of the analytical model. Additional problems like the low frequency at which the PLC can sample, as well as the length and losses difference between the analytical model and the test bench led to only the validation of the outlet temperatures. This approach is considered valid since each equation is linked both thermally and hydraulically to each other. If one can validate the outlet temperatures it is a reasonable assumption that the steady state values of the hydrodynamic domain are also validated.

The energy visualisation is derived based on a technique developed by Bejan [1]. This visualisation technique involves plotting the terms of the first and second law of thermodynamics as interaction vectors on an entropy-energy axis. This technique is termed entropy interaction–energy interaction graphs (S–E graphs). Several fault models were derived including fluid leakage, heat leakage, and fouling models. The purpose of these models is to induce a change in the heat exchanger that will reflect on the S–E graph. Several important characteristics of the S–E graphs can be observed when plotting the S–E graphs for the fault models. Firstly, one can see the dependency of the nodes on each other in the S–E graph. If, for instance, a fault is introduced at node M_{C1} the S–E graph of node M_{C2} will change to reflect that fault as well. A second important property is that the S–E graphs are sensitive to changes in the heat exchanger operation. To evaluate the sensitivity of the S–E graph, a residual was defined that is based on the properties of the vectors in the S–E graph. During the evaluation of the sensitivity of the energy

representation, three test cases were investigated: 1) single faults; 2) multiple faults; and 3) faults of varying severity. Even when the fault induced was subtle, as in the case of test 3, the S–E graph would change to reflect that a change has occurred in the heat exchanger.

In order to uniquely identify the faults, error codes were defined based on the values of the residual. Although each fault or combination of faults could not be identified uniquely, there is some degree of validity to the energy approach as a tool for FDI. If one were to define a better residual, it might be possible to uniquely identify each of the fault combinations. The last property of the S–E graph, which is of importance, is that the entropy generation rate is shown on the graph. Entropy generation is a measure of the effectiveness of a system and as a means of optimisation, the generated entropy can be minimised.

6.3 Recommendations

Validation was done on only a single component of the heat exchanger test bench. To obtain a complete description of the CO_2 in the cycle, it would be beneficial to model the entire test bench as a closed system and then visualise the energy thereof. This would eliminate most of the problems that were encountered during the validation phase of this study and could prove insightful as to the changes CO_2 undergoes in such a closed cycle.

During this study two possible applications of the energy visualisation were identified, namely: (i) fault detection and isolation and (ii) optimisation. Although this study could not uniquely identify each change or fault, an investigation into the definition of a better residual by defining more features may be able to uniquely identify each fault including the scenario where multiple faults are present.

The S–E graph can be used as a means to optimise heat transfer. The entropy generation rate is shown on the S–E graph. To optimise the heat exchanger the entropy generation rate can be minimised. This, in turn, can be used as a means of control. One can, for instance, develop a controller that minimises the entropy generation rate, but at the same time maximises the amount of heat transferred by manipulating the mass flow rate.

6.4 Closure

The development of an energy based representation for a single-phase counter flow heat exchanger was achieved. The energy based representation was evaluated using a sensitivity analysis to demonstrate that the energy representation is sensitive to small changes in the operation of the heat exchanger. The usefulness, as well as two possible applications of the

energy representation were identified. Both of these were identified as areas that will require additional research.

BIBLIOGRAPHY

[1] A. Bejan, *Entropy Generation Minimization: The Method of Thermodynamic Optimization of Finite-Size Systems and Finite-Time Processes*, 1st ed. Florida: CRC Press LLC, 1996.

[2] H. B. Mahood, A. N. Campbell, R. B. Thorpe, and A. O. Sharif, “Heat transfer efficiency and capital cost evaluation of a three-phase direct contact heat exchanger for the utilisation of low-grade energy sources,” *Energy Convers. Manag.*, vol. 106, pp. 101–109, 2015.

[3] Y. Chen, “Novel Cycles Using Carbon Dioxide as Working Fluid New Ways to Utilize Energy from Low - by,” p. 95, 2006.

[4] J. Rose, T. R. Nielsen, J. Kragh, and S. Svendsen, “Quasi-steady-state model of a counter-flow air-to-air heat-exchanger with phase change,” *Appl. Energy*, vol. 85, no. 5, pp. 312–325, 2008.

[5] S. Kakac and H. Lui, “Heat exchangers; Selection, rating and thermal design.” 2002.

[6] Q. Wang, M. Zeng, T. Ma, X. Du, and J. Yang, “Recent development and application of several high-efficiency surface heat exchangers for energy conversion and utilization,” *Appl. Energy*, vol. 135, pp. 748–777, 2014.

[7] A. P. Fraas and N. M. Ozisik, *Heat exchanger design*. John Wiley & Sons Inc., 1965.

[8] T. a. Ameel, R. O. Warrington, R. S. Wegeng, and M. K. Drost, “Miniaturization technologies applied to energy systems,” *Energy Convers. Manag.*, vol. 38, no. 10–13, pp. 969–982, 1997.

[9] R. . Perry and D. . Green, *Perry’s Chemical Engineers' Handbook*, 8th ed. McGraw-Hill, 2007.

[10] J. Banks, J. S. Carson, B. L. Nelson, and N. D. M, *Discrete-Event System Simulation*, 5th ed. Upper Saddle River: Pearson Education Inc, 2010.

[11] T. L. Paez, “Introduction to Model Validation,” *27th Int. Modal Anal. Conf. Orlando, FL*, 2009.

[12] B. I. Master, K. S. Chunangad, a. J. Boxma, D. Kral, and P. Stehlík, “Most Frequently Used Heat Exchangers from Pioneering Research to Worldwide Applications,” *Heat Transf. Eng.*, vol. 27, no. 6, pp. 4–11, Jun. 2006.

[13] J. Zhou, S. Wu, Y. Chen, and C. Shao, “Semi-numerical analysis of heat transfer performance of fractal based tube bundle in shell-and-tube heat exchanger,” *Int. J. Heat Mass Transf.*, vol. 84, pp. 282–292, 2015.

[14] University of Washington, “Explanatory & Analytical Models,” 2002. .

[15] T.-C. Hung, H.-C. Chen, D.-S. Lee, H.-H. Fu, Y.-T. Chen, and G.-P. Yu, “Optimal design of a concentric heat exchanger for high-temperature systems using CFD simulations,” *Applied Thermal Engineering*, no. 0. .

[16] M. Mohanraj, S. Jayaraj, and C. Muraleedharan, “Applications of artificial neural networks for thermal analysis of heat exchangers - A review,” *Int. J. Therm. Sci.*, vol. 90, pp. 150–172, 2015.

[17] M. L. Aime and C. Maffezzoni, “Modelling and simulation of combined lumped and distributed systems by an object-oriented approach,” *Math. Comput. Simul.*, vol. 53, no. 4–6, pp. 345–351, 2000.

[18] Z.-M. Xu, Z. Liu, and Y. Zhang, “Irreversibility and available energy loss in a heat exchanger,” *Int. J. Heat Mass Transf.*, vol. 88, pp. 552–557, 2015.

[19] J. Wang, Z. Liu, F. Yuan, W. Liu, and G. Chen, “Convective heat transfer optimization in a circular tube based on local exergy destruction minimization,” *Int. J. Heat Mass Transf.*, vol. 90, pp. 49–57, 2015.

[20] I. Dincer and Y. A. Cengel, “Energy, Entropy and Exergy Concepts and Their Roles in Thermal Engineering,” *Entropy*, vol. 3, no. 3, pp. 116–149, 2001.

[21] K. Muralikrishna and U. V. Shenoy, “Heat exchanger design targets for minimum area and cost,” *Trans IChemE*, vol. 78, no. Part A, pp. 161–167.

[22] M. Picón-Núñez, G. T. Polley, and G. Martínez-Rodríguez, “Graphical tool for the preliminary design of compact heat exchangers,” *Applied Thermal Engineering*, vol. 61, no. 1. pp. 36–43, 2013.

[23] J. Yang, S. R. Oh, and W. Liu, “Optimization of shell-and-tube heat exchangers using a general design approach motivated by constructal theory,” *Int. J. Heat Mass Transf.*, vol. 77, pp. 1144–1154, 2014.

[24] J. Guo, L. Cheng, and M. Xu, “Optimization design of shell-and-tube heat exchanger by entropy generation minimization and genetic algorithm,” *Appl. Therm. Eng.*, vol. 29, no. 14–15, pp. 2954–2960, 2009.

[25] J. Guo and M. Xu, “The application of entransy dissipation theory in optimization design of

heat exchanger," *Appl. Therm. Eng.*, vol. 36, pp. 227–235, 2012.

[26] V. K. Patel and R. V. Rao, "Design optimization of shell-and-tube heat exchanger using particle swarm optimization technique," *Appl. Therm. Eng.*, vol. 30, no. 11–12, pp. 1417–1425, 2010.

[27] V. C. Mariani, A. R. K. Duck, F. A. Guerra, L. dos S. Coelho, and R. V. Rao, "A chaotic quantum-behaved particle swarm approach applied to optimization of heat exchangers," *Appl. Therm. Eng.*, vol. 42, pp. 119–128, 2012.

[28] B. Khalifeh Soltan, M. Saffar-Avval, and E. Damangir, "Minimizing capital and operating costs of shell and tube condensers using optimum baffle spacing," *Appl. Therm. Eng.*, vol. 24, no. 17–18, pp. 2801–2810, 2004.

[29] S. Sanaye and H. Hajabdollahi, "Multi-objective optimization of shell and tube heat exchangers," *Appl. Therm. Eng.*, vol. 30, no. 14–15, pp. 1937–1945, 2010.

[30] S. U. S. Choi, "Enhancing thermal conductivity of fluids with nanoparticles," in *American Society of Mechanical Engineers, Fluids Engineering Division (Publication) FED*, 1995, vol. 231, pp. 99–105.

[31] X.-Q. Wang and A. S. Mujumdar, "Heat transfer characteristics of nanofluids: a review," *Int. J. Therm. Sci.*, vol. 46, no. 1, pp. 1–19, 2007.

[32] A. K. Tiwari, P. Ghosh, and J. Sarkar, "Performance comparison of the plate heat exchanger using different nanofluids," *Exp. Therm. Fluid Sci.*, vol. 49, pp. 141–151, 2013.

[33] L. Godson, K. Deepak, C. Enoch, B. Jefferson, and B. Raja, "Heat transfer characteristics of silver/water nanofluids in a shell and tube heat exchanger," *Arch. Civ. Mech. Eng.*, vol. 14, no. 3, pp. 489–496, 2014.

[34] H. Maddah, M. Alizadeh, N. Ghasemi, S. Rafidah, and W. Alwi, "Experimental study of Al 2 O 3 / water nanofluid turbulent heat transfer enhancement in the horizontal double pipes fitted with modified twisted tapes," *Int. J. Heat Mass Transf.*, vol. 78, pp. 1042–1054, 2014.

[35] V. Kumar, A. K. Tiwari, and S. K. Ghosh, "Application of nanofluids in plate heat exchanger: A review," *Energy Convers. Manag.*, vol. 105, pp. 1017–1036, 2015.

[36] H. Li and V. Kottke, "Effect of baffle spacing on pressure drop and local heat transfer in shell-and-tube heat exchangers for staggered tube arrangement," *Int. J. Heat Mass Transf.*, vol. 41, no. 2, pp. 1303–1311, 1998.

[37] J. P. Gupta, *Fundamentals of heat exchanger and pressure vessel technology*, 1st ed. Hemisphere Publishing Corporation, 1986.

[38] M. M. Abu-Khader, “Plate heat exchangers: Recent advances,” *Renew. Sustain. Energy Rev.*, vol. 16, no. 4, pp. 1883–1891, May 2012.

[39] B. Parikshit, K. R. Spandana, V. Krishna, T. R. Seetharam, and K. N. Seetharamu, “A simple method to calculate shell side fluid pressure drop in a shell and tube heat exchanger,” *Int. J. Heat Mass Transf.*, vol. 84, pp. 700–712, 2015.

[40] J.-F. Yang, M. Zeng, and Q.-W. Wang, “Numerical investigation on combined single shell-pass shell-and-tube heat exchanger with two-layer continuous helical baffles,” *Int. J. Heat Mass Transf.*, vol. 84, pp. 103–113, 2015.

[41] F. P. Incropera and D. P. DeWitt, *Fundamentals of heat and mass transfer*, 5th ed. John Wiley & Sons Inc., 2002.

[42] S. Patankar, “Numerical heat transfer and fluid flow,” *Series in coputational methods in mechanics and thermal sciences*. pp. 1–197, 1980.

[43] C. Bornarke and Richard E. Sonntag, *Fundamentals of Thermdynamics*. 2008.

[44] J. Welty, C. E. Wicks, G. L. Rorrer, and R. E. Wilson, *Fundamentals of Momentum, heat, and mass transfer*, 5th ed. John Wiley & Sons Inc., 2008.

[45] H. Park, “CDF advantages and practical applications.” .

[46] F. Zaversky, M. Sánchez, and D. Astrain, “Object-oriented modeling for the transient response simulation of multi-pass shell-and-tube heat exchangers as applied in active indirect thermal energy storage systems for concentrated solar power,” *Energy*, vol. 65, pp. 647–664, 2014.

[47] Modelica, “Modelica and the modelica association,” 2015. .

[48] I. Dincer and Y. A. Cengel, “Energy, Entropy and Exergy Concepts and Their Roles in Thermal Engineering,” *Entropy*, vol. 3, no. 3, pp. 116–149, 2001.

[49] H. Sadighi Dizaji, S. Jafarmadar, and M. Hashemian, “The effect of flow, thermodynamic and geometrical characteristics on exergy loss in shell and coiled tube heat exchangers,” *Energy*, vol. 91, pp. 678–684, 2015.

[50] J. Wang, Z. Liu, F. Yuan, W. Liu, and G. Chen, “Convective heat transfer optimization in a circular tube based on local exergy destruction minimization,” *Int. J. Heat Mass Transf.*, vol. 90, pp. 49–57, 2015.

[51] H. Sadighi Dizaji, S. Jafarmadar, and M. Hashemian, “The effect of flow, thermodynamic and geometrical characteristics on exergy loss in shell and coiled tube heat exchangers,” *Energy*, vol. 91, pp. 678–684, 2015.

[52] L. Q. Huang, G. Q. Chen, Y. Zhang, B. Chen, and S. J. Luan, “Exergy as a unified measure of water quality,” *Commun. Nonlinear Sci. Numer. Simul.*, vol. 12, no. 5, pp. 663–672, 2007.

[53] R. Saidur, J. U. Ahamed, and H. H. Masjuki, “Energy, exergy and economic analysis of industrial boilers,” *Energy Policy*, vol. 38, no. 5, pp. 2188–2197, 2010.

[54] D. Tarlet, Y. Fan, S. Roux, and L. Luo, “Entropy generation analysis of a mini heat exchanger for heat transfer intensification,” *Exp. Therm. Fluid Sci.*, vol. 53, pp. 119–126, 2014.

[55] S. Huang, Z. Ma, and P. Cooper, “Optimal design of vertical ground heat exchangers by using entropy generation minimization method and genetic algorithms,” *Energy Convers. Manag.*, vol. 87, pp. 128–137, 2014.

[56] D. Tarlet, Y. Fan, S. Roux, and L. Luo, “Entropy generation analysis of a mini heat exchanger for heat transfer intensification,” *Exp. Therm. Fluid Sci.*, vol. 53, pp. 119–126, 2014.

[57] X. Cheng and X. Liang, “Entransy, Entransy Dissipation and Entransy Loss for Analyses of Heat Transfer and Heat-Work Conversion Processes,” *J. Therm. Sci. Technol.*, vol. 8, no. 2, pp. 337–352, 2013.

[58] Z. Guo, H. Zhu, and X. Liang, “Entransy — A physical quantity describing heat transfer ability,” vol. 50, pp. 2545–2556, 2007.

[59] L. Kang and Y. Liu, “Multi-objective optimization on a heat exchanger network retrofit with a heat pump and analysis of CO2 emissions control,” *Appl. Energy*, vol. 154, pp. 696–708, 2015.

[60] Z. Wang and Y. Li, “Irreversibility analysis for optimization design of plate fin heat exchangers using a multi-objective cuckoo search algorithm,” *Energy Convers. Manag.*, vol. 101, pp. 126–135, 2015.

[61] K. Juslin, “A Companion Model Approach to Modelling and Simulation of Industrial Processes,” 2005.

[62] G. P. Greyvenstein, “An implicit method for the analysis of transient flows in pipe networks,” *Int. J. Numer. Methods Eng.*, vol. 53, no. 5, pp. 1127–1143, 2002.

[63] H. A. Ibrahim, “Fouling in Heat Exchangers,” *MATLAB - A Fundam. Tool Sci. Comput. Eng.*

Appl., vol. 3, pp. 57–96, 2012.

[64] J. J. Gertler, *Fault detection and diagnosis in Engineering Systems*. New York: Marcel Dekker Inc, 1998.

APPENDIX A

Appendix A lists the properties of the heat exchanger and fluids used for all the simulations conducted during this study in tables.

Table A-1: The geometry of the heat exchanger pipes

Parameter	Value	Unit
Inner pipe radius	7.9	[mm]
Outer pipe radius	13.3	[mm]
Separation wall thickness	2.75	[mm]
Pipe length	24	[m]

Table A-2: The values of the electrical components used in the differential equations

Component	Symbol	Value
Compressibility of hot fluid	$C_{h,h}$	$V_h\rho_h/B_h$
Compressibility of cold fluid	$C_{h,c}$	$V_c\rho_c/B_c$
Momentum of hot fluid	L_h	l_h/A_h
Momentum of cold fluid	L_c	l_c/A_c
Friction loss of hot fluid	$R_{h,h}$	$\left(\frac{f_h l_h}{d_h}+K_{s,h}\right)\frac{1}{2\rho_h A_h^2}$
Turbulent loss of hot fluid	$R_{turb,h}$	$-\left(\frac{f_h l_h}{d_h}+K_{s,h}\right)\frac{1}{4\rho_h A_h^2}$
Friction loss of cold fluid	$R_{h,c}$	$\left(\frac{f_c l_c}{d_c}+K_{s,c}\right)\frac{1}{2\rho_c A_c^2}$
Turbulent loss of cold fluid	$R_{turb,c}$	$-\left(\frac{f_c l_c}{d_c}+K_{s,c}\right)\frac{1}{4\rho_c A_c^2}$
Thermal energy storage - hot fluid	$C_{t,h}$	$V_h c_{p,h}\rho_h$
Thermal energy storage - cold fluid	$C_{t,c}$	$V_c c_{p,c}\rho_c$
Thermal energy storage - heat conductive wall	$C_{t,w}$	$V_w c_{p,w}\rho_w$
Convection heat transfer - hot fluid	$R_{t,h}$	$1/h_h A_h$

Convection heat transfer – cold fluid	$R_{t,c}$	$1/h_cA_c$

Table A-3: The thermodynamic properties of carbon dioxide used during simulation of the model

Property	Value	Unit
Density - S_{H1}	111	[kg/m^3]
Density - S_{H2}	141	[kg/m^3]
Density - S_{H3}	203	[kg/m^3]
Density - M_{H1}	150	[kg/m^3]
Density - M_{H2}	239	[kg/m^3]
Specific Heat - M_{H1}	3052	[J/kg.K]
Specific Heat - M_{H2}	4185	[J/kg.K]
Enthalpy - S_{H1}	554816	[J/kg]
Enthalpy - S_{H2}	493011	[J/kg]
Enthalpy - S_{H3}	454256	[J/kg]
Convection Coefficient - M_{H1}	2871	[W/m^2.K]
Convection Coefficient - M_{H2}	4225	[W/m^2.K]

Table A-4: The thermodynamic properties of water used during simulation of the model

Property	Value	Unit
Bulk Modulus	2.2x10^9	[Pa]
Density	987	[kg/m^3]
Specific Heat	4185	[J/kg.K]
Convection Coefficient M_{C1}	3510	[W/m^2.K]
Convection Coefficient M_{C2}	4300	[W/m^2.K]

Table A-5: The thermodynamic properties of the separation wall used during simulation of the model

Property	Value	Unit
Density	8933	[kg/m^3]
Specific Heat	390	[J/kg.K]

Table A-6: The simulation parameters used during simulation of the model

Parameter	Variable	Value	Unit
Pressure in - Hot side	$P_{h,in}$	7000000	[Pa]
Pressure in - Cold Side	$P_{c,in}$	286000	[Pa]
Pressure out - Hot Side	$P_{h,out}$	6882995	[Pa]
Pressure out - Cold Side	$P_{c,out}$	277080	[Pa]
Inlet Temperature - Hot Side	$T_{h,in}$	396	[K]
Inlet Temperature - Cold Side	$T_{c,in}$	302	[K]

Table A-7: The initial conditions used during simulation of the model

Parameter	Variable	Value	Unit
Pressure – M_{H1}	P_{h1}	6949870	[Pa]
Pressure – M_{H2}	P_{h2}	6910405	[Pa]
Pressure - M_{C1}	P_{c1}	283026	[Pa]
Pressure – M_{C2}	P_{c2}	280053	[Pa]
Mass flow rate – S_{H1}-S_{H3}	$\dot{m}_{h1}$-$\dot{m}_{h3}$	0.1823	[kg/s]
Mass flow rate – S_{C1}-S_{C3}	$\dot{m}_{c1}$-$\dot{m}_{c3}$	0.1345	[kg/s]
Temperature – M_{H1}	T_{h1}	346	[K]
Temperature - M_{H2}	T_{h1}	322	[K]
Temperature – M_{C1}	T_{c1}	314	[K]
Temperature - M_{C2}	T_{c2}	334	[K]
Temperature – M_{W1}	T_{w1}	340	[K]
Temperature – M_{W2}	T_{w2}	337	[K]

Table A-8: The geometry of the pipe used to model the fluid leak

Parameter	Value	Unit
Leak pipe diameter	0.001	[m]
Leak pipe length	0.00275	[m]

Table A-9: The thermodynamic properties of carbon dioxide used during simulation of the heat leak

Property	Value	Unit
Density - S_{H1}	111	[kg/m^3]
Density - S_{H2}	141	[kg/m^3]
Density - S_{H3}	203	[kg/m^3]
Density - M_{H1}	150	[kg/m^3]
Density - M_{H2}	239	[kg/m^3]
Specific Heat - M_{H1}	3052	[J/kg.K]
Specific Heat - M_{H2}	4185	[J/kg.K]
Enthalpy - S_{H1}	554816	[J/kg]
Enthalpy - S_{H2}	493011	[J/kg]
Enthalpy - S_{H3}	454256	[J/kg]
Convection Coefficient - M_{H1}	2871	[W/m^2.K]
Convection Coefficient - M_{H2}	4225	[W/m^2.K]

Table A-10: The simulation conditions for validation

Parameter	Variable	Experiment 1	Experiment 2
Pressure in - Hot side	$P_{h,in}$	6890000 Pa	7190000 Pa
Pressure out - Hot side	$P_{h,out}$	6510000 Pa	6780000 Pa
Pressure in - Cold side	$P_{c,in}$	286000 Pa	286000 Pa
Pressure out - Cold side	$P_{c,out}$	250949 Pa	250949 Pa
Temperature in - Hot side	$T_{h,in}$	330.25 K	334.85 K
Temperature in - Cold side	$T_{c,in}$	288.55 K	288.55 K
Mass flow rate - Hot side	$\dot{m}_{h1}$-$\dot{m}_{h3}$	0.169 kg/s	0.187 kg/s
Mass Flow rate - Cold side	$\dot{m}_{c1}$-$\dot{m}_{c3}$	0.267 kg/s	0.267 kg/s
Secondary loss - Hot side	$K_{s,h}$	158	187
Secondary loss - Cold side	$K_{s,c}$	0	0

Table A-11: Initial conditions for validation

Parameter	Variable	Value - Experiment 1	Value - Experiment 2	Unit
Pressure - Hot side 1	P_{h1}	6463556	6715610	[Pa]
Pressure - Hot side 2	P_{h2}	6350393	6602934	[Pa]
Pressure - Cold Side 1	P_{c1}	274020	274020	[Pa]
Pressure - Cold Side 2	P_{c2}	262267	262267	[Pa]
Mass flow rate - Hot side	$\dot{m}_{h1}$-$\dot{m}_{h3}$	0.138	0.169	[kg/s]
Mass flow rate - Cold side	$\dot{m}_{c1}$-$\dot{m}_{c3}$	0.267	0.267	[kg/s]
Temperature - Hot side 1	T_{h1}	312	307	[K]
Temperature - Hot side 2	T_{h1}	300	297	[K]
Temperature - Cold side 1	T_{c1}	296	292	[K]
Temperature - Cold side 2	T_{c2}	305	297	[K]

Table A-12: The fluid properties of carbon dioxide for validation

Property	Value	Unit
Density - S_{H1}	111	[kg/m^3]
Density - S_{H2}	141	[kg/m^3]
Density - S_{H3}	203	[kg/m^3]
Density - M_{H1}	150	[kg/m^3]
Density - M_{H2}	239	[kg/m^3]
Specific Heat - M_{H1}	3052	[J/kg.K]
Specific Heat - M_{H2}	4185	[J/kg.K]
Enthalpy - S_{H1}	554816	[J/kg]
Enthalpy - S_{H2}	493011	[J/kg]
Enthalpy - S_{H3}	454256	[J/kg]
Convection Coefficient - M_{H1}	2871	[W/m^2.K]
Convection Coefficient - M_{H2}	4225	[W/m^2.K]

Table A-13: The fluid properties of water for validation

Property	Value	Unit
Bulk Modulus	$2.2x10^9$	[Pa]
Density	987	[kg/m^3]
Specific Heat	4185	[J/kg.K]
Convection Coefficient M_{C1}	3510	[$W/m^2.K$]
Convection Coefficient M_{C2}	4300	[$W/m^2.K$]

Table A-14: Entropy values of water for the energy representation under normal conditions

Property	Value
Specific entropy S_{C1}	420 J/kg.K
Specific entropy S_{C2}	594 J/kg.K
Specific entropy S_{C3}	858 J/kg.K

Table A-15: Entropy values of water for the energy representation during shifting of operating point

Property	Value
Specific entropy S_{C1}	420 J/kg.K
Specific entropy S_{C2}	539 J/kg.K
Specific entropy S_{C3}	756 J/kg.K

Table A-16: Entropy values of water for the energy representation during a leakage

Property	Value
Specific entropy S_{C1}	420 J/kg.K
Specific entropy S_{C2}	573 J/kg.K
Specific entropy S_{C3}	877 J/kg.K

Table A-17: Entropy values of water for the energy representation during a heat leakage

Property	Value
Specific entropy S_{C1}	420 J/kg.K
Specific entropy S_{C2}	218 J/kg.K
Specific entropy S_{C3}	625 J/kg.K

Table A-18: Entropy values of water for the energy representation during fouling

Property	Value
Specific entropy S_{C1}	420 J/kg.K
Specific entropy S_{C3}	1053 J/kg.K
Specific entropy S_{C2}	727 J/kg.K

APPENDIX B

Appendix B lists the experimental data gathered during the two experiments conducted on the CO_2 test bench.

Experimental results for step from 35Hz to 40Hz

Sensor Number	Time	41	W20	40	39	54	55
Unit	s	°C	°C	°C	°C	bar	bar
6/30/2015 14:39	0	14.4	30.9	51.5	26.5	66.2	62.4
6/30/2015 14:39	5	14.4	30.9	51.5	26.5	66.2	62.4
6/30/2015 14:39	10	14.4	30.9	51.5	26.5	66.2	62.4
6/30/2015 14:40	15	14.4	30.9	51.5	26.5	66.1	62.4
6/30/2015 14:40	20	14.4	30.9	51.5	26.5	66.1	62.4
6/30/2015 14:40	25	14.4	30.9	51.5	26.5	66.1	62.4
6/30/2015 14:40	30	14.4	30.9	51.5	26.5	66.1	62.4
6/30/2015 14:40	35	14.4	30.9	51.5	26.5	66.1	62.4
6/30/2015 14:40	40	14.4	30.9	51.5	26.5	66.1	62.4
6/30/2015 14:40	45	14.4	30.9	51.5	26.5	66.1	62.5
6/30/2015 14:40	50	14.4	30.9	51.5	26.5	66.1	62.5
6/30/2015 14:40	55	14.4	30.9	51.5	26.5	66.1	62.5
6/30/2015 14:40	60	14.4	30.9	51.5	26.5	66.1	62.5
6/30/2015 14:40	65	14.4	30.9	51.5	26.5	66.1	62.5
6/30/2015 14:40	70	14.4	30.9	51.5	26.5	66.1	62.5
6/30/2015 14:41	75	14.4	30.9	51.5	26.5	66.2	62.5
6/30/2015 14:41	80	14.4	30.9	51.5	26.5	66.2	62.5
6/30/2015 14:41	85	14.4	30.9	51.5	26.5	66.2	62.5
6/30/2015 14:41	90	14.4	30.9	51.5	26.5	66.2	62.5
6/30/2015 14:41	95	14.4	30.9	51.5	26.5	66.2	62.5
6/30/2015 14:41	100	14.4	30.9	51.5	26.5	66.2	62.5
6/30/2015 14:41	105	14.4	31.3	53.2	27.3	68.3	64.5
6/30/2015 14:41	110	14.4	31.3	53.2	27.3	68.3	64.5
6/30/2015 14:41	115	14.4	31.3	53.2	27.3	68.3	64.5
6/30/2015 14:41	120	14.4	31.3	53.2	27.3	68.3	64.5
6/30/2015 14:41	125	14.4	31.3	53.2	27.3	68.3	64.5
6/30/2015 14:41	130	14.4	31.3	53.2	27.3	68.3	64.5

Sensor Number	Time	41	W20	40	39	54	55
Unit	s	°C	°C	°C	°C	bar	bar
6/30/2015 14:42	135	14.4	32.2	54.5	27.9	68.7	64.9
6/30/2015 14:42	140	14.4	32.2	54.5	27.9	68.7	64.9
6/30/2015 14:42	145	14.4	32.2	54.5	27.9	68.7	64.9
6/30/2015 14:42	150	14.4	32.2	54.5	27.9	68.7	64.9
6/30/2015 14:42	155	14.4	32.2	54.5	27.9	68.7	64.9
6/30/2015 14:42	160	14.4	32.2	54.5	27.9	68.7	64.9
6/30/2015 14:42	165	14.4	33.2	55.2	27.9	68.8	65
6/30/2015 14:42	170	14.4	33.2	55.2	27.9	68.8	65
6/30/2015 14:42	175	14.4	33.2	55.2	27.9	68.8	65
6/30/2015 14:42	180	14.4	33.2	55.2	27.9	68.8	65
6/30/2015 14:42	185	14.4	33.2	55.2	27.9	68.8	65
6/30/2015 14:42	190	14.4	33.2	55.2	27.9	68.8	65
6/30/2015 14:43	195	14.4	33.5	55.5	27.9	68.9	65
6/30/2015 14:43	200	14.4	33.5	55.5	27.9	68.9	65
6/30/2015 14:43	205	14.4	33.5	55.5	27.9	68.9	65
6/30/2015 14:43	210	14.4	33.5	55.5	27.9	68.9	65
6/30/2015 14:43	215	14.4	33.5	55.5	27.9	68.9	65
6/30/2015 14:43	220	14.4	33.5	55.5	27.9	68.9	65
6/30/2015 14:43	225	14.4	33.5	55.5	27.9	69	65
6/30/2015 14:43	230	14.4	33.5	55.5	27.9	69	65
6/30/2015 14:43	235	14.4	33.5	55.5	27.9	69	65
6/30/2015 14:43	240	14.4	33.5	55.5	27.9	69	65
6/30/2015 14:43	245	14.4	33.5	55.5	27.9	69	65
6/30/2015 14:43	250	14.4	33.5	55.5	27.9	69	65
6/30/2015 14:44	255	14.4	33.8	55.8	27.9	68.9	65.1
6/30/2015 14:44	260	14.4	33.8	55.8	27.9	68.9	65.1
6/30/2015 14:44	265	14.4	33.8	55.8	27.9	68.9	65.1
6/30/2015 14:44	270	14.4	33.8	55.8	27.9	68.9	65.1
6/30/2015 14:44	275	14.4	33.8	55.8	27.9	68.9	65.1
6/30/2015 14:44	280	14.4	33.8	55.8	27.9	68.9	65.1
6/30/2015 14:44	285	14.4	33.8	55.8	27.9	68.9	65.1
6/30/2015 14:44	290	14.4	33.8	55.8	27.9	68.9	65.1
6/30/2015 14:44	295	14.4	33.8	55.8	27.9	68.9	65.1

Sensor Number	Time	41	W20	40	39	54	55
Unit	s	°C	°C	°C	°C	bar	bar
6/30/2015 14:44	300	14.4	33.8	55.8	27.9	68.9	65.1
6/30/2015 14:44	305	14.4	33.8	55.8	27.9	68.9	65.1
6/30/2015 14:44	310	14.4	33.8	55.8	27.9	68.9	65.1
6/30/2015 14:45	315	14.4	33.8	56.1	28.2	68.9	65.2
6/30/2015 14:45	320	14.4	33.8	56.1	28.2	68.9	65.2
6/30/2015 14:45	325	14.4	33.8	56.1	28.2	68.9	65.2
6/30/2015 14:45	330	14.4	33.8	56.1	28.2	68.9	65.2
6/30/2015 14:45	335	14.4	33.8	56.1	28.2	68.9	65.2
6/30/2015 14:45	340	14.4	33.8	56.1	28.2	68.9	65.2
6/30/2015 14:45	345	14.4	33.8	56.1	28.2	68.9	65.1
6/30/2015 14:45	350	14.4	33.8	56.1	28.2	68.9	65.1
6/30/2015 14:45	355	14.4	33.8	56.1	28.2	68.9	65.1
6/30/2015 14:45	360	14.4	33.8	56.1	28.2	68.9	65.1
6/30/2015 14:45	365	14.4	33.8	56.1	28.2	68.9	65.1
6/30/2015 14:45	370	14.4	33.8	56.1	28.2	68.9	65.1
6/30/2015 14:46	375	14.4	33.8	56.1	28.2	68.9	65
6/30/2015 14:46	380	14.4	33.8	56.1	28.2	68.9	65
6/30/2015 14:46	385	14.4	33.8	56.1	28.2	68.9	65
6/30/2015 14:46	390	14.4	33.8	56.1	28.2	68.9	65
6/30/2015 14:46	395	14.4	33.8	56.1	28.2	68.9	65
6/30/2015 14:46	400	14.4	33.8	56.1	28.2	68.9	65
6/30/2015 14:46	405	14.4	33.8	56.1	28.2	69	65.1
6/30/2015 14:46	410	14.4	33.8	56.1	28.2	69	65.1
6/30/2015 14:46	415	14.4	33.8	56.1	28.2	69	65.1
6/30/2015 14:46	420	14.4	33.8	56.1	28.2	69	65.1
6/30/2015 14:46	425	14.4	33.8	56.1	28.2	69	65.1
6/30/2015 14:46	430	14.4	33.8	56.1	28.2	69	65.1
6/30/2015 14:47	435	14.4	33.8	56.1	28.2	68.9	65
6/30/2015 14:47	440	14.4	33.8	56.1	28.2	68.9	65
6/30/2015 14:47	445	14.4	33.8	56.1	28.2	68.9	65
6/30/2015 14:47	450	14.4	33.8	56.1	28.2	68.9	65
6/30/2015 14:47	455	14.4	33.8	56.1	28.2	68.9	65
6/30/2015 14:47	460	14.4	33.8	56.1	28.2	68.9	65

Sensor Number	Time	41	W20	40	39	54	55
Unit	s	°C	°C	°C	°C	bar	bar
6/30/2015 14:47	465	14.4	33.8	56.1	28.2	69	65.1
6/30/2015 14:47	470	14.4	33.8	56.1	28.2	69	65.1
6/30/2015 14:47	475	14.4	33.8	56.1	28.2	69	65.1
6/30/2015 14:47	480	14.4	33.8	56.1	28.2	69	65.1
6/30/2015 14:47	485	14.4	33.8	56.1	28.2	69	65.1
6/30/2015 14:47	490	14.4	33.8	56.1	28.2	69	65.1
6/30/2015 14:48	495	14.4	33.8	56.1	28.2	68.9	65.1

Experimental results for a step from 40Hz to 45Hz

Sensor number	Time	41	W20	40	39	54	55
Unit	s	°C	°C	°C	°C	bar	bar
6/30/2015 14:54	0	14.4	33.6	56.1	28.1	68.9	65
6/30/2015 14:54	5	14.4	33.6	56.1	28.1	68.9	65
6/30/2015 14:54	10	14.4	33.9	56.1	28.1	68.9	65
6/30/2015 14:54	15	14.4	33.9	56.1	28.1	68.9	65
6/30/2015 14:54	20	14.4	33.9	56.1	28.1	68.9	65
6/30/2015 14:54	25	14.4	33.9	56.1	28.1	68.9	65
6/30/2015 14:54	30	14.4	33.9	56.1	28.1	68.9	65
6/30/2015 14:54	35	14.4	33.9	56.1	28.1	68.9	65
6/30/2015 14:55	40	14.4	33.6	56.1	28.1	69.6	65.8
6/30/2015 14:55	45	14.4	33.6	56.1	28.1	69.6	65.8
6/30/2015 14:55	50	14.4	33.6	56.1	28.1	69.6	65.8
6/30/2015 14:55	55	14.4	33.6	56.1	28.1	69.6	65.8
6/30/2015 14:55	60	14.4	33.6	56.1	28.1	69.6	65.8
6/30/2015 14:55	65	14.4	33.6	56.1	28.1	69.6	65.8
6/30/2015 14:55	70	14.4	34.2	58.4	29.4	71.4	67.4
6/30/2015 14:55	75	14.4	34.2	58.4	29.4	71.4	67.4
6/30/2015 14:55	80	14.4	34.2	58.4	29.4	71.4	67.4
6/30/2015 14:55	85	14.4	34.2	58.4	29.4	71.4	67.4
6/30/2015 14:55	90	14.4	34.2	58.4	29.4	71.4	67.4
6/30/2015 14:55	95	14.4	34.2	58.4	29.4	71.4	67.4
6/30/2015 14:56	100	14.4	35.4	59.4	29.7	71.7	67.8
6/30/2015 14:56	105	14.4	35.4	59.4	29.7	71.7	67.8

Sensor number	Time	41	W20	40	39	54	55
Unit	s	°C	°C	°C	°C	bar	bar
6/30/2015 14:56	110	14.4	35.4	59.4	29.7	71.7	67.8
6/30/2015 14:56	115	14.4	35.4	59.4	29.7	71.7	67.8
6/30/2015 14:56	120	14.4	35.4	59.4	29.7	71.7	67.8
6/30/2015 14:56	125	14.4	35.4	59.4	29.7	71.7	67.8
6/30/2015 14:56	130	14.4	35.9	59.8	29.7	71.9	67.9
6/30/2015 14:56	135	14.4	35.9	59.8	29.7	71.9	67.9
6/30/2015 14:56	140	14.4	35.9	59.8	29.7	71.9	67.9
6/30/2015 14:56	145	14.4	35.9	59.8	29.7	71.9	67.9
6/30/2015 14:56	150	14.4	35.9	59.8	29.7	71.9	67.9
6/30/2015 14:56	155	14.4	35.9	59.8	29.7	71.9	67.9
6/30/2015 14:57	160	14.4	36.2	60.1	29.7	71.8	67.8
6/30/2015 14:57	165	14.4	36.2	60.1	29.7	71.8	67.8
6/30/2015 14:57	170	14.4	36.2	60.1	29.7	71.8	67.8
6/30/2015 14:57	175	14.4	36.2	60.1	29.7	71.8	67.8
6/30/2015 14:57	180	14.4	36.2	60.1	29.7	71.8	67.8
6/30/2015 14:57	185	14.4	36.2	60.1	29.7	71.8	67.8
6/30/2015 14:57	190	14.4	36.2	60.4	29.9	71.8	67.8
6/30/2015 14:57	195	14.4	36.2	60.4	29.9	71.8	67.8
6/30/2015 14:57	200	14.4	36.2	60.4	29.9	71.8	67.8
6/30/2015 14:57	205	14.4	36.2	60.4	29.9	71.8	67.8
6/30/2015 14:57	210	14.4	36.2	60.4	29.9	71.8	67.8
6/30/2015 14:57	215	14.4	36.2	60.4	29.9	71.8	67.8
6/30/2015 14:58	220	14.4	36.2	60.4	29.9	71.9	68.1
6/30/2015 14:58	225	14.4	36.2	60.4	29.9	71.9	68.1
6/30/2015 14:58	230	14.4	36.2	60.4	29.9	71.9	68.1
6/30/2015 14:58	235	14.4	36.2	60.4	29.9	71.9	68.1
6/30/2015 14:58	240	14.4	36.2	60.4	29.9	71.9	68.1
6/30/2015 14:58	245	14.4	36.2	60.4	29.9	71.9	68.1
6/30/2015 14:58	250	14.4	36.2	60.4	29.9	71.9	67.8
6/30/2015 14:58	255	14.4	36.2	60.4	29.9	71.9	67.8
6/30/2015 14:58	260	14.4	36.2	60.4	29.9	71.9	67.8
6/30/2015 14:58	265	14.4	36.2	60.4	29.9	71.9	67.8
6/30/2015 14:58	270	14.4	36.2	60.4	29.9	71.9	67.8

Sensor number	Time	41	W20	40	39	54	55
Unit	s	°C	°C	°C	°C	bar	bar
6/30/2015 14:58	275	14.4	36.2	60.4	29.9	71.9	67.8
6/30/2015 14:59	280	14.4	36.2	60.7	29.9	71.9	68
6/30/2015 14:59	285	14.4	36.2	60.7	29.9	71.9	68
6/30/2015 14:59	290	14.4	36.2	60.7	29.9	71.9	68
6/30/2015 14:59	295	14.4	36.2	60.7	29.9	71.9	68
6/30/2015 14:59	300	14.4	36.2	60.7	29.9	71.9	68
6/30/2015 14:59	305	14.4	36.2	60.7	29.9	71.9	68
6/30/2015 14:59	310	14.4	36.6	60.7	29.9	71.9	67.8
6/30/2015 14:59	315	14.4	36.6	60.7	29.9	71.9	67.8
6/30/2015 14:59	320	14.4	36.6	60.7	29.9	71.9	67.8
6/30/2015 14:59	325	14.4	36.6	60.7	29.9	71.9	67.8
6/30/2015 14:59	330	14.4	36.6	60.7	29.9	71.9	67.8
6/30/2015 14:59	335	14.4	36.6	60.7	29.9	71.9	67.8
6/30/2015 15:00	340	14.4	36.2	60.7	29.9	71.9	67.8
6/30/2015 15:00	345	14.4	36.2	60.7	29.9	71.9	67.8
6/30/2015 15:00	350	14.4	36.2	60.7	29.9	71.9	67.8
6/30/2015 15:00	355	14.4	36.2	60.7	29.9	71.9	67.8
6/30/2015 15:00	360	14.4	36.2	60.7	29.9	71.9	67.8
6/30/2015 15:00	365	14.4	36.2	60.7	29.9	71.9	67.8
6/30/2015 15:00	370	14.4	36.2	60.7	29.9	71.9	67.8
6/30/2015 15:00	375	14.4	36.2	60.7	29.9	71.9	67.8
6/30/2015 15:00	380	14.4	36.2	60.7	29.9	71.9	67.8
6/30/2015 15:00	385	14.4	36.2	60.7	29.9	71.9	67.8
6/30/2015 15:00	390	14.4	36.2	60.7	29.9	71.9	67.8
6/30/2015 15:00	395	14.4	36.2	60.7	29.9	71.9	67.8
6/30/2015 15:01	400	14.4	36.6	60.7	29.9	71.8	67.8
6/30/2015 15:01	405	14.4	36.6	60.7	29.9	71.8	67.8
6/30/2015 15:01	410	14.4	36.6	60.7	29.9	71.8	67.8
6/30/2015 15:01	415	14.4	36.6	60.7	29.9	71.8	67.8
6/30/2015 15:01	420	14.4	36.6	60.7	29.9	71.8	67.8
6/30/2015 15:01	425	14.4	36.6	60.7	29.9	71.8	67.8
6/30/2015 15:01	430	14.4	36.3	60.7	29.9	71.9	67.7
6/30/2015 15:01	435	14.4	36.3	60.7	29.9	71.9	67.7

Sensor number	Time	41	W20	40	39	54	55
Unit	**s**	**°C**	**°C**	**°C**	**°C**	**bar**	**bar**
6/30/2015 15:01	440	14.4	36.3	60.7	29.9	71.9	67.7
6/30/2015 15:01	445	14.4	36.3	60.7	29.9	71.9	67.7
6/30/2015 15:01	450	14.4	36.3	60.7	29.9	71.9	67.7
6/30/2015 15:01	455	14.4	36.3	60.7	29.9	71.9	67.7
6/30/2015 15:02	460	14.4	36.3	60.7	29.9	71.9	67.8
6/30/2015 15:02	465	14.4	36.3	60.7	29.9	71.9	67.8
6/30/2015 15:02	470	14.4	36.3	60.7	29.9	71.9	67.8
6/30/2015 15:02	480	14.4	36.3	60.7	29.9	71.9	67.8
6/30/2015 15:02	485	14.4	36.3	60.7	29.9	71.9	67.8